

# ACTA MATERIALIA TRANSYLVANICA

Material Sciences Publications

Volume 6, Issue 2



ERDÉLYI MÚZEUM-EGYESÜLET  
Cluj-Napoca  
2023

A folyóirat megjelenését támogatta a Communitas Alapítvány, a Magyar Tudományos Akadémia, a Bethlen Gábor Alapkezelő Zrt. és az EME Műszaki Tudományok Szakosztálya / The publication of this magazine was supported by the Communitas Foundation, by the Hungarian Academy of Sciences, by the Bethlen Gábor Fund and by the TMS – Department of Engineering Sciences.



**Főszerkesztő / Editor-in-Chief:** Bitay Enikő

**Nemzetközi Tanácsadó testület / International Editorial Advisory Board:**

Prof. Biró László Péter, MTA Energiatudományi Kutatóközpont, Budapest, Magyarország  
 Prof. emer. B. Nagy János, University of Namur, Namur, Belgium  
 Prof. Czigány Tibor, Budapesti Műszaki és Gazdaságtudományi Egyetem, Budapest, Magyarország  
 Prof. Diószegi Attila, Jönköping University, Jönköping, Svédország  
 Dobránszky János, ELKH–BME Kompozittechnológiai Kutatócsoport, Budapest, Magyarország  
 Prof. Dusza János, Institute of Materials Research of Slovak Academy of Sciences, Kassa, Szlovákia  
 Prof. Kaptay György, Miskolci Egyetem, Miskolc, Magyarország  
 Dr. Kolozsváry Zoltán, Plasmaterm Rt., Marosvásárhely, Románia  
 Prof. Mertinger Valéria, Miskolci Egyetem, Miskolc, Magyarország  
 Prof. Porkoláb Miklós, Massachusetts Institute of Technology, Cambridge, MA, USA  
 Prof. Réger Mihály, Óbudai Egyetem, Budapest, Magyarország  
 Prof. emer. Réti Tamás, Óbudai Egyetem, Budapest, Magyarország  
 Prof. emer. Roósz András, Miskolci Egyetem, Miskolc, Magyarország  
 Dr. Spenik Sándor, Ungvári Nemzeti Egyetem, Ungvár, Ukrajna  
 Prof. Zsoldos Ibolya, Széchenyi István Egyetem, Győr, Magyarország

**Lapszámszerkesztők / Editorial Board:**

Dobránszky János, HUN-REN–BME Kompozittechnológiai Kutatócsoport, Budapest, Magyarország  
 Csavdári Alexandra, Babeş–Bolyai Tudományegyetem, Kolozsvár, Románia  
 Gergely Attila, Sapientia Erdélyi Magyar Tudományegyetem, Marosvásárhely, Románia  
 Kovács Tünde, Óbudai Egyetem, Budapest, Magyarország

**Kiadó / Publisher:** Erdélyi Múzeum-Egyesület

**Felelős kiadó / Responsible publisher:** Biró Annamária

**Olvasószerkesztő / Proofreader:** Szenkovics Enikő (magyar), David Speight (English)

**Szerkesztőségi titkár / Editorial secretary:** Kisfaludi-Bak Zsombor

**Borítóterv / Cover:** Kőnczey Elemér

**Nyomdai munkálatok / Printed at:** F&F International Kft., Gyergyószentmiklós

**Copyright** © a szerzők / the authors, EME/ TMS 2023

**ISSN 2601-1883, ISSN-L 2601-1883**

**DOI: 10.33923/amt-2023-02**

**A folyóirat honlapja:** <https://www.eme.ro/publication-hu/acta-mat/mat-main.htm>

**The journal website:** <https://www.eme.ro/publication/acta-mat/mat-main.htm>

*Az Acta Materialia Transylvanica. Anyagtudományi Közlemények* az Erdélyi Múzeum-Egyesület (EME) Műszaki Tudományok Szakosztályának folyóirata, amely az anyagtudományok területéről közlő tudományos közleményeket: szakcikkeket, összefoglalókat (szemléket), tanulmányokat. A folyóirat célja összképet adni kiemelten a Kárpát-medencei kutatási irányokról, tudományos eredményeiről, s ezt széles körben terjeszteni is. A folyóirat az EME felvállalt céljaihoz híven a magyar szaknyelv ápolását is támogatja, így a nyomtatott folyóirat magyar nyelven jelenik meg, mely az Erdélyi digitális adattárban elérhető (<https://eda.eme.ro/handle/10598/30356>). A széles körű nemzetközi terjesztés érdekében a folyóirat teljes angol nyelvű változatát is közzétesszük.

*Acta Materialia Transylvanica* – Material Sciences Publications – is a journal of the Technical Sciences Department of the Transylvanian Museum Society, publishing scientific papers, issues, reviews and studies in the field of material sciences. Its mission is to provide and disseminate a comprehensive picture focusing on research trends and scientific results in the Carpathian basin. In accordance with the general mission of the Transylvanian Museum Society it aims to support specialized literature in Hungarian. The printed version of the journal is published in Hungarian and is available in the Transylvanian Digital Database (<https://eda.eme.ro/handle/10598/30356>). However, we would like to spread it internationally, therefore the full content of the journal will also be available in English.

## Tartalom / Content

---

BARABÁSSY Miklós .....	64
<i>A Szent Korona süllyesztett rekeszománcai</i>	
<i>The Recessed Apertures of the Holy Crown</i>	
Borhy Levente, Szabó Gábor .....	74
<i>A ragasztóanyag rétegvastagsága hatásának vizsgálata fém és kompozit közötti kötésekben</i>	
<i>Investigation of the Effect of Layer Thickness of Adhesive Material on Metal to Composite Joints</i>	
Dobránszky János .....	80
<i>Egy meghibásodott turbófeltöltő károsodáselemzése</i>	
<i>Failure Analysis of a Damaged Turbocharger</i>	
Egerszegi Boglárka Fanni.....	84
<i>Orvoseszköz-tervezés a kézmozgás támogatására</i>	
<i>Medical Device Design to Support Hand Movement</i>	
Fekete L. Mátyás .....	90
<i>A pozdorjaadalékos beton elemzése</i>	
<i>Analysis of Concrete with Chaff</i>	
Nagy Balázs, Kovács Tünde Anna .....	95
<i>A maximális hézag meghatározása lézeres hegesztéshez</i>	
<i>Determination of maximal gap for laser welding</i>	
Szovák Benedek, Maróti János Endre, Orbulov Imre Norbert .....	100
<i>Részecskeerősítésű nyílt cellás fémhabok</i>	
<i>Particle Reinforced, Open Cell Metal Foams</i>	
Tamás-Bényei Péter .....	105
<i>A sós víz hatása a bazaltszál erősítésű kompozit tulajdonságaira</i>	
<i>The Effect of Salt Water on the Properties of Basalt Fibre Reinforced Composites</i>	

Tóth László..... 114

*Szerszámacélok tulajdonságainak változása a hőkezelés hatására*

*Effect of Heat Treatment on the Properties of Tool Steel*

Vincze Kata Dóra..... 121

*Ortopédiai ortézis károsodási folyamatainak vizsgálata*

*Examination of damage Processes of Orthopaedic Orthosis*



# The Recessed Apertures of the Holy Crown

Miklós BARABÁSSY

KEMPELEN Academy of Sciences Foundation, Budapest, Hungary, [miklos.barabassy@gmail.com](mailto:miklos.barabassy@gmail.com)

## Abstract

One of the most important questions in the study of the Holy Crown concerns the technique of making the enamel cloisonné. The importance of this is that the manufacture of cloisonné enamel reached its peak in the 10<sup>th</sup> and 11<sup>th</sup> centuries in Byzantium and Western Europe. The figural enamels of the Holy Crown are all images of top-quality products of this process. Archaeometric analysis of the Holy Crown has not been carried out. My work attempts to fill this gap. The knowledge of the techniques used will help to determine the place and time of the various parts. For the time being, the aim is to recognise the techniques only from the colour side, but if possible from both sides. With this tutorial I would like to describe what I have learned so far.

**Keywords:** *Holy Crown, diaphragm making, archeaometry.*

## 1. Technical evolution of the émail cloisonné

The enamel itself, known in French as émail cloisonné, is made of glass. It is not crystalline like ceramics, but amorphous. The enamel is made by fusing several layers of different coloured glass powder into a recess delimited by metal walls – the recipient. The different coloured parts of the image are separated by strips.

The study deals exclusively with gold recipes

made using the sunken sandwich technique, which were used in Byzantium and Western Europe from the 10<sup>th</sup> to middle of the 11<sup>th</sup> centuries. All the figural enamel works on the Holy Crown (a total of 19) were made using this technique. The sandwich construction of the recipient is due to the fact that they are typically made of two layers of plates soldered together, and the lower plate is often recessed.

### 1.1. The Vollschmelz (full melt) enamel

By definition, the Vollschmelz of full enamel fills the entire surface of the plate. To achieve this, the edge of the plate was folded up or, alternatively, a thicker sub-plate was framed around it. This was necessary to prevent the molten glass from flowing over the edge; this can be observed in [Figure 1](#)

### 1.2. Recipient with cut-out, sandwich structure

In this case, two plates were soldered together. A piece of the upper one was cut out where the enamel is visible and then soldered on top of each other. The depth of the recipient is thus equal to the thickness of the upper plate. This method of making the recipient evolved naturally from the solution shown in [Figure 2](#). If the recipient is created by soldering two plates together, I call it the sandwich technique.



**Figure 1.** *Vollschmelz (full) enamel on the main panel of the Martvili Triptych, Tbilis.*

### 1.3. Sandwich technique combined with sinking

In my opinion, it was realised early on that considerable savings in gold could be made in the production of enamel images if the required depth of the recipient was not achieved by using a thick and a thin plate, but by sinking the lower of the two thin plates.

The same procedure was used for all the figurative pictures of the Holy Crown, regardless of where they were made - in Western Europe or Byzantium. The present study focuses on this type of technical realisation. The aim is to formulate criteria that will allow us to identify, from the colour side only, the way in which the recipient was executed. By defining the recipient created, we can obtain important information for determining the date and place of the Holy Crown's creation. Still, the use of chronology justifies the presentation of this technique alongside the practice of the earlier (full melt) and subsequent ages, the Limoges and the „only” sinking techniques.

### 1.4. Recessed recipients

By the turn of the 10<sup>th</sup> and 11<sup>th</sup> centuries, gold was running out in the West as well as in Byzantium. In Byzantium, from the second third of the 11<sup>th</sup> century onwards, recipients were not made using the sandwich technique, but simply by sinking a thin gold plate. The earliest compartment enamel I know of made using this technique is the Monomachos Crown (1045-1050) from the Hungarian National Museum (MNM).

One of the reasons why this work of art was described as a technical forgery by Nicolas Oikonomides was precisely because of the simple technique of sinking [1]. Other enamel paintings made with a similar technique were identified later, as shown in Figure 5 (c. 1100). By this time, Byzantine enamel was already used mainly in opalescent (not translucent, similar to polished marble) enamel. Another striking feature is the denser walls of the compartment strips.

### 1.5. Limoges or champlevé enamels

From the middle of the 11<sup>th</sup> century until the second half of the 12<sup>th</sup> century, there were no gold compartment enamels made. This may have been partly due to changing fashions, and partly to the extreme shortage of gold in the German-Roman Empire (no gold coins were minted for a long time after 1000), while in Byzantium (mainly due to warfare) the gold stock was extremely low. In the 12<sup>th</sup> century, gold enamels were replaced in



Figure 2. Christ on enamel medallion, Cleveland.



Figure 3. 11<sup>th</sup> century medal, Metropolitan Museum of Art (MET) (colour side-on left; back side-on right).



Figure 4. Image of Christ with sandwich recipient, British Museum, London.



Figure 5. Byzantine Christ, enamel c. 1100, Metropolitan Museum of Art (MET).

the west by so-called *champlevé* enamels. In this case, recesses were made in the copper or bronze (sometimes silver and very rarely gold) plates by engraving „pits”. Importantly, the enamel they used was light-absorbing, opalescent, so it did not glitter like the earlier diaphragm enamels (German: *Grubenschmelz*; hence the term „pit enamel”).

## 2. The technique of the sandwich recessed diaphragm recipient

From the 10<sup>th</sup> century onwards, the relationship between Byzantium and the German-Roman Empire became very strong. This was thanks to the efforts of Princess Theophanu, who arrived in Italy on 14 April 972, thanks to the efforts of Otto I (the Great), who did everything he could to re-establish the Roman Empire, but Byzantium considered itself the heir to the Roman Empire, and in fact despised the Frankish Empire. The result of Otto's long and intense efforts was that Otto II was eventually able to bring a wealthy, high-ranking princess from Byzantium, but not from the narrow imperial family. Theophanu arrived with a huge court and dowry, and was married to Otto II. From then on, countless documents have survived confirming the strong Byzantine influence. A bilingual hymn-book, codices, clothing, carpets, textiles and, last but not least, importantly for us, Byzantine-style gold enamels belonging to strict Christian religious artefacts, relics or depicting saints. In 983, after the death of Otto II, Theophanu reached the height of his power as regent of the German-Roman Empire. The Greek language and style was mixed with Latin on countless works of art produced at this time. Numerous works of art from this period mix Greek language and style with Latin. The first Byzantine enamel I know of and date, made using the recessed-sandwich technique, is the Preslav hoard, dating from the first third of the 10<sup>th</sup> century. The treasure, which was restored in Mainz, was described by Antje Bosselmann-Ruickbie [2]. The lower plate of the

two-layer recipient is about 0.1 mm thick and is pure gold, while the upper plate, from which the contour was cut, is 0.2 -0.3 mm thick. The lower plate was deepened by *trébing*. It is probable that the technique of recessed sandwiching in enamel was first used in Byzantium. I do not know of any enamels made in Western Europe using this technique from the first half of the 10<sup>th</sup> century.

As can be seen from the above, enamel making is a multi-phase process and it is therefore necessary to examine the process, the advantages and the time of use of the solutions. In Theophanu's time, enamel works became widespread in Western Europe, north of the Alps. The enamel paintings created at this time were of two styles.

The first, with the previously known full-enamel technique, and the second with the recessed sandwich technique. In this period, the recessed sandwich technique was more common. This was also verifiably in use in the art workshops that Egbert managed.

Since all the figural enamel paintings of the Holy Crown are made using the recessed sandwich technique, a thorough knowledge of this technique is required. Latin and Byzantine languages are also mixed on the Holy Crown, which was more common in the late 10<sup>th</sup> and early 11<sup>th</sup> century artefacts, in the Saxon Liudolfinger period, and even characteristic of Ottonian objects, so much so, that until the end of the last century many decorative enamel plates in Western Europe were believed to be of Byzantine origin.

Among the mixed Byzantine and Eastern Frankish monuments of the Ottoman period, the *Pericope* of Henry II (Bible fragment) and the *Morgengabe* cross stand out, but we must not forget



**Figure 6.** *The Death of Thomas Becket, Limoges enamel, c. 1180. V&A, foto: Marie-Lan Nguyen.*



**Figure 7.** *Enamel pulp on the Preslav site, Bulgarian National Museum.*

the Relic of St. Marius, the most outstanding piece in the Essen treasury, which was unfortunately destroyed during the secularisation (Figures 8–9).

It is scientifically certain that the ring of the tyre on the Holy Crown was aligned with the cross-strap, and that the pediment, the pendilias and other parts were mounted on the hoop according to the cross-strap. It is also likely that the integral cross-strap was made in the Egbert workshop. Consequently, if it can be shown that the six definitely original enamel figures on the hoop are from the 10<sup>th</sup> century, then the greatest likelihood that the Western and Eastern enamels, created at almost the same time at the end of the 10<sup>th</sup> century, were on the same artefact is precisely in the Ottoman Empire. Although I have searched through some 2,000 enamels, relics and other artefacts from Byzantium and West of it, I have not found any artefacts, certainly made around 1,000 AD, which would have featured enamels from the two geographical areas in question at the same time, anywhere other than in the German-Roman Empire. This fact is confirmed by the similarity of the strap widths and the two Pantocrator images of the same size and appearance.

To determine the age of enamel works, it may be important to know the materials and technology used. To this end, we have set ourselves the goal of investigating whether it is even possible to identify this technique of making the recipients

from the colour side (front side) of the images.

The recognition of the recessed sandwich enamel images is not always easy, since it involves the combined use of two different recipient-making techniques. The first is the sandwich (subsection 1.2), the second is the embossing (subsection 1.4). To understand this complex technique, they are first discussed separately.

## 2.1. The sandwich recipient

A pure sandwich recipient, which consists of two sheets of gold soldered together, is often impossible to recognise. Sometimes it cannot be distinguished from engraving. The question is, how can one tell that the medallion in Figure 3 is not engraved? In this case, the fact that the top left side of the head has a damaged plate (Figure 10. and 11). is helpful. In this case, a damage on the edge of the enamelling will help us to recognise it from the colour side. At the time of the damage, the edge of the recipient is turned out and it is possible to see well into the bottom of the recipient. The fact that it is turned out is evidence that the bottom plate is much thinner than the top plate. This is confirmed by the injury shown in the image on the back. High quality images are needed to identify it, but even then it is difficult. It is also advisable to examine the edge of the plate carefully. This requires either a high-resolution 3D digital model nor a stereo microscope. In the



Figure 8. Prayer book of Henry II Pericope (Munich).



Figure 9. Henry II, detail of the Morgengabe cross, after P. Schramm.



Figure 10. Detail from Figure 3.



Figure 11. Detail from Figure 3.

case of the Holy Crown, as the crown cannot be examined, it is essential to have a 3D computer-processable model.

In the 10<sup>th</sup> and 11<sup>th</sup> centuries, the sandwich recipient was used not very often, but it was used. The fact is that until the end of the 20<sup>th</sup> century, we knew too little about the types of recipient used or even how to recognise them. In Hungary, D. Buckton was the first to draw attention to the variations of recipients when he described the „Latin crown [3]. From the 12<sup>th</sup> century onwards, when cloisonné enamels were replaced by champlevé enamels, the recesses in the copper plates were already engraved, and it was even necessary to vary the depth of the engravings for stylistic reasons. The depth of the recipient of the gold diaphragm enamel is constant. Another aspect is that engraving creates chips of variable size, which have a greater loss than cutting, and this is an important consideration for gold. It is therefore easy to understand why the sandwich technique was preferred to the kidney technique for cloisonné enamels. This idea should also be considered in the light of a more recent and thorough examination of the Reichskrone enamel plates, which are considered to have been made by engraving [4].

In summary: the upper plate is thick, the cut edges of the contour are intact, sharp and defined. From the reverse side, the lower plate is not completely smooth. This is often due to heating.

## 2.2. The sandwich recessed recipients

Recognition of the sandwich technique is much easier if the reverse side of the enamel plate is known. Note [Figure 4](#). What is immediately noticeable are the recesses of the letters. These are not visible on the reverse side, whereas where the Christ image is visible, the recesses are also visible on the reverse side. So, in similar cases, where the front and back can be examined, there is no particular difficulty in recognising them. The aim of this study is to identify features that will allow us to determine the process from the colour side of the enamel (front side).

Before demonstrating, by means of concrete examples, the processes used in different workshops, it is necessary to assess the possibilities. From an engineering point of view, the possible technological sequence is as follows:

1. the outline of the enamel image is drawn on a thin plate, the upper one. This is then cut out.

Two options are then possible:

a) 1.a. First the two plates are soldered together, and then the countersinking.

- 2.a. The lower plate and the upper plate are welded together.
- 3.a. The lower plate is recessed where the upper plate is cut out. The advantage of this procedure is that the recess will often be within a few tenths of a millimetre of the cut contour.
- 4.a. The compartment strips are then placed in the recess and soldered in place.
- 5.a. Enamelling follows in several steps.
- b) 1.b. First the recessing and then the soldering.
- 2.b. The contour is also drawn on the bottom plate.
- 3.b. The drawn contour is recessed. In this case, in most cases the upper edge of the resulting recess is larger than the cut-out of the upper plate. This may often have been intentional.
- 4.b. The compartment strips are inserted into the bottom sheet and soldered to the top plate at the same time. In this case, the compartment strips are often intentionally placed under the top plate, and often the strips are inserted under the edge of the top plate in the same direction as the top plate. In this way, the strips may be in contact with the edge of the contour.
- 4.c. An alternative to the previous solution is to solder the joints one after the other, rather than all at once. This can be done by soldering the compartment strips first and then the top plate. The result is as above, so the strip can be placed under the top plate. But it is also possible to solder the two plates together and then press the strips under the top plate.

Before we go any further, let us first examine [Figure 4](#). The most characteristic descriptive signs of the technique in question:

- 1. the relatively low gold consumption,
- 2. the recipient is cornered, forming a precise transition at the junction of the gold and glass at the face of the plate.
- 3. The „b” or „c” versions have a more closed edge at the corners and are therefore much less sensitive to contours.

The simplest technological process of the recessed sandwich process is to solder immediately after cutting the top plate and then to recess it. In other words, the recipient is formed according to procedure ‚a’ above.

The countersunk sandwich process is the result of a clear process that started with the full enamel, continued with the sandwich technique and reached the highest level of enamel art with the recessed sandwich recipient. I believe it started in

Byzantium and was carried over into the practice of the Egbert workshop. Now let us look again at **Figure 4**. What stands out is the nimbus of Christ, and within it the cross belonging to the nimbus. The two horizontal cross stems belong to the upper plate, but the vertical stem is separate, separated from the upper plate.

So, if you look at the back of the plate, you can see that the nimbus of Christ is completely recessed, even where the cross-bars are.

This means that they were recessed before the two plates were welded together. This procedure offers several possibilities. If the recessing is done before the two plates are welded together, it is possible to extend the recessing beyond the contour. The reverse side of **Figure 13** shows that the sandwich design has been made with the bottom plate smaller than the face plate. This also occurs so that even less gold is needed. The point, however, is that Peter's right hand is much more graceful than it appears on the reverse.

It follows that a wider recess than that shown in the enamelled image was intentionally used. But further special solutions were also possible, namely to allow the partitions to reach the edge of the cut-out contour without obstruction, and even to intentionally push it underneath. In the case of letter designs, such as the letters O, P, A, etc., it was necessary to replace the part that had fallen out, which, when the partitions were soldered, were also inserted. Letters were not usually countersunk, but they were often not countersunk for staves, cross stems, spears, etc., which were outside the figure. In these cases, the enamel layer is of small thickness and therefore the enamel has often fallen out as shown in **Figure 13**.

In **Figure 12** are some examples from the Trier-Essen workshop to illustrate this procedure. The noteworthy specialities are shown with arrows. All of the examples shown are from the Trier-Essen workshop and are all from before 1000.

### 3. Recognising the sandwich technique from the colour side

A way to create a recess in a thin plate other than a sandwich technique is to create a recess in it by embossing: **Figure 14**. The recessing by embossing involves the sheet hardening at the point of plastic deformation, and the resulting near-vertical recess wall supporting the part of the sheet that has not been embossed. Therefore, when later pressed from the face of the enamel picture, as on a decorative book cover, the con-

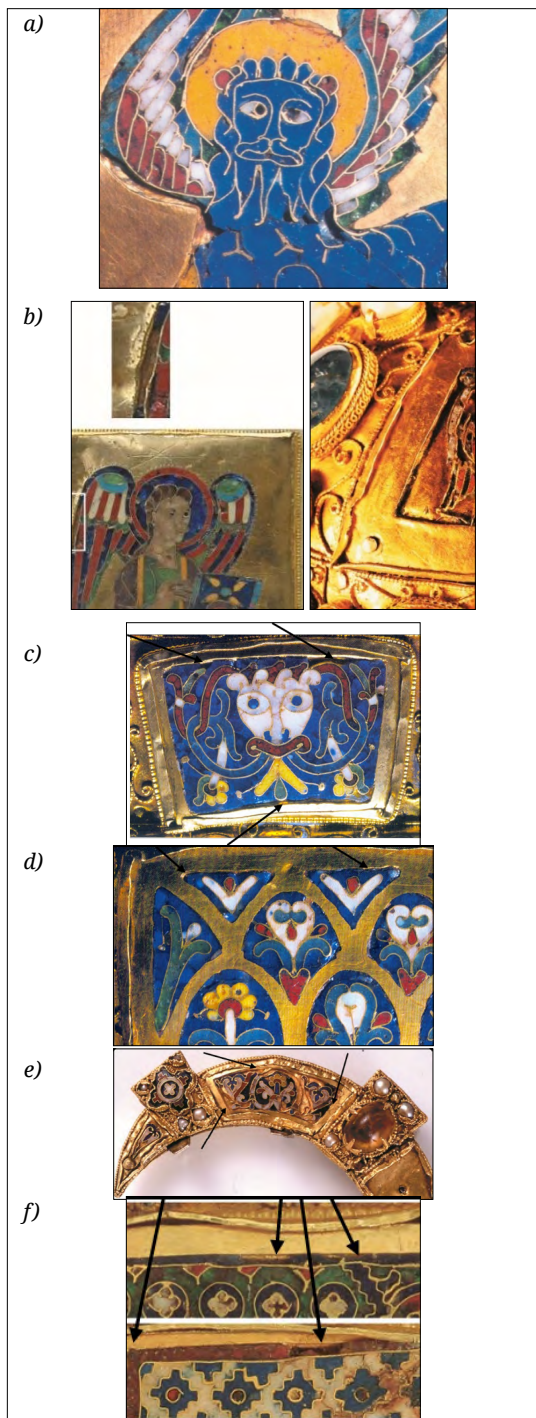


**Figure 12.** a) Cross with the large countersunk melts, Dom Essen; b) Peter's staff, Dom Limburg; c) Egbert shrine, Dom Trier; d) Cross nail reliquary, Dom Essen; e) Theophanu cross, Dom Essen; f) Chris nimbus, Dom Essen; g) Images of the apostles from the Holy Crown.

tour is accentuated. The features that emerge from the colour side (front side) in the case of simple recessing are as follows.

- The edge of the outline, which is visible from the colour side, is rounded, smooth and blunt along its entire length. This is unavoidable, but is particularly noticeable on thin gold plates. One can assume that for the more demanding enamel designs, this was precisely the reason for choosing the more complex sandwich construction. In the latter case, the transition between enamel and gold is much more perfect.
- If this enamel plate has been subjected to pressure from the colour side, then, as in the case of the image in **Figure 14**, a pronounced bend is visible from the colour side.

Colour-side characteristics of recessed sandwich enamel plates:

1. The top plate had to be cut out where the enamel was placed. The cut is clearly distinguishable from the rounded edge at a higher resolution. The edge is sharp. The cut was usually made with a sharp tool.
2. In this case, the cutting edge is left with burrs, material that is often applied to the enamel surface by post-grinding: **Figures 15 c.** and **e.**
3. The cutting out of the letters, because of their size and the absence of a tool specially designed for this operation, is rather irregular in contour: **Figure 15 b.**
4. If the upper plate is damaged during cutting, the recipient is enlarged there **Figure 15 k.**
5. In the case where the enamel and often the diaphragm go under the top plate, the top plate and diaphragm may also fuse together during soldering; creating thickening and special shapes that are unique to the recessed sandwich construction **Figure 16. h.** and **Figure 17. h.** or **Figure 4.**
6. The diaphragm wall must not go under the top plate if the recessing has been made after the two plates have been welded together. Therefore, this technique can only be detected if enamel has fallen out at the already thin edges. In this case, it is notable that the beginning of the sinking of the lower plate becomes visible below the thickness of the upper plate: **Figures 12. a–g.**
7. Often the upper plate is damaged and peeling occurs. See under details **Figures 15. c; f; g; i; j.**
8. It is interesting to note that the technique of the recessed sandwich has been known to almost all enamel experts since the last third



**Figure 13.** Enamelled image of St Peter, MET.



**Figure 14.** Enamelled image of St Nicholas, MET.

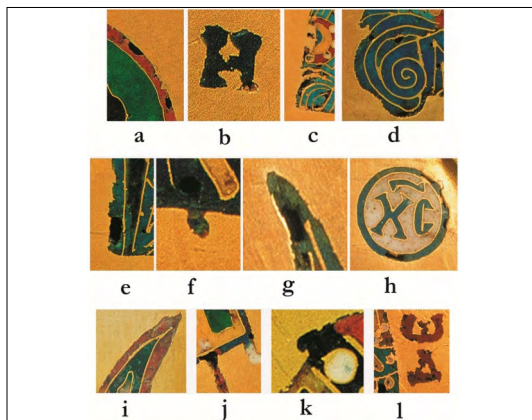


**Figure 15.** Recognising the sandwich technique from the colour of the Holy Crown enamel images.

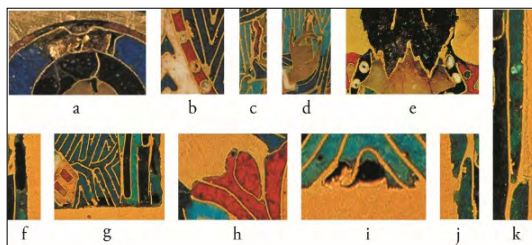


**Figure 16.** Recognising the sandwich technique from the colour of the Holy Crown enamel images.

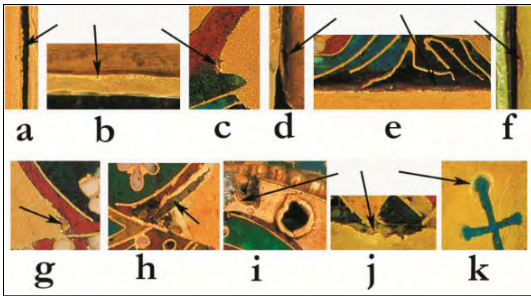


**Figure 17.** *Recognising the sandwich technique from the colour sides of the Holy Crown enamel images.*



**Figure 18.** *Recognising the sandwich technique from the colour side, Bibliotheca Marciana, Venice.*

of the 20<sup>th</sup> century, but unfortunately it is ignored in Hungary. My own observation is that the Byzantine enamel workshops were characterised by the technique of recessing the plates first and then soldering them together. I detect the same thing on the lower part of the Holy Crown. As an example, here are some Byzantine enamel plates of the Bibliotheca Marciana book cover in Venice: (Figure 18).

The features described above are also clearly visible in Byzantine enamel paintings from the 10<sup>th</sup> century. I have marked them with arrows.

In the case of the enamel medallions in the Cathedral of San Marco, it is noticeable that the enamel wall is smeared in many places on the enamel. Typically, this is very noticeable when there are defects or air bubbles left in the enamel.

#### **4. Recognise the sandwich technique if both sides of the enamel picture are known**

Recognising the sandwiching from the side is not always possible. If the enamel is intact and the edge is covered, the sandwich technique can be recognised from the colour side, but the countersinking can only be determined from indirect signs. Such a sign could be, for example, the recognition of the edge of the letters. As you know, the unevenness of the edges of the letters is characteristic of soft and thin plates. Thick plate usually provides better edges. Backside characteristics: not all the colour-side enamel elements appear to be bulged on the backside. Think here of the letters or parts that fall outside the body, such as the stick, cross, spear, etc.

It is also advisable to use a computer. Take a photograph of the front and the undersides. In the computer, we make a vertical mirror image of the back and superimpose the colour side and the mirror image. We align them exactly according to the edges. If the recessed contour on the back is larger than the enamelled surface then this is obviously a sandwich technique, and the one I have seen above in the Greek enamelling technique, and in addition it is of better quality. If the recessed contour is everywhere less than or equal to the size of the enamel, then you must first ascertain from the colour side whether you are dealing with the sandwich or direct recessing technique, as per the properties listed above. If we are satisfied that it is, then it was probably made according to technique 3.2.a, i.e. the sandwich plate pair was created first and then countersunk.



**Figure 19.** Recognition of the technique from the colour: St. George and St. Cosmas, San Marco, Venice

## 5. A summary of the recessed sandwich technique

The technique is most often clearly recognisable from the colour side of the enamel picture. This technique was used around the first millennium in Western Europe and also in Byzantium for gold recipients. There is a difference between the processes used north of the Alps and those used in Byzantium, so it can be an important reference for the location and time when the enamel was made. Thus, the enamel pictures on the Holy Crown could not have been made at any other time than this period. After this period, the production of gold enamel stopped north of the Alps, while in Byzantium they returned to full enamel or simple recessing and switched to the use of opaline glass. There was no other way of soldering the two plates together than the so-called reaction soldering, which had been forgotten for centuries and which allowed for repeated soldering in several steps. It is thus possible that the figural enamel images of the crown could have been made by a later forgery.

## References

- [1] N. Oikonomides: *La couronne dite de Constantin Monomaque, in Travaux et Mémoires*. Centre de Recherche d' Histoire et Civilisation de Byzance, 12, 1994, 241–262.
- [2] A. Bosselmann-Ruichbie: *Byzantinischer Schmuck des 9. bis frühen 13. Jahrhunderts*. Reichert, Wiesbaden, 2011, 88.
- [3] Buckton David: *Vorläufige Ergebnisse einer optischen Untersuchung des Emails der Krone*. In Ferenc Fülep – Éva Kovács – Lovag Zsuzsa: *Insignia Regni Hungarie. Studien zur Machtsymbolik des mittelalterlichen Ungarn*. MNM, Budapest, 1983. 129–144.
- [4] S. E. Eckenfels-Kunst: *Goldemails*. Pro Business, Berlin, 2008, 135.



# Investigation of the Effect of Layer Thickness of Adhesive Material on Metal to Composite Joints

Levente BORHY,<sup>1,a</sup> Gábor SZEBÉNYI<sup>1,2,b</sup>

<sup>1</sup> Department of Materials Science and Engineering, Faculty of Mechanical Engineering, Budapest University of Technology and Economics, Budapest, Hungary

<sup>2</sup> MTA-BME Lendület Lightweight Polymer Composites Research Group, Budapest, Hungary

<sup>a</sup> [borhy.levente@edu.bme.hu](mailto:borhy.levente@edu.bme.hu)

<sup>b</sup> [szebenyi@pt.bme.hu](mailto:szebenyi@pt.bme.hu)

---

## Abstract

In this research, fiberglass-reinforced epoxy composite plates and additively manufactured titanium inserts are adhesively bonded. The samples are investigated by tensile and shear bond test methods. After the mechanical tests, topographical evaluations are conducted over the failure surface areas. A 3D profiling method for the inspection of bonded joints has been developed to quantify and compare failure types. It was found that varying the thickness of the adhesive has a significant effect on the load-carrying capacity of the structure under normal direction loading, whereas under shear loading the effect is modest. The research methodology used allows for the qualification and comparison of further bonded structures.

**Keywords:** adhesive bonding, metal-composite joint, tensile bond test, shear bond test, topographical examination.

---

## 1. Introduction

The significance of adhesives, used to manufacture load-bearing structures is rapidly increasing in recent years in modern industries (such as in the automotive, construction and E&E industries [1]).

Structural adhesives are used for applications, where adherends may be exposed to large stresses. Establishing joints with structural adhesives are favorable in multi-material systems (where materials with dissimilar chemical structure are joined together), thanks to potential advantages such as flexibility in design, simple fabrication, and exceptional strength-to-weight ratio. On the other hand, the load-bearing capacity of adhesively bonded structures is usually limited and several parameters play important roles that can influence the lifespan of these products [2].

Therefore, it is necessary to examine the effect of different parameters in the fabrication of adhesively bonded structures, such as the adhesive layer thickness.

### 1.1. Failure modes of adhesive bonds

Adhesive bonding is a phenomenon where the connection between two dissimilar structures is established with an adhesive in a way that the transmission of load occurs between the two bodies until the failure of the bond. An adhesive material, when applied on the surfaces of structures (Figure 1) connects them as a result of the adhesive bonding process [3].

There are three different failure modes that need to be considered when designing and investigating adhesive joints. In the case of adhesive failure (Figure 2a), separation occurs between the adhesive and one of the adherends. In the case of cohesive failure, subsequent failure can occur in the adhesive layer while all the adherends' surfaces remain covered with the adhesive material (Figure 2b), or failure can occur in one of the adherends further away from the bond (Figure 2c) [4, 5]. In many cases, the failure of the bonded joint occurs as a combination (partly adhesive and partly cohesive) of these failure modes [6].



**Figure 1.** Typical structure of an adhesive bond.

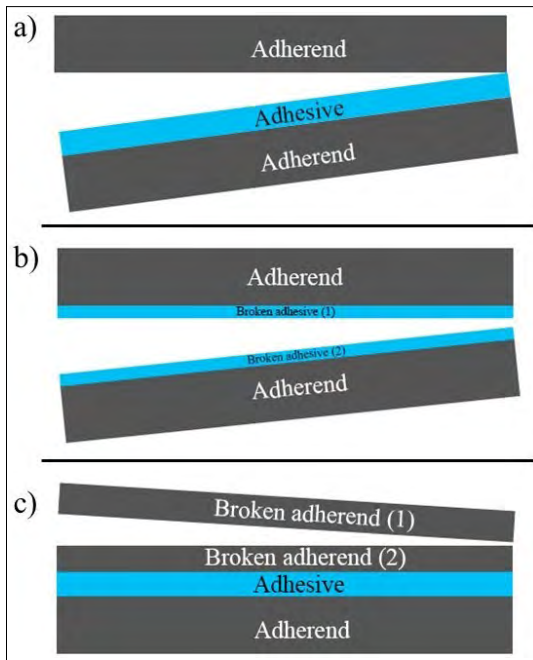


**Figure 2.** Typical failure modes of adhesive bonds: (a) adhesive failure, (b) cohesive failure in the adhesive layer, (c) cohesive failure in one of the adherends.

## 1.2. Test method

One of the most common methods for evaluating the strength of an adhesively bonded joint is to perform mechanical tests until failure, such as tensile bond strength, and shear bond strength tests [7]. These measurements are suitable to examine the performance and load-bearing capacity of adhesively bonded structures [8, 9].

The quality of adhesive joints cannot be determined by destructive tests alone, there are several properties of the structure that can only be revealed by topographical examinations. This is because, in many cases, the combination of basic failure modes occurs. The ratio of adhesive and cohesive failure areas is an indicator of the quality of the adhesive joint and the whole bonded structure [10, 11].

In this research, normal and shear bond tests were carried out on adhesively bonded multi-

material hybrid structures, and the failure surface areas were subjected to visual surface topography. The manufacturer has specified the optimum adhesive thickness (0.05 - 0.1 mm) for shear-loaded joints only, so our aim is to determine its suitability for normal directional loading [12].

## 2. Materials and methods

### 2.1. Materials

For the fabrication of composite plates EPIKOTETM Resin MGS LR 235 with EPIKURETM MGS LH 235 two-component (100:35) medium viscosity casting, laminating, and resin system was used as matrix material, with bidirectionally woven glass fiber sheets as reinforcement.

EOS Titanium Ti64 powder (Ti6Al4V), with a grain size of 20  $\mu\text{m}$  was used in the additive manufacturing process of the titanium inserts.

For the adhesive bonding, Araldite™ 2011 two-component (100:80) epoxy adhesive by Huntsman Ltd. Corporation was used.

### 2.2. Preparation of specimens

#### 2.2.1. Fabrication of the composite plates

The composite plates in the research were manufactured by vacuum-infusion method. In each case, 4 sheets of glass fiber ([0,90]) with a size corresponding to the chosen plate size were placed on top of each other. Particular attention was paid to the surface quality and the uniformity of the structure of the whole plate in order to ensure the repeatability of measurements. Following the crosslinking of the composite, the edges were removed, and 80×80 mm square-shaped pieces were cut from the plates.

#### 2.2.2. Additive manufacturing of the titanium inserts

The titanium inserts were additively manufactured by selective laser melting (SLM) technology using an EOS M100 metal 3D printer. 6 titanium inserts with a base diameter of 25 mm and a height of 14 mm were additively manufactured uniformly and with the same process parameter values.

#### 2.2.3. Establishing the adhesive bonds

For the mechanical and topographical tests, samples were created with five different adhesive layer thickness values. To set the thickness of the glue, metal wires with specified diameter values were distributed between the composite plates and the titanium inserts.

In the first group, as a control group, no metal wire was used. In the following groups metal wires with a diameter of 0.18 mm, 0.23 mm, 0.43 mm, and 1.30 mm were used consequently.

The steps of creating the bonded structure in all cases were similar (Figure 3). All samples were left to crosslink for at least 24 hours in room temperature.

### 2.3. Methods of measurement

The load-bearing capacity and failure topography of the fabricated samples were evaluated with mechanical and macrostructural investigations. Firstly, after the crosslinking of the adhesive, the specimens were subjected to tensile-, or shear bond tests. For these tests, the same 6 titanium inserts were used in each case, and at the end of each test, the adhesive was burnt off their surfaces at 550 °C so that they could be reused. After the destructive tests, the fractured area of each specimen was examined by a surface 3D optical profilometer.

#### 2.3.1. Tensile bond tests

The tensile bond tests were performed with a Zwick Z005 universal testing machine. The machine was equipped with a  $\pm 5$  kN measuring cell. The measurements were implemented with a preload speed of 2 mm/min and a test speed (speed of the crosshead) of 10 mm/min. To carry out the measurement, a special clamping device had to be used in the setup (Figure 4).

#### 2.3.2. Shear bond tests

The shear bond tests were implemented with a Zwick Z250 universal material testing machine. The device was equipped with a  $\pm 20$  kN measuring cell. The same measurement speeds were applied as in the case of the tensile bond tests. In this case, a different clamping tool was necessary in order to perform the tests (Figure 5).

#### 2.3.3. Surface topography visualization

The visual investigation was carried out by a Keyence VR-5200 optical microscope. During the examination, a low magnification (12 $\times$ ) was used with a wide field of vision. The measurement accuracy of the device is  $\pm 2.5$   $\mu\text{m}$ , and it is equipped with a 4-megapixel monochrome CMOS image-capturing system. After setting the base layer on each specimen, the ratio between the area of adhesive and cohesive failure was calculated using the program of the measuring device. During evaluation, the modes of failure were determined by the height differences on the surface area.

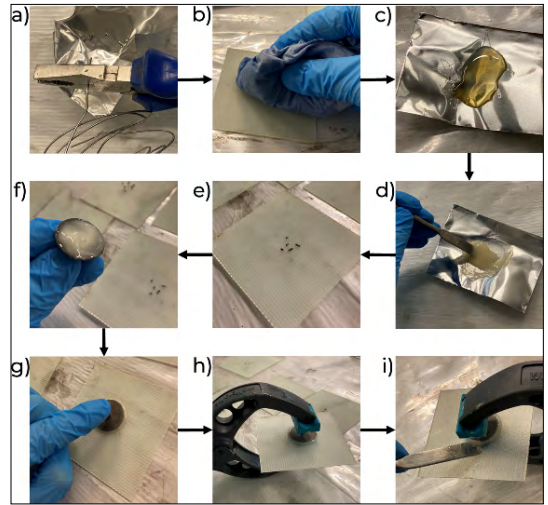


**Figure 3.** Steps of establishing the adhesive bonds: (a) cutting wires, (b) cleaning the surface with acetone, (c) proportioning the components of the adhesive, (d) mixing the components, (e) distributing the wires, (f) spreading the adhesive evenly, (g) placing the insert on top of the plate, (h) compression, (i) removing residual adhesive.

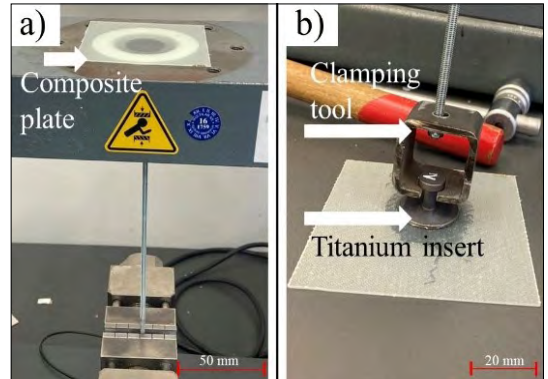


**Figure 4.** Tensile bond test: (a) special clamping tool, (b) test setup.

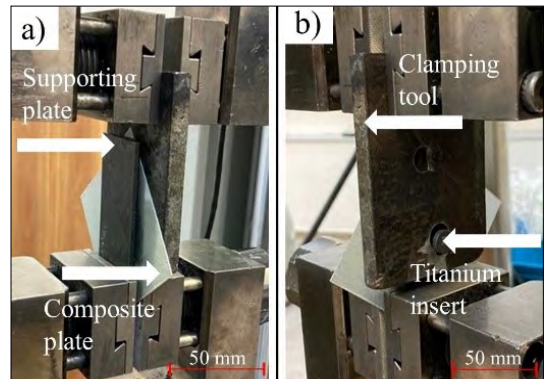


**Figure 5.** Shear bond test: (a) backside, (b) front side.

### 3. Results

Tensile tests were performed on all five previously mentioned adhesive thickness groups. There were 5 samples in the first group (the control group) and 6 in all others, summing up a total amount of 29 samples.

Shear tests were performed on the first and the fifth group (in which samples were manufactured using 1.30 mm thick wire pieces). Both groups consisted of 6 samples, but one sample had to be excluded from the latter mentioned group due to errors during sample preparation, resulting in a total of 11 samples.

Surface topography was applied to all 40 samples. From the obtained data and the help of the analysis software, the ratio of adhesive (Figure 6) and cohesive failure (Figure 7) area was determined for each sample.

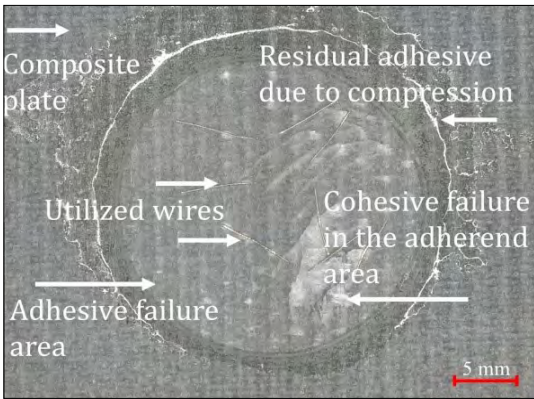


Figure 6. Surface topography image of a sample with adhesive failure

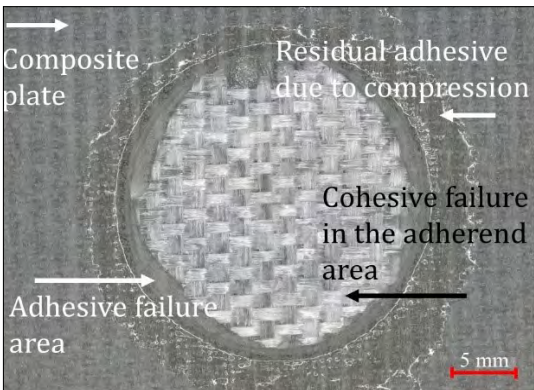


Figure 7. Surface topography image of a sample with mainly cohesive failure

### 3.1. Results of the tensile bond tests

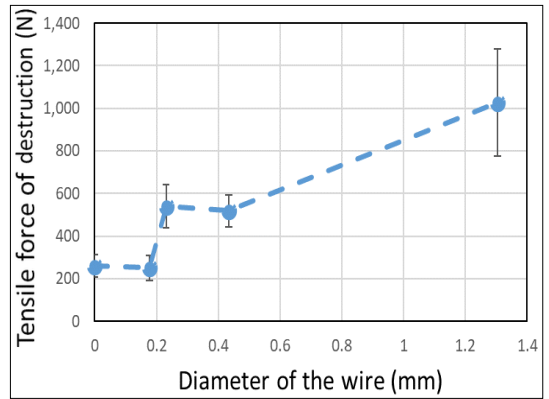
The result of the tests can be observed on the depicted diagrams below, where the tensile breaking force as a function of the diameter of the applied wire (and thus, adhesive thickness) is displayed (Figure 8).

After the tensile tests, the topographical tests were performed on the same samples. The results are represented below, where the percentage of cohesive failure as a function of wire thickness is depicted (Figure 9).

### 3.2. Results of the shear bond tests

Figure 10 illustrates the outcome of the shear bond tests, with the wire diameter on the x-axis, and the shear breaking force on the y-axis.

Similarly to the tensile tests, the topographical investigation was carried out for all samples after the shear bond tests (Figure 11).



8. ábra. Results of the tensile bond tests

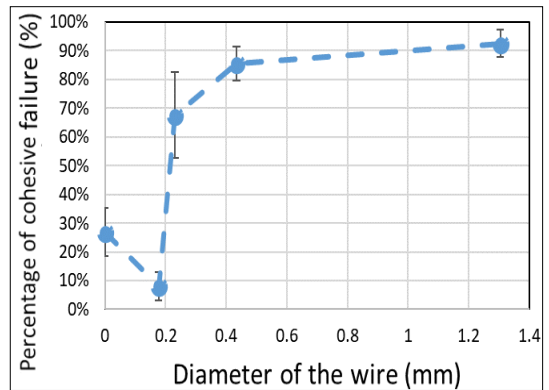
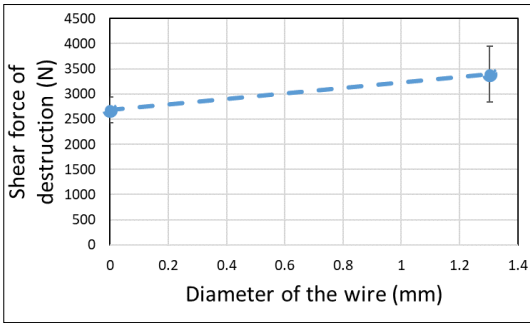
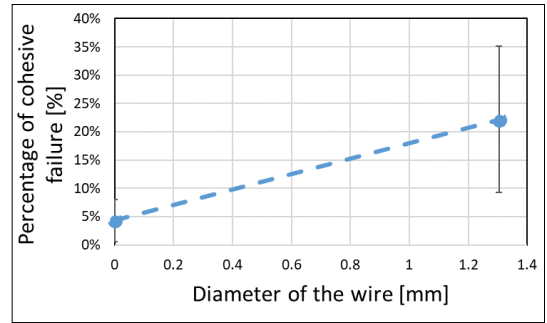


Figure 9. Topographical investigation results of the tensile bond tests.



**Figure 10.** Results of the shear bond tests



**Figure 11.** Topographical investigation results of the shear bond tests.

#### 4. Conclusions

A total of 40 specimens were made and examined by mechanical and topographical investigation methods successfully in this research. The outcome provides a basis for further comparative examinations of adhesively bonded structures. At the Department of Polymer Engineering of the Budapest University of Technology and Economics, we developed a 3D profiling method for the analysis of adhesive-bonded joints, which allows for the quantification and comparison of failure types, thus facilitating further research in this field.

Changing the adhesive layer thickness has a significant effect on the tensile breaking force. It can be stated that the load direction strongly influences the load capacity of the structure and that the optimal layer thickness is different in each direction.

It can be observed that mainly shear loads should affect adhesively bonded multi-material hybrid structures, since these can withstand remarkably greater forces under shear load compared to tensile load.

Compared to the tensile tests, the adhesive layer thickness did not affect the load-bearing capacity of the bond as substantially as in the case of shear stress.

It is shown that the optimal adhesive layer thickness recommended by the manufacturer (0.05–0.1 mm) is not adequate for normal directional loading, by increasing the layer thickness we were able to increase the bond strength by a factor of 4–5 times.

The results from the mechanical and the topographical investigations show the same tendency, and they are comparable. The percentage of cohesive failure in the fracture area of those samples that withstood greater loads was consistently

higher, which may be due to a larger proportion of solid bonding material at the bonding surface.

Considering that the structures we examined are subject to complex loading modes rather than pure shear, which would be favorable from a bonding perspective, it is of great significance to investigate different directional loads. Our research can serve as the basis for further studies in this field. By employing the measurement methodology utilized here, it is possible to optimize the resistance of bonded structures against complex loading.

In summary, it can be stated that this research can provide a starting point for further perfecting adhesively bonded structures and has demonstrated the importance of adhesive layer thickness in the manufacture of complex bonded structures.

#### Acknowledgements

The publication of the work reported herein has been supported by the NTP-SZKOLL-22-0080 National Talent Program of the Ministry of human Capacities. The research reported in this paper and carried out at BME has been supported by the NRDI Fund (TkP2022 IEs, Grant No. BME-IE-NAT; TkP2022 NC, Grant No. BME-NCS) based on the charter of bolster issued by the NRDI Office under the auspices of the Ministry for Innovation and Technology. The research was supported by the Hungarian National Research, Development, and Innovation Office (NKFIH) by projects OTKA FK 142540, 2019-1.1.1-PIA-CI-KFI-2019-00139, 2022-2.1.1-NL-2022-00012.

#### References

- [1] Adams R. D.: *Adhesive bonding: science, technology and applications*. 2. ed. Woodhead Publishing, Cambridge, 2021. 3–4.
- [2] Pethrick R. A.: *Design and ageing of adhesives for structural adhesive bonding-A review*. Proc. Inst.

- Mech. Eng. Part L J. Mater. Des. Appl., 229. (2015) 349–379.  
<https://doi.org/10.1177/1464420714522981>.
- [3] Baldan A.: *Adhesion phenomena in bonded joints*. Int. J. Adhes. Adhes., 38. (2012) 95–116.  
<https://doi.org/10.1016/j.ijadhadh.2012.04.007>.
- [4] Banea M. D., Da Silva L. F. M., Campilho R. D. S. G.: *The effect of adhesive thickness on the mechanical behavior of a structural polyurethane adhesive*. J. Adhes., 91. (2014) 331–346.  
<https://doi.org/10.1080/00218464.2014.903802>.
- [5] Seong M. S., Kim T. H., Nguyen K. H., Kweon J. H., Choi J. H.: *A parametric study on the failure of bonded single-lap joints of carbon composite and aluminum*. Compos. Struct., 86. (2008) 135–145.  
<https://doi.org/10.1016/j.compstruct.2008.03.026>.
- [6] Davis M. J., McGregor A.: *Assessing adhesive bond failures: mixed-mode bond failures explained*. ISASI Aust. Saf. Semin. Canberra, (2010) 1–13.
- [7] Valenza A., Fiore V., Fratini L.: *Mechanical behaviour and failure modes of metal to composite adhesive joints for nautical applications*. Int. J. Adv. Manuf. Technol., 53. (2011) 593–600.  
<https://doi.org/10.1007/s00170-010-2866-1>.
- [8] Banea M. D., Da Silva L. F. M.: *The effect of temperature on the mechanical properties of adhesives for the automotive industry*. Proc. Inst. Mech. Eng. Part. L. J. Mater. Des. Appl., 224. (2010) 51–62.  
<https://doi.org/10.1243/14644207JMDA283>.
- [9] Li J., Yan Y., Zhang T., Liang Z.: *Experimental study of adhesively bonded CFRP joints subjected to tensile loads*. Int. J. Adhes. Adhes., 57. (2015) 95–104.  
<https://doi.org/10.1016/j.ijadhadh.2014.11.001>.
- [10] Marshall S. J., Bayne S. C., Baier R., Tomsia A. P., Marshall G. W.: *A review of adhesion science*. Dent. Mater., 26. (2010) 11–16.  
<https://doi.org/10.1016/j.dental.2009.11.157>.
- [11] Saraç İ., Adin H., Temiz Ş.: *Experimental determination of the static and fatigue strength of the adhesive joints bonded by epoxy adhesive including different particles*. Compos. Part. B. Eng., 155. (2018) 92–103.  
<https://doi.org/10.1016/j.compositesb.2018.08.006>.
- [12] Huntsman Advanced Materials GmbH Switzerland, Araldite® 2011 *Structural Adhesives technical data sheet*. 2014. <https://docs.rs-online.com/afb0/0900766b81331047.pdf> (letöltve: 2023. július 4.)

# Failure Analysis of a Damaged Turbocharger

János DOBRÁNSZKY

Hungarian Research Network, HUN-RE-BME Research Group for Composite Science and Technology,  
Budapest, Hungary, Dobranszky.Janos@eik.bme.hu

## Abstract

Failure analysis, carried out in order to explore the causes of the failure of equipment, is one of the most complex types of material testing work. It is not only necessary to know a wide range of material testing procedures, but also to have sufficient experience in performing a significant part of them and evaluating the test results. As an example of this, the article describes the investigation of the cause of failure of a car engine component that became damaged during normal service. The examinations include various methods of optical microscopy, scanning electron microscopy, EDS analysis and fractography. From the results of the failure analysis, it can be concluded that the root cause of the failure was, most probably, abnormal wear of some components, wear that can be traced back to small manufacturing inaccuracies.

**Keywords:** failure analysis, optical microscopy, scanning electron microscopy, wear.

## 1. The damaged equipment

The internal components of the turbocharger tested for damage are shown in **Figure 1**. The assembly drawing of the assemblies is shown in **Figure 2**, with the names of the components. The purpose of the study was to determine the forms of damage and possible causes. According to the rules of damage analysis [1, 2, 3], the components were examined with optical and scanning electron microscopes, and the composition was also analysed with EDS analysis.



**Figure 1.** Parts of the internal assembly of the failed turbocharger; the total length of the turbine + shaft assembly is 120 mm.

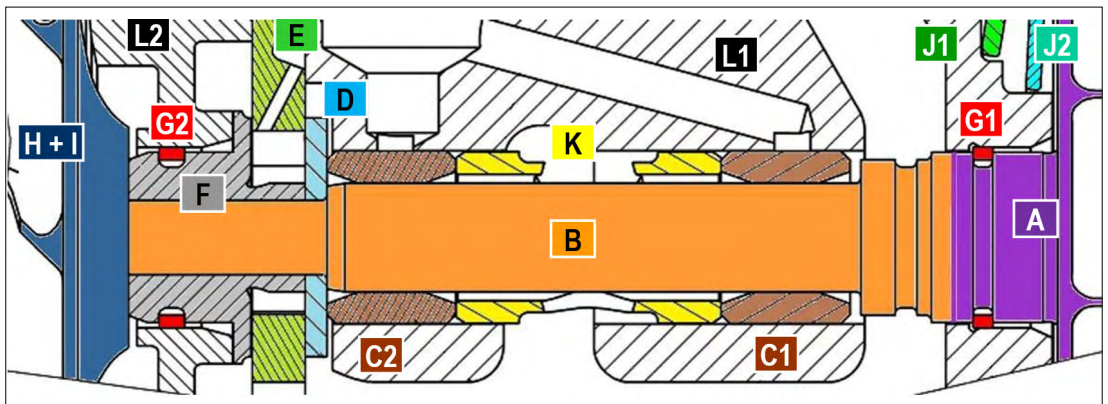


**Figure 2.** Internal assemblies the turbocharger: A = turbine wheel, B = shaft, C = bearing, D = thrust ring, E = axial bearing, F = sealing bush, G = labyrinth ring, H = back plate, I = compressor wheel, J = heat shield plate (belleveille spring), K = journal bearing spacer, L = housing.

Based on **Figure 2** it is easy to see that it is an extremely complex device consisting of many components, the operating stress of which should be known as it can operate at tens of thousands of revolutions per minute. **Figure 3** shows the assembled internal assembly; the damage locations and modes detected by visual inspection are marked in the figure.

From the wear shown in **Figure 3** it can be concluded that the axis of rotation of the moving parts of the turbine has tilted, and because of this, the moving parts have come into contact with the fixed or stationary parts. In the case of possible wear, the possibility of contact with opposite surfaces of the housing casting must be mentioned. The customer of the damage analysis did not hand over this component for testing, so there is no data on it. Nevertheless, it is not at all excluded that the parts that are clearly visible in **Figure 2** close to some of the surfaces of the housing have experienced friction and wear.

## 2. Examination of turbine and shaft

The material of the turbine wheel is heat-resisting nickel alloy: Ni-12.5Cr-6Al-4.5Mo-2Nb-Fe-Ti, and the material of the shaft is 1.5Cr-0.5Mo alloyed heat-resistant steel. The friction-welded turbine + shaft assembly can be seen in **Figures 4, 5**

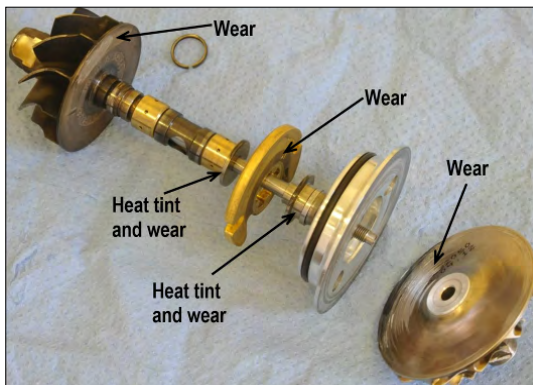


**Figure 3.** The internal fittings of the turbocharger are loosely assembled.



**Figure 4.** The welded turbine and shaft.

and **6** which show signs of wear on the faceplate and shaft of the turbine

The damage to the turbine wheel shown in **Figure 5** on the blade holder base plate is conspicuous. The wear is only around the circumference of the circular base plate. It extends to a third, but it is strong there. Since the surface is almost completely clean, it can be assumed that the turbocharger was not in operation or only for a very short time after the breakdown leading to wear. Another element of the wear process was presumably the opposite surface of the heat shield and/or the turbine housing.

Shaft wear is indicated by the polishing of the surface under the bearing bushings. Diameter reduction cannot be measured with a measuring device with micrometre accuracy, but surface wear can be easily detected.

## 3. Inspection of bearing bushings

A burr can be seen on the front of the cylindrical ring of the bearing bushings (**Figure 7**).

The formation of grey spots on the brass material is noticeable both on the outer and inner surface (**Figure 8**). According to the EDS analysis, the spots are material smears, the material of which is mainly Fe, Cr, Ni, in some places Sn and Pb. A change of shape indicating a strong heating of



**Figure 5.** Wear traces on the turbine wheel.



**Figure 6.** Wear marks on the shaft.

the edge can be seen in the holes, and in some cases partial blockage.

The piece of material shown in **Figure 9** was attached to the inner surface of one bearing. Based on the EDS analysis, it could be identified as austenitic steel: Fe-1.7Al-2.7Si-1.9Mo-16.9Cr-2.5Mn-9.4Ni.

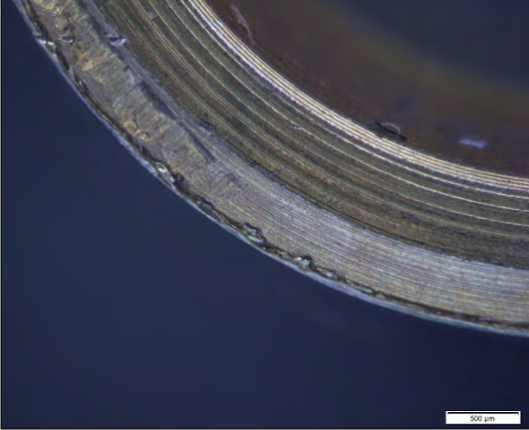


**Figure 7.** Traces of burr formation on the bearing.

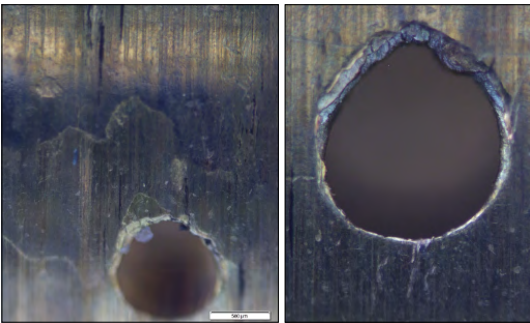


**Figure 8.** Wear of the bore rim on the bearing.

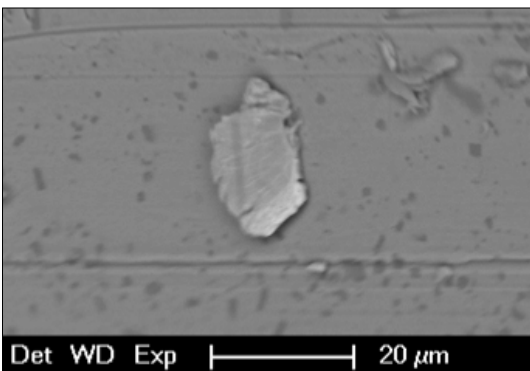


**Figure 9.** A chip stuck to the bearing surface.



**Figure 10.** Wear marks on the axial bearing.

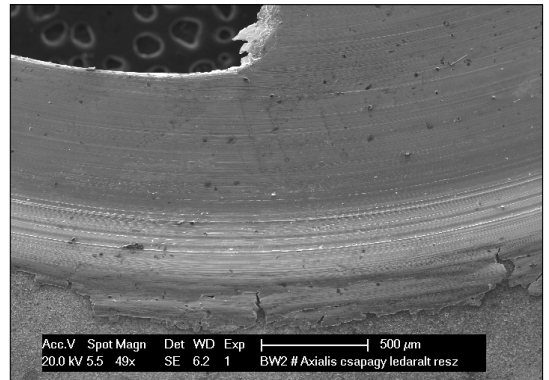


**Figure 11.** Wear marks on the support bearing.

#### 4. Examination of the axial bearing

The wear marks on the support bearing (**Figure 10**) can be seen in **Figure 11**. Rough wear grooves formed on the surface, squeezing the upper material layer out of the contact surface as a burr.

#### 5. Inspection of the compressor wheel

The material of the compressor wheel shown in **Figure 12**: Al-2Mg-2Ag-1Fe-2Ni-3Cu-0.1Zn-0.2Ti-0.35Si-0.1Mn; coating material: nickel alloy with ~10% phosphorous. The most typical mechanism for the wear process is the cracking and flaking of the brittle coating

#### 6. Assessment of damage analysis

The main findings of the evaluation of the nature of the damage to the turbocharger are as follows:



**Figure 12.** Wear marks on the compressor wheel.

Foreign substances have been placed on the surface of the components; they are the product of organic contamination and wear of other components. No material connection between foreign materials and the wear of any of the parts can be demonstrated.

There is such an amount of material missing from the various components due to wear and

tear that this alone makes general and heavy wear the essence of the damage process.

We could not determine the amount of material missing from the various parts, as we do not know the exact weight of the parts before installation. It would be advisable to pay attention to this in the analysis of damage processes.

Damage to the turbine-side labyrinth ring groove and labyrinth ring (G1 and G2 in [Figure 2](#)) is usually key, but in this case the wear on the parts in question was not significant.

On the large-diameter components – turbine wheel, compressor wheel – the wear occurred on their surfaces far from the axis of rotation, namely not circularly.

Consequently, the wear-causing displacement spread to the entire axle assembly. The responsibility of the tested components for this development could not be established. For this reason, the only hypothesis that seems to be correct is that the surfaces of the cast housing began to wear intensively, and these surfaces are meant to ensure the uniaxiality of the shaft assembly. Additionally, the crumbs we identified on some of the filter inserts indicate the wear of the housing.

## References

- [1] Zima A., Greuter E.: *Engine Failure Analysis - Internal Combustion Engine Failures and Their Causes*. SAE International, 2012.
- [2] Brooks C. R., Choudhury A.: *Failure Analysis of Engineering Materials*. McGraw-Hill, 2001.
- [3] Baratto G., Guérin J. J., Mongis J., Tournier C., Vieu A.: *Analyse morphologique des défaillances d'organes de machines*. CETIM, 2005.



# Medical Device Design to Support Hand Movement

Boglárka Fanni EGRSZEGI

*Budapest University of Technology and Economics, Faculty of Mechanical Engineering, Budapest, Hungary*  
*egerszegibogi@gmail.com*

---

## Abstract

After accidents, neurological disorders, and cerebrovascular diseases, patients must learn to perform their daily tasks with their new, changed life situation, in which they can be helped by various ergotherapy aids. In the course of my work, I aimed to develop an aid that not only tries to correct the errors of products found on the market, but also a multifunctional aid that serves several types of disability, and which can be worn by individuals with upper limb involvement and living with locomotor diseases/locomotor disorders/changes. An important aspect in the design of the aid was, among other things, that it can be used in any environment and during any activity and that it should be comfortable to wear.

**Keywords:** *special design, 3D modelling, product design, ergotherapy.*

---

## 1. Introduction

In some countries ergotherapy and ergotherapist terms are used instead of occupational therapy and occupational therapist. The hieroglyphic sign of life (𓅓) from ancient Egyptian writing was chosen as the symbol of the profession [1].

Occupational therapy helps to treat hand dysfunction caused by rheumatic diseases. The main anatomical area of therapeutic interventions for the hand is the wrist and finger joints, and the task is the postoperative or conservative treatment of these parts of the body. The aim of occupational therapy is to maintain joint mobility, strengthen muscles, correct deformities, relieve pain or treat inflammation [2].

In Hungary, the first publication on occupational therapy was published almost 80 years ago [3], and the most recent just a few months ago [4]. Szilvia Mogánné Tölgyesy gives a detailed account of the development of the field in Hungary [5], and describes treatments specifically used to improve mobility in a study with her co-author Adél Bartos [6].

*Rehabilitation* has been an independent Hungarian-language journal of the profession for more than 30 years.

## 2. Selection of topics, definition of users

I have chosen to design a medical device that facilitates the daily activities of people with upper limb musculoskeletal disorders or neurological disorders. My aim is that the medical device I design will help users to live their lives from the simplest tasks to the most complex ones.

In selecting the users, I have chosen people with severe disabilities who suffer from one of the musculoskeletal disorders listed below:

- hemiplegia (paralysis of one side),
- hemiparesis (weakness of the opposite side of the body),
- cerebral palsy,
- rheumatoid arthritis.

Another target group is the so-called intermittent users, who need to use certain assistive devices due to an injury or trauma, such as a broken hand.

When defining the user group, it was important to include as many groups as possible, as the main objective of the design task was to design a device that would provide a complex solution.

To determine the dimensions of a medical device of the type designed, it was not sufficient to examine the geometric characteristics of the analogues. I reviewed the relevant chapters of the PeopleSize catalogue to determine the dimen-

sions of the adult human hand, and examined the ranges of reach for specific cases. Data that were not included in the catalogue, such as wrist size determinations, were determined by a thirty sample measurement.

After evaluating the results, I also determined the mean and percentile values, broken down by gender.

### 3. Testing the standard

All products on the market are subject to different rules and standards that they must comply with. In my work, the standards to be respected were those relating to universal design, including accessibility rules.

The ISO 9999:2007 standard [7], also published in Hungarian, defines the classification of assistive devices manufactured specifically for or generally available to people with disabilities. It also includes assistive devices that require the assistance of another person for use. Currently, the most recent standard for the product I am developing is MSZ EN ISO 9999:2023 [8] which has been significantly revised in its title.

### 4. Material selection

My product has to meet a number of hygienic, mechanical and physiological criteria, of which the biocompatibility property is key. Since I have tried to cover a very wide range of disorders when identifying the user group, I have also had to take into account the diseases that may occur with the disorders, such as skin diseases in which the skin of the patient concerned becomes ulcerated and the protective function of the skin is not complete.

To meet these requirements, I chose a silicone suitable for use as a medical device as the material for the strap.

In terms of its hygienic properties, silicone is the easiest to keep clean, as it does not soak through, is water-repellent and easy to disinfect. In terms of physical characteristics, it is impact resistant, stretchable, yet soft to the touch. It is non-irritating to the skin, making it safe to wear for extended periods.

Of the two-component mouldable silicones, I chose the RTV two-component material. As I am using it for the preparation of a skin contact product, I have considered the use of a catalyst suitable only for food applications.

Among the Hungarian based manufacturers, Bondex Ltd.'s peroxide silicone product Rubosil

SR-30 meets the above criteria as it is one of the few materials that are approved by OÉTI (National Institute of Food and Nutrition). The main characteristics of the product are shown in **Table 1. [9]**.

**Table 1.** Material properties of Rubosil SR30

<b>Processing time, pot life</b>	20 min
<b>Binding, curing time</b>	30 min
<b>Hardness</b>	30±5 ShoreA
<b>Heat resistance</b>	-55–200 °C
<b>Viscosity</b>	26 500 ± 1500 m·Pas (or cP)
<b>Density</b>	1.40 g/cm <sup>3</sup>
<b>Resistance to splitting</b>	4.86 N/mm
<b>Tensile strength</b>	1.88 N/mm <sup>2</sup>
<b>Elongation at break</b>	140 %

For the Rubosil SR-30 silicone, the manufacturer recommends the Rubosil K Food catalyst, for which the manufacturer has also obtained OETI approval. To 1kg of silicone, 50 mL of catalyst is added. The most typical applications for the chosen silicone are in food and confectionery moulds. In addition, skin contact products such as toe separators and spacers and other prostheses can be made from it.

For the 3D printed parts - functional heads, staples - I used a polyamide filament: a white 3D Printer Tough Resin from the manufacturer 3D JAKE. This is a high hardness photopolymer resin that can be used with SLA printers. The composition of the material has not been made public by the factory, the choice of material being justified by previous prototyping processes. First, parts were made of docamide material using the FDM process variant of the fibre compression [10] additive manufacturing process. Due to the manufacturing process, the surface roughness of the elements is high and the spherical elements are separated from their base by tensile stress. The manufacturing method was then changed to SLA; a high hardness but inelastic resin [11].

The parts became brittle due to the choice of material, the snap-in joint suffered a permanent deformation on the third snap-in and then broke. These experiences justified the use of the modified product. The hardness and wear resistance of the parts were found to be better, and the intact

bond did not deform, despite more than twenty cycles of connection and disconnection.

## 5. Definition of the product concept

In my information gathering work, I analysed a number of competing products. I examined the strengths and weaknesses of these products in order to adapt and adapt the positive features and eliminate the negative ones to create a product proposal that would meet as many user needs as possible. After processing the information, a list of requirements was drawn up.

During the market research, I tested several holders and handles, and the idea of a silicone strap (Figures 1 and 2), with a 3D-printed base to which, on request, a detachable snap-on bandage can be attached to some multifunctional heads that help to grip specific objects and perform specific activities; e.g. holding cutlery, toothbrush, writing utensil, buttoning a button, zipping a zipper.

The plastic insert is located on the palm side of the strap, built into an increased thickness silicone pad (the so-called core) so that only the part that can be snapped in protrudes from the strap. This way, the user is not disturbed even when not in use.

I have placed anti-slip ribs on the palm side of the hand to allow the skin to come into contact with the air and reduce the amount of material used, which in turn affects the weight and price of the product.

Perforations should be made on the back of the hand to allow the skin to come into contact with the air and reduce the amount of material used, which in turn affects the weight and price of the product.

I have designed heads and straps for the product that can be used in as few but as many ways as possible, and that can fit in a pocket or a small bag. I wanted to design a fashionable, inconspicuous, compact and discreet product to help users who want to distract themselves from their changing situation.

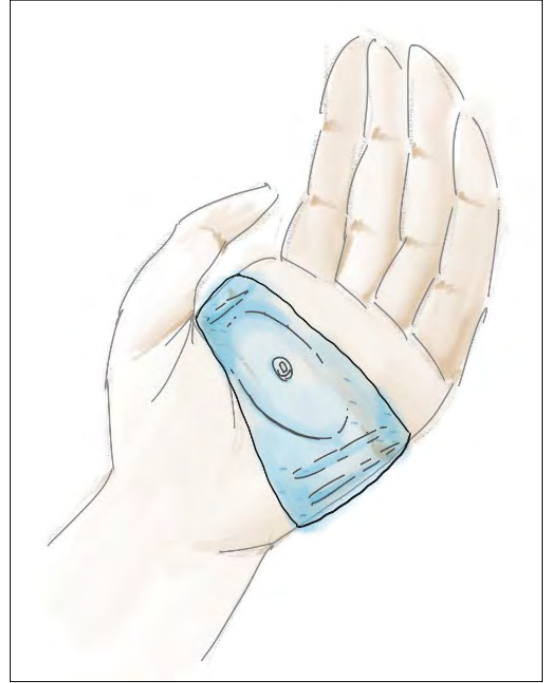


**Figure 1.** The front of hand side of the first product concept.

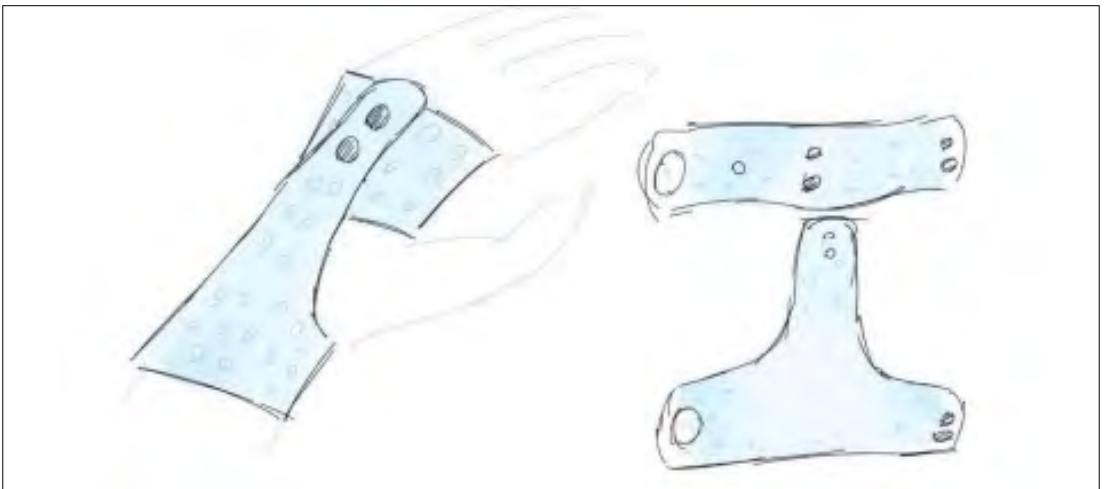


**Figure 2.** The back-of-hand side of an improved product concept.

## 6. Developing the product concept

### 6.1. Evaluation of the first product concept

To conduct the interviews, I visited rehabilitation centres. During my visits, I consulted stakeholders and specialists on the product concept. I received many comments from these people, which allowed me to improve my product proposal accordingly.

The first criticism concerned the donning and doffing of the strap: the hand wrapping is not an appropriate method for a person with limited upper limb mobility. It is therefore necessary to replace the strap with a strap-like geometry, which can be adjusted to several sizes by means of a buckle. It is also important that a ring-shaped perforation is provided at one end of the strap to allow users with limited finger mobility to put it on independently. They can then hook their finger into the ring and pull the strap to the correct size. In addition to all these aspects, I have also identified the need to design several accessories to ensure that the concept, which is evolving into a product family, can meet as many user needs as possible.

During the visits I also examined the geometry of the functional heads. The feedback showed that the heads should be able to hold small and large diameter products, as well as assist with dressing. Users have the most problems with buttoning, putting on socks and tying shoes. Some users also need help with typing and using touch screen phones. This requires the design of a head that allows accurate tapping even for people whose fingers do not allow it due to a restricted range of motion.

The analysis of complex workflows has also highlighted the flaws in the head-strap connection. During everyday activities, gripping and using certain tools requires a different direction of movement, which is not always possible depending on the user's condition. For this reason, the connection must be able to rotate so that these actions can be carried out by everyone, and therefore users are not hindered by possible shortcomings in the product design. Therefore, the geometry of the snap-in connection has been modified. It thus behaves as a ball joint in a given range, ensuring the right amount of rotation and bending.

When discussing aesthetic features, the perforation of the strap was supported by the respondents. So I was tasked with designing a pattern that would not tear when pulled, would be aesthetical-

ly pleasing and would leave as much skin surface area free as possible. In addition, it had to provide the necessary conditions for fastening: it had to fit the fastener precisely and allow for adjustability.

### 6.2. Design the perforations

When designing the pattern, I tried to keep the aesthetic features in mind and to cover as little skin surface as possible, so that the strap can still hold the tool holder head and the tool inside. This requires a ratio between the wall thickness and the area of the perforations, which should not be less than 1:2.

The patterns were evaluated using the Copeland method on the basis of various criteria: aesthetics, wall thickness, novelty. The scores obtained were summed up to select the right pattern for the perforations (Figure 3).

## 7. Conclusions: presentation of the final design of the instrument

The range of occupational therapy aids for hand movement that I have designed is a range of aesthetic, multifunctional devices to help people with upper limb impairments, musculo-skeletal disorders or neurological disorders to carry out their daily activities.

All frequently used parts of the products can be replaced separately, making them cost-effective for both the manufacturer and the customer, and extending product life. The different strap geometries allow specific users to select and use the right tools for their condition and reach, reflecting their individual needs.

The skin-contact straps are made of a two-component bio-compatible silicone with a unique pattern that not only provides aesthetic function but also ensures air contact with the skin, preventing



Figure 3. The prototype of the product line.

skin irritation due to penetration. In addition, the perforations help to connect the two ends of the strap so that the right size can be easily adjusted, ensuring a proper fit.

Due to the choice of materials, the product does not need to be put on and taken off when in contact with water, as all its components are waterproof. It is easy to keep hygienic, as it is not sensitive to commercial skin and tool disinfectants. It allows the grip of many tools used for everyday activities. Easy to adjust to size, it can be used not only on the palm side but also on the palm side.

I considered this feature of transformability important to include because the identified user group includes a large number of individuals with a high degree of hand lesion. The presence of these lesions - contactures, ossified cartilage - does not allow the user to insert anything into the palm of the hand. I believed that by fixing them to the back of the hand, they would also be able to access a number of functions that were previously inaccessible.

In designing the special device heads, I focused not only on the proper performance of the functions, but also on the fit of each accessory, its secure connection and its interchangeability without causing difficulties for the user.

In terms of securing the utensils, I looked at the easiest way to secure them so that they do not move during use. To solve this problem, I have designed a number of designs, some of which include proposals for additional fasteners made of compressible material depending on the type and

geometry of the utensils to be captured.

I also tested the validity of the working principles in practice with a hemiplegic patient who survived a stroke and with occupational therapists. The results of the study clearly demonstrated the validity of the concept. The positive feedback and the suggestions on the individual elements have led me to continue the development of the project.

My product is niche and meets the objective set at the beginning of this work, i.e. to provide a complex solution without compromises for the specific user group identified. These people are all hand or palm mobility impaired, which makes it very difficult for them to carry out their daily activities. During hospital rehabilitation they learn how to adapt to their changed living situation, but after rehabilitation almost all of them need to use some form of assistive device. My product range is designed to meet their needs.

## References

- [1] Söderback I.: *Occupational Therapy: Emphasis on Clinical Practic.* In: *International Handbook of Occupational Therapy Interventions.* (Ed.: Söderback I.). Springer, Dordrecht, 2009. 14–35. <https://doi.org/10.1007/978-0-387-75424-6>
- [2] Bureck W., Illgner U.: *Hand ergotherapy for rheumatic diseases and the special importance of hand surgery.* *Zeitschrift für Rheumatologie*, 73/5. (2014) 424–433. <https://doi.org/10.1007/s00393-013-1342-3>
- [3] „Ego Te Restaurabo”. *Az ergoterapia az egészség-helyreállítás szolgálatában.* Magyar Kórház, 13/17. (1944) 437–438.



**Figure 4.** Photorealistic image of the final product range proposal.

- [4] Szívügyem az ergoterápia. Császár Gabriellával Bajkay Ágnes beszélgetett. Fizioerápia. A Magyar Gyógytornász-Fizioerapeuták Társasága szakmai folyóirata, 32/1–2. (2023) 47–50.
- [5] Mogánné Tölgyesy Szilvia: Az ergoterápia hazai fejlődése. Egészségügyi Gazdasági Szemle, 45/5–6. (2007) 37–39.
- [6] Bartos A., Józsa J., Tajthy K., Tapa G., Cselovszki T., Hum K., Szigeti J., Gasparicsné Csillag Á.: Ergoterápia a mozgásjavítóban. Fizioerápia: A Magyar Gyógytornász-Fizioerapeuták Társasága szakmai folyóirata, 21/1. (2012) 23–27.
- [7] MSZ EN ISO 9999:2007 Fogyatékkal élő személyek segédeszközei. Osztályozás és szakkifejezések (ISO 9999:2007)
- [8] MSZ EN ISO 9999:2022 Segédeszközök. Osztályozás és terminológia (ISO 9999:2022)
- [9] MSZ EN ISO/ASTM 52900:2017 Additív gyártás. Általános alapelvek. Terminológia (ISO/ASTM 52900:2015)
- [10] Bondex Kft. „OÉTI engedélyes folyékony szilikon Rubosil. 2022 (accessed on : 2022. okt. 19.). <https://szilikonwebaruhaz.hu/id/02767-OETI-engedelyes-folyekony-szilikon-Rubosil-SR38>
- [11] Bondex Kft. „OÉTI engedélyes élelmiszeripari katalizátor önthető szilikonhoz Rubosil K Food 50 ml”. 2022. (accessed on : 2022. okt. 19.). <https://szilikonwebaruhaz.hu/id/02763-OETI-engedelyes-elelmiszeripari-katalizator-ontheto-szilikonhoz-Rubosil-K-Food-50-ml>



# Analysis of Concrete with Chaff

Fekete L. Mátyás

Építőmérnöki Kar, Kolozsvári Műszaki Egyetem, e-mail: [feketematyas01@gmail.com](mailto:feketematyas01@gmail.com)

Theme leaders: dr. Raluca Iştoan, e-mail: [raluca.fernea@ccm.utcluj.ro](mailto:raluca.fernea@ccm.utcluj.ro)  
and dr. Elena Jumate, [elena.jumate@ccm.utcluj.ro](mailto:elena.jumate@ccm.utcluj.ro)

---

## Abstract

Can the reintroduction of a traditional building material lessen the emission of greenhouse gas emissions of the construction industry? The study below will present the search for the answer to this question. Given that the used hemp shives, compared to cement, have low mechanical strength but act as a great thermal insulator, I tried four recipes to find the best ratio among the elements after determining the bending, compressive and tensile strengths. The study also analyzes the price of hempcrete, comparing it to the price of hollow bricks, to examine the material's viability from a financial perspective. Additionally, it compares the carbon dioxide emissions of hempcrete and bricks.

**Keywords:** *environmentally friendly, sustainable, pollutant-free, natural, thermal insulator.*

---

## 1. Introduction

In recent years, there has been a growing trend towards using green building materials, and it is expected that this market will double by 2030 [1]. The needs of this market can be met by creating new and innovative materials or by improving existing ones.

In recent years, the textile industry has reintroduced hemp into production. As the demand for hemp fiber increases, and this industry only utilizes the outer fiber of the plant, the rest of the plant is considered waste. This „waste” consists of the woody fiber, from which hempcrete is made.

The construction and manufacturing industries together account for 21% of greenhouse gas emissions, while also influencing energy consumption, which constitutes 40% of the emitted gases [2]. A well-insulated building needs 10% less energy [3], so the use of materials with lower thermal conductive properties results in saving energy.

Hemp shives have a density of 85–90 kg/m<sup>3</sup> [4], can be mixed with cement and lime to obtain a material with low thermal conductivity and low mechanical strength. This material has been studied for years by the scientific community.

## 2. Materials and methods

### 2.1. Materials used

To establish a starting point, we replicated the HH1 recipe developed by Nguyen et al in 2010 [5]. In this recipe, the ratio between the binder and the shives is 2.12, and the ratio between water and binder is 1.52. The shives used were from Hempflax Romania, the cement was Holcim ExtraDur 52, and the hydrated lime was Carmeuse Super Calco M. The compaction was done manually.

The hemp shives had a diameter of less than 3 millimeters. The cement was of high strength, grade 52.5.

In all mixes, there was 2.14 times more binder than shives and 1.52 times more water than binder. The difference among the four recipes lay in the composition of the binder: in the control recipe (R0), we used 100% hydrated lime, in the first recipe (R1) 33% cement and 67% hydrated lime, in the second recipe (R2) 67% cement and 33% hydrated lime, and in the third recipe (R3) 100% cement.

**1. táblázat.** Quantities for 5.43 dm<sup>3</sup> of material

	Hemp (g)	Cement (g)	Lime (g)	Water (L)
R0	535	0	1145	1.74
R1	535	378	767	1.74
R2	535	767	378	1.74
R3	535	1145	0	1.74

**2.2. Determining the density**

We conducted all tests under laboratory conditions at a temperature of 15-20°C and a relative humidity of 30-50%.

To determine the initial density, the prepared material was placed in a 1-liter (1000 cm<sup>3</sup>) cylinder, and then the mass of the material was measured.

For determining the density curve, the mass of the test samples was measured before the mechanical strength tests.

**2.3. Determining the bending strength**

To determine the material's bending strength, tests were conducted at 3, 7, 14, 28, and 90 days using a hydraulic press.

The bending strength can be calculated using formula (1) [6]

$$R_{ti} = \frac{3}{2} \cdot \frac{P \cdot l}{b \cdot h^2} \tag{1}$$

where  $R_{ti}$  is the strength,  $P$  is the force expressed in Newtons,  $l$  the distance measured in millimeters between the supports of the machine,  $b$  the width, and  $h$  the height of the cross-section, expressed in millimeters.

**2.4. Determining the compressive strength**

To determine the material's compressive strength, tests were conducted at 3, 7, 14, 28, and 90 days using a hydraulic press. The compressive strength can be calculated using formula (2).

$$R_c = \frac{P}{A} \tag{2}$$

where  $R_c$  is the strength,  $P$  is the force in newtons,  $A$  is the cross sectional area.

**3. Results**

**3.1. Density**

As observed in Figure 3, the material density significantly decreased in the first 3 days when the water content fell dramatically from an average of 50.88% to 47.64%.



Figure 1. Mixing the ingredients.



Figure 2. Determining the density.

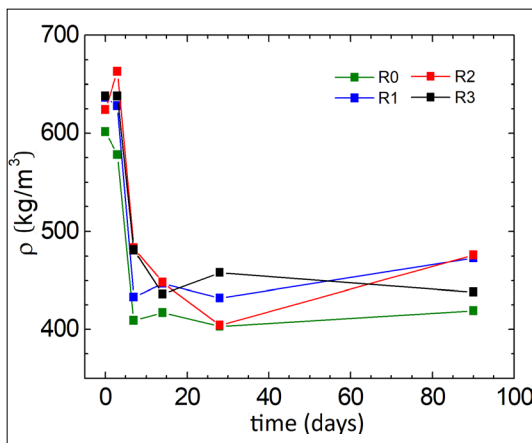


Figure 3. Variation of binder density as a function of drying time.

By the 7th day, the density had almost reached the final value for all samples. The recipes containing a significant amount of cement (R2 – 66.67% binder, R3 – 100% binder) dried more slowly compared to lime-based recipes.

Despite talking about drying, the density of lime-based recipes increased during the drying period - the last two weeks were rainy, leading to increased environmental humidity.

**3.2. Tensile strength**

Concrete is not known for its tensile strength and hemp shives are too short to significantly resist tension in a way that steel would have. The results support this observation.

The maximum tensile strength of the control material (R0) was 0.41 N/mm<sup>2</sup> after 14 days, and its final value was 0.24 N/mm<sup>2</sup>. The modeled recipe had a tensile strength of 0.105 N/mm<sup>2</sup> after 90 days. The difference in results was caused by the lime used, as they were not of the same brand - the shives were the same size for both materials.

In terms of tension, the best resistance was achieved by the R2 mix, where 33.33% of the binder was lime and 66.67% was 52.5-grade cement, because cement-based mortar has higher strength than lime-based ones. The high initial resistance was due to additives in the cement, which was labeled ‚R,‘ indicating the rapid-setting cement used.

**3.3. Compressive strength**

The shives have low density and mechanical strength, causing the resulting hempcrete to have lower strength properties than traditional concrete.

The final compressive strength of the control recipe (R0) reached 0.2625 N/mm<sup>2</sup>, contrasting with Nguyen’s result of 0.7 N/mm<sup>2</sup>. Although the material based on the R0 recipe achieved better values than Nguyen’s HH1, it performed worse during the compressive strength test, suggesting a different orientation of the hemp shives. Despite identical mixing methods, it is possible that during manual compaction, the fibers in the model material aligned along their length, significantly contributing to tensile strength at the expense of compressive strength.

**4. Economic considerations**

**4.1. Price of raw materials**

The price of a 40-kilogram bag of Holcim Extra-dur 52 cement is 35 RON. The price of a 20-kilogram bag of CL-70-S lime is 30 RON. The price of a

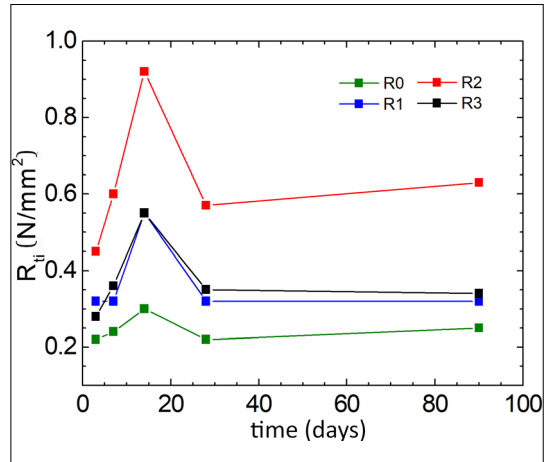


Figure 4. Tensile strength

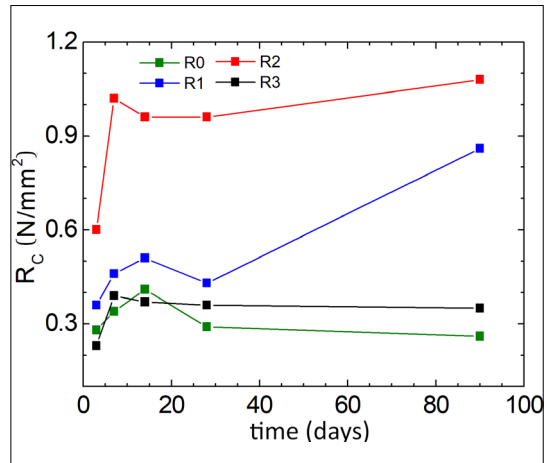


Figure 5. Compressive strength variation

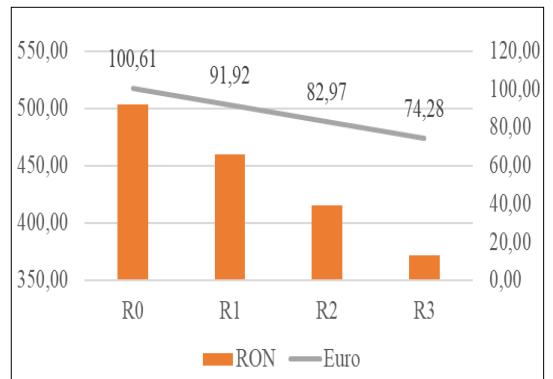


Figure 6. Prices of recipes.

**Table 2.** Prices of materials

Recipe	5.43 dm <sup>3</sup> = 0.00543 m <sup>3</sup>				1 m <sup>3</sup>	1 m <sup>3</sup>
	Hemp	Cement	Lime	Total	RON	Euro
R0	1.0165	0	1.7175	2.734	503.056	100.6112
R1	1.0165	0.33075	1.1505	2.49775	459.586	91.9172
R2	1.0165	0.671125	0.567	2.254625	414.851	82.9702
R3	1.0165	1.001875	0	2.018375	371.381	74.2762

14-kilogram bag of hemp is 5.4145 euros, which is equivalent to 1 kilogram costing 1.92 RON.

Comparing the price of 1 cubic meter of hempcrete with 1 cubic meter of hollow bricks (520 RON/m<sup>3</sup>), it can be concluded that each tested recipe is more economical than a brick wall.

These prices need to be supplemented with indirect costs (water, laboratory services, labour) that are not included in the material costs and account for 10% of the formulation's cost. In the case of larger procurement, negotiations with suppliers regarding the prices of raw materials (cement, lime, hemp) are possible, leading to reduced production costs.

## 4.2. Ease of implementation

The successful implementation of new technologies largely depends on how easy it is to transition from the old model. In the case of hempcrete, the process is intuitive as it closely resembles traditional concrete work: everything is mixed in a concrete mixer, gradually adding water, and then poured into molds.

The only drawback to this method is that due to the lime content, the walls reach their final strength only after 90 days. This delay can cause issues if the project schedule doesn't account for the new method.

## 5. Ecological considerations

### 5.1. Carbon-dioxide emissions

An environmentally friendly material should have a low carbon dioxide emission compared to the „old” alternative. Every kilogram of cement used produces 0.81 kg of CO<sub>2</sub> [7], and every kilogram of used lime generates 0.75 kg CO<sub>2</sub> [8]. 1 kg of hemp absorbs 1.29 kg CO<sub>2</sub> [9].

**Table 3.** Emissions of 1 m<sup>3</sup> hempcrete

	Kender (kg)	Cement (kg)	Mész (kg)	Összesen (kg)
R0	-127.12	0	157.5	31.925
R1	-127.12	56.94	105	36.36
R2	-127.12	113.87	52.5	40.80
R3	-127.12	170.81	0	45.23

It can be stated that hempcrete is nearly carbon neutral. Converted, it emits 50.8-71.43 kg of CO<sub>2</sub> per ton. Considering that a ton of bricks emits 258 kg of CO<sub>2</sub> [10], the difference is significant.

## 6. Conclusions

Ultimately, it can be concluded that hempcrete can serve as an alternative to bricks, but only in non-structural functions as it lacks the necessary properties for a structural task – in this regard, it falls short of traditional bricks.

From an environmental perspective, the material produced emits one-third of the carbon dioxide compared to glass bricks, but its carbon dioxide balance is still not negative, so it can be considered only a partial success.

From an economic standpoint, the material is more cost-effective than traditional brickwork, making it an improvement in the construction industry, even if it doesn't consider the positive environmental impact.

## References

- [1] Sushant M.: *Green Building Materials Market by Product Type (Exterior Products, Interior Products, Building Systems, Solar Products, and Others) and Application (Residential Buildings and Non-Residential Buildings): Global Opportunity Analysis and Industry Forecast, 2021-2030s*. Allied Market Research, (2022).

- [2] Aydogan H., Hirz M. et al.: *The use and future of biofuels*. International Journal of Social Sciences (2014).
- [3] US Department of Energy, Guide to Home Insulation. Energy Efficiency and Renewable Energy, [https://www.energy.gov/sites/prod/files/guide\\_to\\_home\\_insulation.pdf](https://www.energy.gov/sites/prod/files/guide_to_home_insulation.pdf)
- [4] Jiang Y. et al.: *Cell wall microstructure, pore size distribution and absolute density of hemp shiv*. The Royal Society Publishing, (2018).
- [5] Nguyen T., Picandet V. et al.: *Effect of compaction on mechanical and thermal properties of hemp concrete*. European Journal of Environment and Civil Engineering, (2010).
- [6] Netea A., Manea D., et al.: *Materiale de Construcții*. Chimie. UTPress (2019).
- [7] Kavitha S.: *Evaluation of CO2 emissions for green concrete with high volume slag, recycled aggregate, recycled water to build eco environment*. International Journey of Civil Engineering and Technology, (2017).
- [8] European Environment Agency, Jeronen Kuenen, et al., *Lime Production. Lime. Manufacture of cement, lime and plaster*. EMEP/EEA air pollutant emission inventory guidebook 2016.
- [9] Scrucca F., Ingrao C., et al.: *Energy and carbon footprint assessment of production of hemp hurds for application in buildings*. Environment Assessment Review, 84. (2020).
- [10] Henning Larsen: *Recycled Bricks Reduces CO2 Emissions Enormously*. Henninglarsen.com (2017).



# Determination of Maximal Gap for Laser Welding

Nagy Balázs,<sup>1</sup> Kovács Tünde Anna<sup>2</sup>

Óbuda University, Bánki Donát Faculty of Mechanical and Safety Engineering, Budapest, Hungary

<sup>1</sup> [nagy.balazs@bgk.uni-obuda.hu](mailto:nagy.balazs@bgk.uni-obuda.hu)

<sup>2</sup> [kovacs.tunde@bgk.uni-obuda.hu](mailto:kovacs.tunde@bgk.uni-obuda.hu)

---

## Abstract

Nowadays laser welding is widely used in industrial applications. Often, steel sheets are welded without welding material by using this process. The research aims to determine the maximal gap size and the related welding parameters for the laser welding of a 3 mm thick steel sheet of S235J2 steel grade. During welding, a joint gap may occur due to inadequate edge preparation, which must be considered during the design of the technology. The result of the experiments is that using the Trumpf TLF 5000 turbo-type carbon dioxide laser of 4.5 kW power, 3000 mm/min welding speed, with a focus the maximal gap size is 0.10 mm, while at 2000 (mm/min) welding speed, with 5 mm above focus the maximal gap size is 0.27 mm which can be welded with acceptable seam quality.

**Keywords:** *unalloyed steel, laser welding, welded joint, joint gap.*

---

## 1. Introduction

In the 1970s, laser machining systems were introduced to the market, providing advantages across a broader technological spectrum compared to existing manufacturing systems. It also opened up entirely new application possibilities. Development in this field is ongoing. Today, laser technology has also reached the realms of both the economy and private life. Some examples include essential technological elements in automotive manufacturing (cutting, drilling, welding, hardening) [1, 2].

For high-power lasers used in material processing, the raw laser beam diameter is reduced by focusing to create the appropriate power density in the spot and to ensure that the spot size aligns with the processing area. Focusing can be achieved by lenses and mirrors. The spot size linearly changes with the distance between the focus and the optics, allowing the determination of the spot diameter at a given distance from the focal plane [3, 4]. „If the workpiece is located outside the focal distance, we refer to positive focal shift; if it is inside, we talk about negative focal shift” [5].

A portion of the laser beam can be reflected on the surface, another part can penetrate the ma-

terial. The fraction that enters may be absorbed, converting into heat. The unabsorbed portion that passes through the workpiece exits from it. These three types of interaction together should determine the initial intensity. During absorption, the intensity decreases exponentially in the depth direction. This decrease depends on the material's composition, structure (crystalline or amorphous), and the wavelength of the laser radiation. The penetration depth is determined based on the 1/e ratio decrease in surface intensity. For metals, laser light transmission is zero, so the amount of reflection and absorption equals the initial intensity. Therefore, if we know one parameter, we can calculate the other. **Figure 1** shows emission among the possible interactions, which is responsible for the laser radiation phenomenon and forms the basis of solid-state lasers.

For metals, absorption occurs at depths of micrometres or less. During the absorption of laser radiation in the material, free electrons near the surface become excited, increasing their kinetic energy. The energy is transmitted towards the atomic nuclei, which vibrate with increasing amplitude. As a result, the temperature rises in the surface layers. The absorbed energy further propagates into deeper layers through heat conduction.

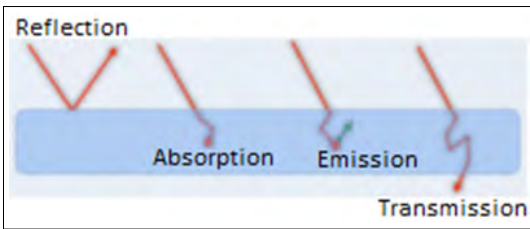


**Figure 1.** Possible forms of light-matter interaction.

With the increase in temperature, absorption also increases. A sudden jump in absorption is observed during the phase change at melting, indicating that the material absorbs laser radiation to varying degrees in the solid and liquid phases.

Laser radiation is classified into seven groups based on its application: everyday and entertainment, industrial and material processing, medical, measurement and control technology, energetic, military, scientific and research. In the case of industrial and material processing laser equipment, the power (energy content) of the laser beam is always used for material processing, which is partially absorbed in the material, turns into heat, and produces various effects (heats, melts, vaporizes, transforms into a plasma state, breaks down compounds, creates material transformation) [4–6].

Lasers are typically categorized into four main groups based on the state of their active laser medium: gas, solid-state, semiconductor, and dye lasers.

### 1.1. Gas Lasers

Gas lasers use gas as the active medium, such as a helium-neon mixture, argon (its ions), excimer ( $\text{Ar}_2$ ,  $\text{F}_2$ )/ exciplex (a noble gas and a halide element mixture, e.g.,  $\text{XeCl}$ ) laser gas mixtures, and carbon dioxide, as applied by us. The advantages of using gas include its homogeneity, relatively low cost, and ease of refilling. However, its drawback, inherent in its physical nature, is that it requires a large quantity of gas due to its low density to achieve population inversion [4, 5].

### 1.2. He-Ne Laser

The He-Ne laser (1961, Bell Laboratories) was the first type of laser that could produce continuous laser radiation. A very popular and widespread laser type in industrial practice. Both gases are contained in a glass tube, where the pressure (a few hundred pascals) is lower than atmospheric pressure, as this is necessary to induce electrical gas discharge [4, 5].

### 1.3. Ar-ion Laser

Argon ion lasers (similar to noble gas ion lasers) emit radiation in the visible and near-UV range. In this laser medium, low-pressure argon is used, and a direct current of 30–50 (A) creates population inversion. Argon ion lasers operate in pulsed mode, but ring discharge can also be applied to achieve continuous output radiation. Their maximum output is in the order of 100 (W) [4, 5].

### 1.4. Excimer / exciplex Laser

The classic meaning of excimer is an excited, homopolar molecule consisting of identical atoms (e.g.,  $\text{Ar}_2$ ,  $\text{F}_2$ ). Nowadays, it's more common to use a mixture of a noble gas and a halide element (heteropolar, e.g.,  $\text{XeCl}$ ), making the correct term exciplex (excited complex) laser, although this term hasn't widely spread in practice (fortunately, these substances function similarly when used as an active laser medium). Excimer lasers typically involve a two-atom molecule formed by a noble gas or a noble gas and a halogen mixture. Excimer lasers are suitable for the heat-free ablation of organic materials and biological tissues, facilitated by the high photon energy and significant absorption characteristic of the UV range. It is also used for the excitation of dye lasers and material processing; in chip manufacturing, they are applied as a light source for photolithography [4, 5].

### 1.5. Carbon-dioxide Laser

The  $\text{CO}_2$  laser operates between the vibrational levels of carbon dioxide molecules and is the most powerful gas laser, boasting the highest efficiency (15–20%). The active laser medium is a mixture of  $\text{CO}_2$ ,  $\text{N}_2$  and He gas or  $\text{H}_2\text{O}$  vapour in roughly a 1:1:8 ratio [4, 5].

### 1.6. Solid-State Lasers

Solid-state lasers have become worthy competitors to  $\text{CO}_2$  lasers in recent times. In this case, the laser medium consists of solid-state materials (Nd: YAG, Nd: glass, alexandrite, Ti: sapphire, etc.). It is worth noting that low-power semiconductor lasers are also grouped with solid-state lasers. The YAG-based version has gained the most popularity, with the essential types being:

- Flashlamp-pumped YAG lasers,
- Diode-pumped YAG lasers,
- YAG disk lasers (hybrids) [1].

Laser welding has seen significant development in the past few decades. Numerous laser machining processes are known and applied in today's

industrial practices. Laser cutting is typically widespread, but laser welding is increasingly applied in various industries. The applications of laser machining are decisively determined by the applied lasers, the achievable power, and the type of laser [7–9].

Several research results are known regarding the laser welding of special materials [8–10].

The aim of the research is to determine the maximum fit-up gap for laser welding, where a suitable weld can still be created using the Trumpf TLF 5000 turbo CO<sub>2</sub> laser.

## 2. Experiments

### 2.1. Materials Used

The experiment was conducted on steel plates of quality S235J2, with its chemical composition provided in Table 1. This steel quality is easily-weldable and suitable for laser welding, given its low reflectivity of the base material surface, thermal conductivity of 54 W/(m<sup>2</sup>·K), and thermal expansion of 1.2·10<sup>-5</sup> 1/°C.

The mechanical properties of the used steel are R<sub>p0.2</sub> = 235 MPa, R<sub>m</sub> = 540 MPa, minimum elongation at fracture A ≥ 24 %, and a density of ρ = 7,85 kg/dm<sup>3</sup>. For the experiments, plates with a thickness of 3 mm were utilized.

### 2.2. Welding Experiments

The experiments were conducted at Bay Zoltán Non-profit Ltd. for Applied Research using a Trumpf TLF 5000 turbo carbon dioxide laser with a wavelength of 10.6 μm, max power of 5 kW, and five-axis CNC control. The device's working area is 1600×1000×400 mm, suitable for cutting, drilling, welding, and heat treatment. To determine the welding parameters, fillet joint test welds were performed. In fillet welding, no joint is formed with another piece (Figure 2).

The constant parameters are included in Table 2. During the welding process, three different speeds (500 mm/min, 2000 mm/min, 3000 mm/min) and three focal positions (0, +5, +10 mm), were applied, resulting in a total of nine welds.

The results of the fillet welding experiments were evaluated, and the parameters of the further experiments were determined based on visual inspection and fusion depth.

To determine the weldable gap, the two plates were welded in the configuration shown in Figure 3 where one side of the plates was matched, and the other side was separated by 1 mm using a gap plate. The welding parameters are summarized in Table 3.

**Table 1.** S235J2 steel chemical composition (m%)

Compo-nents	C	Si	Mn	P	S	Cu	Fe
%	<0.17	–	1.4	0.025	0.025	<0.55	left-overs

**Table 2.** Constant welding parameters.

Filling	Performance (W)	Nozzle distance (mm)
CW (continuous operation)	4500 (90%)	1
Working gas	Gas pressure (bar)	Amount of working gas (l/min)
Helium 4.6	5	6

**Table 3.** Experimental parameters.

Signal of the sample	Focus shift (mm)	Performance (W)	Welding speed (mm/min)
A	0	4500	3000
B	+5	4500	2000

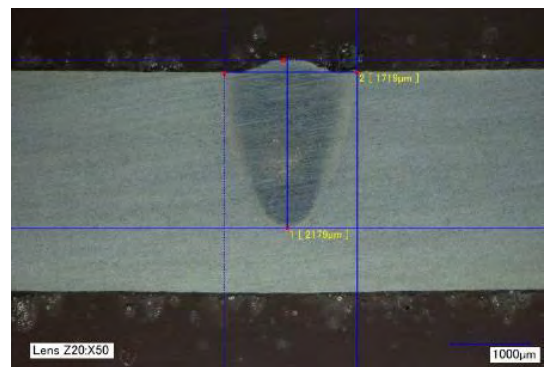


**Figure 2.** Section of a fillet joint.

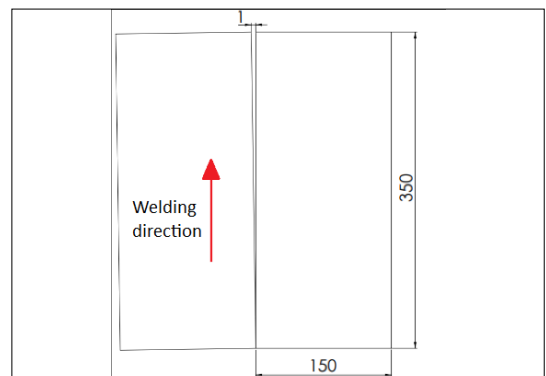


**Figure 3.** Experimental arrangement.

**Table 4.** Hardness values

Signal of the sample	Average Hardness HV10		
	Base material	Heat effect zone	Welded joint
A	130	150	190
B	130	160	200

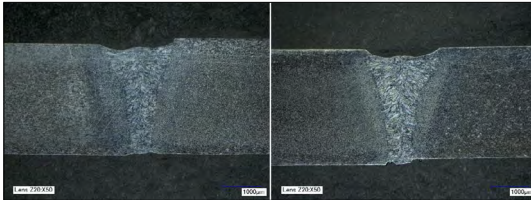


**Figure 4.** Acceptable joint cross-section; focus shift: 0 mm.

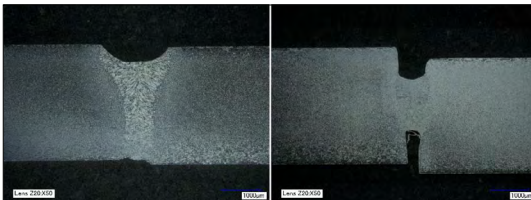


**Figure 5.** Appropriate joint with +5 (mm) focal shift.



**Figure 6.** Tensile test specimens.

### 3. Results

After the test welding, we observed that when welding in focus (0 mm) with a 0.1 mm gap, a satisfactory weld was achieved. **Figure 4** shows the cross-section of the welded joint with a 0.1 mm gap, welded with a power of 4.5 kW and a welding speed of 3000 mm/min.

The fusion of the two plates occurred, and the joint was successfully formed.

We have found that a +5 mm focal shift with a gap of 0.27 mm was weldable, maintaining satisfactory weld quality. **Figure 5** displays the cross-section of the welded joint with a 0.27 mm gap, welded with a power of 4.5 kW and a welding speed of 2000 mm/min.

To verify the adequacy of the weld, a tensile test was conducted. We found that in all cases, the fracture occurred in the base material, confirming the integrity of the welded joint (**Figure 6**).

We also wanted to verify the test results with hardness measurements and found that the hardness in the weld, heat-affected zone, and base material was below the permissible 380 HV10 (**Table 4**).

### 4. Conclusions

During sheet metal cutting, precise alignment is not always achieved, resulting in gaps at the joints of the two plates that are not uniform. Therefore, it is crucial to determine the permissible gap size to allow for the creation of a weld using laser welding without the addition of welding material. Based on the results of the conducted laser welding experiments, it can be stated that using the Trumpf TLF 5000 turbo carbon dioxide laser with a power of 4.5 kW, with welding speed of 3000 mm/min, focal shift of 0 mm, and a gap of 0.1 mm, as well as with the same power, welding speed of 2000 mm/min and a focal shift of +5 mm, a gap of 0.27 mm can be welded with acceptable weld quality.

### References

- [1] Buza G.: *Lézesugaras Technológiák I.*, 1. kiadás. Edutus Főiskola, Budapest, 2012.
- [2] Almási G., Erdélyi M., Fülöp József A., Hebling J., Horváth Z., Kovács Attila P., Rácz B., Smausz Kolumbán T.: *Lézerfizika*. Elektronikus tananyag, (2013) <http://titan.physx.u-szeged.hu/~bubo/Lezerfizika/book.html#id296435> (letöltve: 2023. 09. 30.)
- [3] Markovits T.: *Korszerű lézesugaras technológiák*. Akadémiai Kiadó, 2018.

- [4] R. Crafer, Peter J. Oakley: *Laser processing in Manufacturing*. Springer Science & Business Media, 1992. 292.
- [5] IIW VI-1338r1-2022 Laser welding terms for ISO/TR 25901-5 (2022)
- [6] Bitay E.: *Lézeres felületkezelés és modellezés*. Műszaki Tudományos Füzetek, 4. 2007.  
<https://doi.org/10.36242/mtf-04>
- [7] Halász G.: *Lézer hibrid hegesztés*. 25. Jubileumi Hegesztési Konferencia, Budapest, 2010.
- [8] Xinmin Dong, Guofang Wang, Mohammad Ghaderi: *Experimental investigation of the effect of laser parameters on the weld bead shape and temperature distribution during dissimilar laser welding of stainless steel 308 and carbon steel St 37*. Infrared Physics & Technology, 116. (2021).  
<https://doi.org/10.1016/j.infrared.2021.103774>.
- [9] Kovacs, T.: *Laser welding process specification base on welding theories*. Procedia Manufacturing, 22. (2018), 147–153.  
<https://doi.org/10.1016/j.promfg.2018.03.023>.
- [10] Dobránszky, J., Lőrinc, Zs., Gyimesi, F., Szigethy, A., Bitay, E.: *Laser welding of lean duplex stainless steels and their dissimilar joints*. In: 8th European Stainless Steel and Duplex Stainless Steel Conference, Graz, Austria, April 28-30, 2015. 138–147.



# Particle Reinforced, Open Cell Metal Foams

Szovák Benedek,<sup>1,2,a</sup> Maróti János Endre,<sup>1,2,b</sup> Orbulov Imre Norbert<sup>1,2,c</sup>

<sup>1</sup> Budapest University of Technology and Economics, Faculty of Mechanical Engineering, Department of Materials Science and Engineering, Budapest, Hungary

<sup>2</sup> MTA–BME Lendület „Momentum” High-performance Composite Metal Foams Research Group, Budapest, Hungary

<sup>a</sup> szovak.benedek@edu.bme.hu, <sup>b</sup> maroti.janos.endre@gpk.bme.hu, <sup>c</sup> orbulov.imre.norbert@gpk.bme.hu

---

## Abstract

Salt replicated metal matrix foams are cellular materials with interconnected cells. These materials have some highly specific mechanical properties. They are capable of absorbing high amount of energy during compression. The main goal of this study was to increase these mechanical properties without drastically increasing density with the application of ceramic particles as reinforcing material. In this research salt-replicated metal foams with particle reinforced cell walls were successfully created with pressure infiltration. The energy absorption capacity, the plateau stress and in some cases the specific values were increased approximately by 10 % to 41 % by particle reinforcement.

**Keywords:** *metallic foam, open cell foam, reinforcement material.*

---

## 1. Introduction

In recent decades one of the main lines of material science research has been to optimize the weight specific mechanical properties of engineering materials.

One of the main objectives of this is the lowering of weight and density with the application of porous, cellular materials [1]. These materials have low density and high energy absorption capacity [2]. Metal foams can be categorized into three main groups based on their cell structure: closed cell metal foams [2], open cell foams [2, 3] and syntactic metal foams [4–7].

Another solution is increasing the mechanical properties without drastically increasing the weight. These materials are composites, where the high density-high strength reinforcing material is embedded in the low density-low strength matrix, such as aluminium alloys. These reinforcing materials could be ceramic particles, such as alumina or silicon-carbide or fibers, like carbon fiber for example [8–11].

There is only limited publication concerning the combination of these two solutions. In these sources ceramic particles were applied as reinforcement in syntactic aluminium matrix foams

[12, 13]. During these studies it was concluded that the ceramic reinforcement increases the compressive strength but lowers the plateau stress and the amount of absorbed energy up to 50% engineering strain. Due to this, the application of ceramic reinforcement in metal matrix syntactic foams is only advantageous in particular cases [12, 13].

In this study salt replicated metal matrix foams were created with ceramic particle reinforcement in their metallic struts, and the effect on the mechanical properties of this reinforcement were examined.

## 2. Materials and methods

### 2.1. Materials

Al99,5 aluminium was used as matrix material, the exact chemical composition (wt%) was: Al: 99.68; Si: 0.16; Fe: 0.1; Cu: 0.05; others: 0.01. The measurement was performed in a Zeiss EVO MA 10 scanning electron microscope and was obtained as the average of 4 different measurements.

Common road salt was used as cell forming owing to its low price and wide availability. Gradient salt was used with a grain-size of 2.6–3 mm, a pic-

ture of the cell forming captured with stereomicroscope is shown in [Figure 1.a](#) As reinforcement material alumina and silicon-carbide ceramic particles were used with the same 0.35–0.60 mm grain size, they are shown in [Figure 1 b, c](#). Both were added in 20% of the volume of the matrix material. The reinforcing materials were acquired from Granit Grinding Wheel Ltd. [14].

Based on the microscope images, the average diameter of the salt particle was  $2.73 \pm 0.04$  mm, the grainsize of the reinforcement is shown in [Table 1](#).

## 2.2. Methods

The sample was produced with pressure infiltration in an infiltration furnace.

The cell forming and reinforcing materials were mixed by hand mixing method until they reached an desired level of mixing based on visual investigation. The mixture was poured into mould made of S235J steel with the outer dimensions of 60×60×300 mm. The inner side of the mould was coated with Dueci Electronic N 77 graphite spray. The different mixtures were placed on top of each other separated with paper separators. The installation was closed with AISI 304 steel net prevent the cell forming or the reinforcement material preventing the movement of the filler into the molten matrix during infiltration. On top of the steel net a 2 mm thick alumina quilt was placed. Then the matrix material was placed into the mould. A model of the installation configuration is shown in [Figure 3](#).

The installation was placed into the infiltration furnace at 600°C for 1.5 hours until the vacuum built up to 10-4 Pa. Then the temperature was raised to 750°C and was maintained for 1 hour. Following this, the infiltration was performed with 5 bar argon gas for 5 seconds. The idealized temperature history of the infiltration is shown on [Figure 4](#).

The installation was cooled in air and after it reached room temperature the sample was cut out from the mold with angle grinder. The sample was cut into specimens with the dimension of 20×20×30 mm ([Figure 2](#)) with a Struers Disco-tom-10 cutting machine.

Firstly, the specimens were soaked in water (continuously flowing), to dissolve the cell-forming material and thus form an open cell structure. One specimen from every type was selected for visual investigation. These specimens were grinded with P80 to P2500 silicon-carbide sandpaper with even distribution and polished with 3 μm di-

**Table 1.** The grainsize of the used reinforcing materials

Reinforcement material	Nominal diameter (mm)	Measured grainsize (mm)
Al <sub>2</sub> O <sub>3</sub>	0.35–0.60	0.52 ± 0.07
SiC	0.35–0.60	0.42 ± 0.06

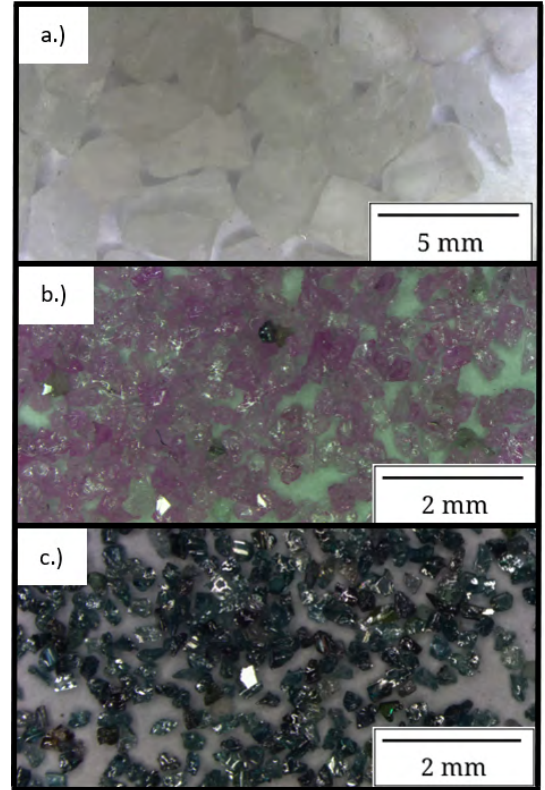


**Figure 1.** a) Cell forming, b) alumina with grainsize of 0.35 – 0.60, c) silicon-carbide with grainsize of 0.35 – 0.60 reinforcement.



**Figure 2.** Picture of the specimens (from left to right open cell meta foam with Al<sub>2</sub>O<sub>3</sub> reinforcement, Reinforcement metal foam by SiC and unreinforcement open cell metal foam.

among suspension. The investigation was carried out on an Olympus PMG 3 microscope.

The mechanical properties were examined with an MTS 810 universal material testing machine with a load bearing capacity of 250 kN, according to ISO 13314:2011 [15]. The tests were uni-axial quasi-static compression tests with 3 mm/min speed up to at least 50 % engineering strain. As lubrication, 0.3 mm thick Kolofol teflon foil was placed between the specimens and the faces of the machine.

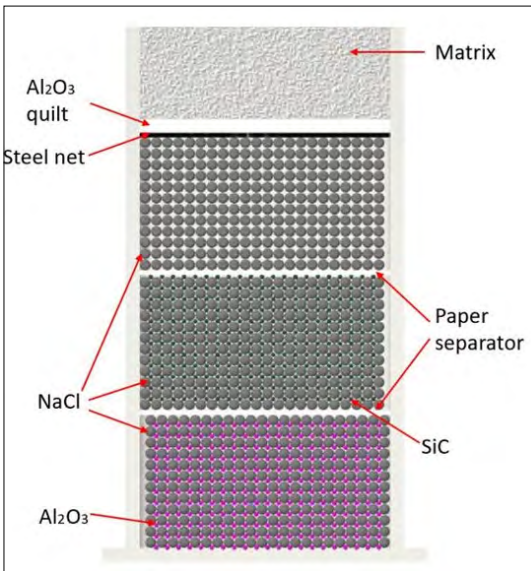


Figure 3. Model of the installation which was used in our research.

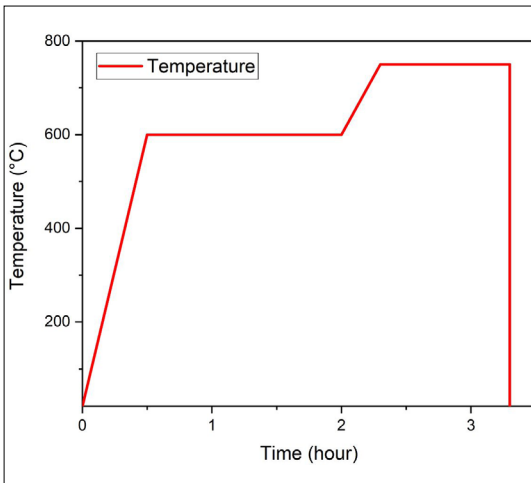


Figure 4. The idealized temperature versus time curve.

### 3. Results

#### 3.1. Visual testing

The results of the micro-structural analysis are shown in Figure 5.

The micro-structural tests have shown that a good connection between the strut's material (acting as matrix in this case) and the reinforcing material has developed, and no large-scale porosities, surface defects, or separations have been observed. It is also clearly visible in the pictures that the salt was well dissolved, and the open-cell structure was formed. Based on these observations, pressure infiltration is an adequate method to produce salt replicated metal foams reinforced in the matrix material.

#### 3.2. Mechanical tests

The force-crosshead displacement data pairs acquired during mechanical tests were transformed into engineering stress-engineering strain curves with the original cross section area and original height of the specimens. On these diagrams, the following mechanical properties and their den-

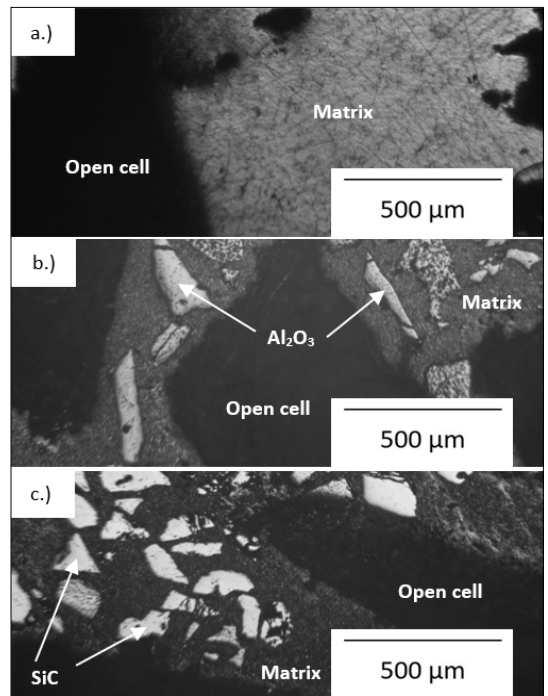


Figure 5. Salt replicated foam reinforced with (a) alumina and (b) silicon-carbide (not every cell, particle of reinforcing material or matrix material is labelled).

sity specific counterparts ('s' index) were examined: compressive offset stress ( $\sigma_{p0,2}$ ,  $\sigma_{fp11}$ ), which is the stress at 1 % engineering strain, the plateau stress ( $\sigma_{pl}$ ,  $\sigma_{fp1}$ ), which is the average stress value between 20 % and 30 % engineering strain, and the absorbed energy in a unit of volume up to 50 % engineering strain ( $W_{50}$ ,  $W_{f50}$ ), which is the area under the engineering stress-engineering strain curve. These mechanical properties are represented in Figure 6.

The averaged curves of the three specimens of the same type and the absorbed energy in a unit of volume is shown in Figure 7.

The main mechanical properties are shown in Table 2. .

After evaluating the results, some of the mechanical properties can be improved by adding a reinforcement material. The density of the metal foams increased by 36% for  $Al_2O_3$  and 19% for SiC.

As we can see, the application of reinforcing materials has increased the plateau strength, by 26% in the case of  $Al_2O_3$  reinforcing material, and by 41% in the case of SiC. The energy absorbed up to a deformation of 50% increased by 24% and 36%, respectively.

However, the value of the conventional compressive yield strength was reduced by 11% in the case of silicon-carbide and increase by 27% by reinforcing  $Al_2O_3$ .

Examining the specific values, it can be concluded that both the plateau stress and absorbed energy increased by 13% and 10% by using the SiC reinforcing material, however, both parameters were decreased by 8% and 10% by application of  $Al_2O_3$  -reinforcement, and the specific conventional compressive yield strength was decreased by an average 21%.

It can be concluded that silicon carbide performed well both in the case of plateau voltage and absorbed energy (and in their specific pairs as well) and improves these properties. Only the conventional yield strength and the specific conventional yield strength were not improved compared to the reference sample.

Out of the examined reinforcing material the usage of the silicon-carbide turned out to be the most advantageous.

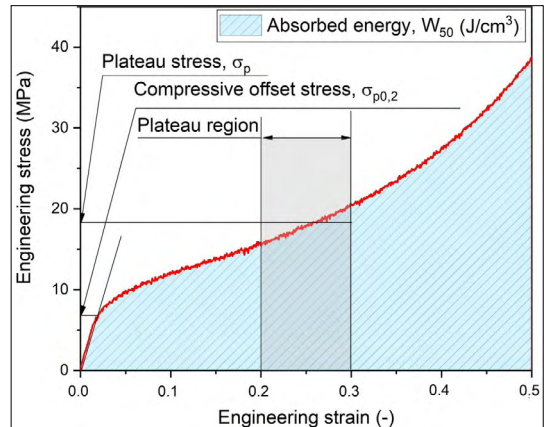


Figure 6. The examined mechanical properties.

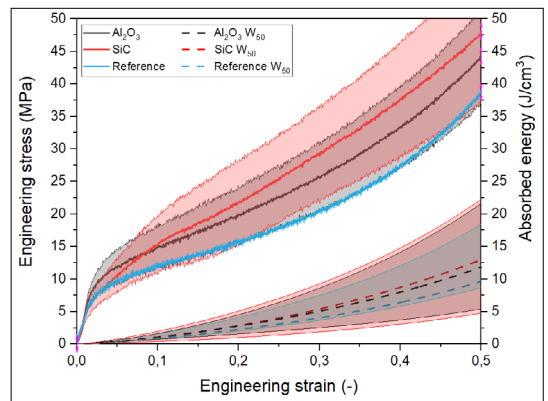


Figure 7. The averaged engineering stress-strain curves and the averaged absorbed energy curves of the specimens.

Table 2. Average values and standard deviations of the studied mechanical properties

	$\sigma_{p11}$ (MPa)	$\sigma_{pl}$ (MPa)	$W_{50}$ (J/cm <sup>3</sup> )
Ref.	6.40 ± 0.12	17.91 ± 0.19	9.66 ± 0.11
$Al_2O_3$	8.18 ± 0.52	22.93 ± 4.19	12 ± 97
SiC	5.78 ± 0.94	25.76 ± 6.18	13 ± 87
	$\sigma_{fp11}$ (MPa*cm <sup>3</sup> /g)	$\sigma_{fp1}$ (MPa*cm <sup>3</sup> /g)	$W_{f50}$ (J/g)
Ref.	5.40 ± 0.14	15.11 ± 0.16	8.15 ± 0.08
$Al_2O_3$	5.15 ± 0.27	14.08 ± 1.45	7.40 ± 0.63
SiC	3.98 ± 0.39	17.46 ± 2.81	8.94 ± 1.25
	Density (g/cm <sup>3</sup> )		
Ref.	1.18 ± 0.01		
$Al_2O_3$	1.60 ± 0.12		
SiC	1.43 ± 0.11		

## 4. Conclusions

The following conclusions were drawn from this research:

- Pressure infiltration is an adequate method to produce salt replicated metal foams reinforced in the matrix material.
- Application of the  $Al_2O_3$  reinforcing material were improved in the case of all parameters, however, in specific cases, the values for all parameters were decreased compared to the reference sample.
- In the case of silicon carbide type reinforcing material, the conventional yield strength and the specific conventional yield strength were improved compared to the unreinforced open-cell metal foam in all cases, except for the specific conventional yield strength.
- Out of the examined reinforcing material the usage of the silicon-carbide proved to be the most advantageous.

## Acknowledgement

The research reported in this paper is part of project no. BME-NVA-02, implemented with the support provided by the Ministry of Innovation and Technology of Hungary from the National Research, Development and Innovation Fund, financed under the TKP2021 funding scheme, and the NRDI Fund (TKP2020 NC, Grant No. BME-NCS) based on the charter of bolster issued by the NRDI Office under the auspices of the Ministry for Innovation and Technology.

This work was supported by the National Research, Development and Innovation Office (NKFIH), under grant agreement OTKA-FK\_21 138505.

## References

- [1] Kádár Cs., Kenesi P.: *Napjaink korszerű anyagai: a fémhabok*. Fizikai Szemle, 7-8. (2008) 279–281.
- [2] Hangai Y., Ando M., Ohashi M., Amagai K., Suzuki R., Matsubara M., Yoshikawa N.: *Compressive properties of two-layered aluminum foams with closed-cell and open-cell structures*. Materials Today Comm., 24. (2020) 101249. <https://doi.org/10.1016/j.mtcomm.2020.101249>
- [3] San Marchi C., Mortensen A.: *Deformation of open-cell aluminum foam*. Acta Materialia, 49/19. (2001) 3959–3969. [https://doi.org/10.1016/S1359-6454\(01\)00294-4](https://doi.org/10.1016/S1359-6454(01)00294-4)
- [4] Santa Maria J. A., Schultz B. F., Ferguson J. B., Rohatgi P. K.: *Al- $Al_2O_3$  syntactic foams - Part I: Effect of matrix strength and hollow sphere size on the quasi-static properties of Al-A206/ $Al_2O_3$  syntactic foams*. Materials Science and Engineering: A, 582. (2013) 415–422. <https://doi.org/10.1016/j.msea.2013.05.081>
- [5] Zukri A., Nazir R., Said K. N. M., Moayed H.: *Physical and mechanical properties of lightweight expanded clay aggregate (LECA)*. MATEC Web Conf 2018; 250. <https://doi.org/10.1051/mateconf/201825001016>
- [6] Kincses D. B., Károly D., Bukor C.: *Production and testing of syntactic metal foams with graded filler volume*. Materials Today. Proc., 45. (2020) 4225–8. <https://doi.org/10.1016/j.matpr.2020.12.163>
- [7] Károly D., Iklódi Z., Kemény A., Kincses D. B., Orbulov I. N.: *Production and Functional Properties of Graded Al-Based Syntactic Metal Foams* 2022:1–12.
- [8] Dhanashekar M., Loganathan P., Ayyanar S., Mohan S. R., Sathish T.: *Mechanical and wear behaviour of AA6061/SiC composites fabricated by powder metallurgy method*. Materials Today. Proceedings, 21. (2019) 335–41. <https://doi.org/10.1016/j.matpr.2019.10.052>
- [9] Kumar N., Chittappa H. C., Ezhil Vannan S.: *Development of Aluminium-Nickel Coated Short Carbon Fiber Metal Matrix Composites*. Materials Today. Proc., 5. (2018) 11336–45. <https://doi.org/10.1016/j.matpr.2018.02.100>
- [10] Zamani NABN, Asif Iqbal AKM, Nuruzzaman DM.: *Fabrication and characterization of  $Al_2O_3$  nanoparticle reinforced aluminum matrix composite via powder metallurgy*. Materials Today. Proceedings, 29. (2019) 190–5. <https://doi.org/10.1016/j.matpr.2020.05.541>
- [11] Zaiemyekheh Z., Liaghat G. H., Ahmadi H., Khan M. K., Razmkhah O.: *Effect of strain rate on deformation behavior of aluminum matrix composites with  $Al_2O_3$  nanoparticles*. Materials Science and Engineering. A, 753. (2019) 276–84. <https://doi.org/10.1016/j.msea.2019.03.052>
- [12] Maróti J. E., Szovák B., Orbulov I. N.: *Reinforced Matrix Syntactic Foams Filled with Ceramic Hollow Spheres*. Acta Mater. Transylvanica 5. (2022) 18–22. <https://doi.org/10.33924/amt-2022-01-05>
- [13] Károly D., Maróti J. E., Lolbert-Szabó J., Kemény A., Orbulov I. N.: *Production of syntactic metal foams reinforced in the matrix material*. IOP Conf. Ser. Mater. Sci. Eng. 2022; 1246:012014. <https://doi.org/10.1088/1757-899x/1246/1/012014>
- [14] Granit Csiszolószerző Kft. <https://www.granit-net.hu/> (accessed on: 2023. 07. 8.).
- [15] ISO13314:2011 Mechanical testing of metals. Ductility testing. Compression test for porous and cellular metals.



# The Effect of Salt Water on the Properties of Basalt Fibre Reinforced Composites

Tamás-Bényei Péter<sup>1,2</sup>

<sup>1</sup> HUN-REN–BME Research Group for Composite Science and Technology, Budapest, Hungary, [tamaspt@pt.bme.hu](mailto:tamaspt@pt.bme.hu)

<sup>2</sup> Budapest University of Technology and Economics, Faculty of Mechanical Engineering, Department of Polymer Engineering, Budapest, Hungary, [tamaspt@pt.bme.hu](mailto:tamaspt@pt.bme.hu)

---

## Abstract

The use of natural or naturally derived reinforcing materials in polymer composites is increasing, thanks to the growing importance of sustainable economy and environmental consciousness. The most promising natural reinforcing material is basalt fibre, which has a very similar chemical structure to glass fibre, which is widely used. However, due to the difference in chemical structure, basalt fibre may be more resistant to more aggressive environments, such as seawater. In this research, the effect of salt water on basalt fibre and its composites was analysed. Unimpregnated basalt, glass and carbon fibre as well as impregnated composites with different concentrations of saltwater solutions were treated for different durations. The effect of salt water was studied by mechanical and morphological tests.

**Keywords:** *basalt fibre, salt water, ageing, polymer composite.*

---

## 1. Introduction

### . Introduction

Modern materials science offers excellent material combinations for the production of parts that are exposed to high loads. Structural materials can basically be divided into three groups, one of which is polymer materials. A special group of polymers is the polymer composites, which are characterized by high specific strength and designable anisotropy. Polymer composites are a combination of a reinforcing material and a matrix material, the reinforcing material is used to provide the structural strength.

The reinforcing material is typically in the form of fibres, the most used being glass fibre and carbon fibre. Nowadays, due to the growing environmental awareness and sustainable economic approach, the use of natural or naturally derived reinforcing materials is becoming increasingly popular.

One of the most promising natural reinforcing materials for polymer composites is basalt fibre. Basalt is a naturally and widely available igneous rock with a very similar chemical composition

to glass fibre, whose main constituents are  $\text{SiO}_2$ ,  $\text{Al}_2\text{O}_3$ ,  $\text{CaO}$ ,  $\text{MgO}$ ,  $\text{FeO}$  and  $\text{Fe}_2\text{O}_3$  [1].

The mechanical properties of basalt fibre are similar to glass fibre, but it also has the advantage of natural, bio-inert, non-irritating and environmentally friendly properties [2], and is resistant to UV and high-energy electromagnetic radiation [3]. The excellent resistance of basalt fibre also extends to its chemical resistance [4].

Continuous basalt fibre with improved mechanical properties can be produced by two-step fibre pulling [5]. The tensile strength of basalt fibres is influenced by many factors besides manufacturing technology, including chemical composition, fibre diameter, fibre structural inhomogeneities. Basalt fibres are less sensitive to fibre ageing because the iron oxides they contain behave as nucleating elements and promote the formation of a fine and relatively homogeneous crystalline structure [6].

Thanks to its beneficial properties, basalt fibre is expected to become more widely used in areas where it is exposed to more aggressive environmental conditions. The environmental exposure can vary widely depending on the application [3].

The impact of seawater on the properties of basalt fibre composites has been evaluated by several researchers [7], but the analyses were not comprehensive.

Wei et al. [8] investigated the effect of seawater on the properties of glass and basalt fibre composites. They showed that the basalt fibre composites were more resistant to seawater than the glass fibre composites. Bonsu et al. [9] analysed the behaviour of glass and basalt fibre in composite and in hybrid composite [10] at constant solvent concentration and different holding times. It was shown that the decrease in mechanical properties is mainly caused by a significant degradation of the fiber-matrix adhesion and the plasticizing effect of water.

In addition, Fourier transform infrared spectroscopy (FTIR spectroscopy) was used to examine the surface of the embedded fibres before treatment and 305 after aging. The results of the tests showed that the seawater treatment changes the chemical composition of the fibre surface.

Davies et al [11] analysed the change in properties of basalt reinforced fibre composites in response to soaking in salt water at different temperatures, using static and cyclic tests. They found that the behaviour of the basalt fibre composites was similar to that of the glass fibre composites. The interlaminar shear strength decreased by around 20% in both cases, caused by degradation and moisture absorption of around 1.5%.

Kaybal et al [12] attempted to compensate for the saltwater-induced delamination by addition of a halloysite nanotube (HNT). They investigated the damage mechanisms in the composites due to applied loads. It was demonstrated that HNT reduced moisture absorption, resulting in higher residual strength in the composites. Several researchers have investigated the effect of holding time [13], and medium temperature [14] on morphological and mechanical properties [15, 16], but the effect of concentration has not been analysed and the property changes of reinforcing materials without matrix material have not been further investigated.

In my research, I analysed, under laboratory conditions, the effect of salt water on the properties of basalt fibre and composites with an epoxy resin matrix using basalt fibre fabric. As a reference, I used the most commonly applied reinforcing materials (glass fibre, carbon fibre) and their composites made with their fabrics and carried out their treatment too.

## 2. Materials, methods and equipment

In this chapter I have summarised the materials used in the research, the procedure for preparing the samples, the test methods and the equipment used for testing the specimens.

### 2.1. Materials

During my research, I used two of the most commonly used reinforcement materials, fibre-glass and carbon fibre, besides basalt fibre fabric (Table 1). The fabrics were plain woven, and all were surface treated to epoxy resin.

For the preparation of the polymer composites, I used a general-purpose laminating epoxy resin type MR3009 bisphenol A („Component A”) with an amine type harder MH3120 („Component B”), prepared by Ipx Chemicals Ltd. The basic properties of the matrix material are summarized in Table 2.

I made the composite laminates by hand lay-up. I ensured proper mixing of the matrix material components by two-step mixing. In the first step, the components were mixed with an IKA RW 16 Basic stirrer at a speed of 5000 rpm for 3 minutes at room temperature. The mixture was then rested for 2 min and the first step was repeated. After impregnating each layer during the laminating process, I used a roller to remove air voids and also remove unnecessary resin from the fabric. The composite sheets were built up using 6 layers of reinforcements. In all cases, I used the manufacturer’s recommended post curing heat treatment of 4 hours at 60 °C in a Heraeus UT20 dryer oven.

For easier identification, I have abbreviated the names of the materials, where GFEP stands for glass, BFEP for basalt and CFEP for carbon fibre reinforced epoxy resin-based composites.

**Table 1.** Main properties of used reinforcements

Materials	Producer	Type	Areal density
Basalt fabric	Basaltex (Belgium)	BAS 220 P	220 g/m <sup>2</sup>
Glass fabric	UNIQUE textiles (Czech Republic)	UTE 220 P	220 g/m <sup>2</sup>
Carbon fabric	SGL Group (Germany)	SIGRATEx C W200-PL1/1	200 g/m <sup>2</sup>

**Table 2.** Main properties of used matrix

Component A	Component B	Mixture	
Dynamic viscosity		Mixing ratio	Pot life
2000 mPas	300 mPas	100 : 20	45 min

## 2.2. Test methods and equipment

The properties of the fabrics were analysed by performing tensile tests according to MSZ EN ISO 13934-1:2013 using a Zwick Z020 universal testing machine. The samples used for the test were 250 mm long and 50 mm wide. The tensile strength and elastic modulus of the fabrics were calculated based on the number and diameter of the rovings that build up the strip, the number and diameter of the elementary fibres that make up the rovings and the tensile strength of the reinforcing fabric. 10-10 samples per fabric were tested at room temperature.

Tensile testing of the composites was carried out according to MSZ EN ISO 527-4:2023 on a ZWICK Z020 universal testing machine using 250 mm long and 2×25 mm cross-section specimens. Tensile strength, elongation at break and Young's modulus were determined from the force-displacement curve recorded during tensile tests. The grip length was 150 mm, and the test speed was 2 mm/min. To make the results more accurate, I also used a video extensometer to measure the elongation during the measurement. I examined 5-5 specimens at room temperature for each composite.

Three-point bending tests of the composites were carried out on a ZWICK Z020 tensile testing machine according to MSZ EN ISO 14125:1999 at ambient temperature. The test specimens of 2×10 mm cross section used for the measurements were tested with a support distance of 64 mm and a test speed of 5 mm/min. The specimens were tested to a limiting deflection of 6.4 mm. From the force-deflection curves, bending stress and bending elastic modulus were calculated. I examined 5-5 specimens for each composite.

Charpy impact test of composites was carried out according to MSZ EN ISO 179-2:2020 using CEAST Resil Impactor Junior machine with 2×10 mm cross section test specimen without notch. The applied impact energy was 25 J, the velocity of the impact 3.3 m/s, and the support distance 80 mm. During the measurement, the energy absorbed by the test specimen was recorded and the Charpy impact strength was calculated. The measurements were carried out on 5 specimens of each composite at room temperature.

The Fourier transform infrared spectroscopy (FTIR) measurements were performed on a Perkin Elmer Spectrum 400 in reflection mode. The light source in the instrument allows measurements in the wavelength range 4000-6500 cm<sup>-1</sup> and 2500-15385 nm.

The ultraviolet (UV) spectroscopic studies were carried out using a Hewlett Packard 8452A spectrometer with diode array detector in absorption mode. The instrument uses a visible UV light source operating in the wavelength range 190-820 nm with a resolution of 2 nm.

Microstructural analysis of the samples was performed with a JEOL JSM-6380LA scanning electron microscope. During the tests, I made images of the fracture surfaces of the broken specimens to characterise the quality of the interfacial adhesion. The examined surfaces were coated with a conductive layer before the measurement to avoid electrostatic charging.

## 3. Results and discussion

In this chapter I have summarised the results and conclusions of the measurements carried out in the experimental part of the research.

### 3.1. The effect of salt water on the properties of reinforcements

Saltwater corrosion is also a real potential risk for the polymer composites that are used to build the blades of offshore wind turbines. In addition to moisture's already identified softening and adhesion damaging effects, in the case of possible damage, the reinforcing fabric could also come into contact with seawater, which could directly damage the reinforcing fabric.

To analyse this influence, I prepared treatment solutions simulating seawater at different concentrations (0, 10, 20, 30, 38%) and placed the reinforcements and composites in them for different durations (1, 2, 4 weeks). To ensure a constant concentration, the treatment was carried out in a closed container, isolated from light. Treatment with a saturating solution (38%) was justified by the possibility of localised increases in concentration on the wind turbine blades. I flushed the surface of the samples with distilled water before each test. The effect of the treatment on fabrics was analysed using strip tensile tests, the results of which are summarised in [Figure 1](#).

The results of the tensile test showed that the tensile strength of each of the reinforcements decreased steadily with increasing solution concentration and treatment exposure time. This decrease was highest for the carbon fibre (76%), followed by the glass fibre (65%) and the most resistant was found to be the basalt fibre (32%). The strength degradation in basalt fibre fabric is caused by the interaction between salt water

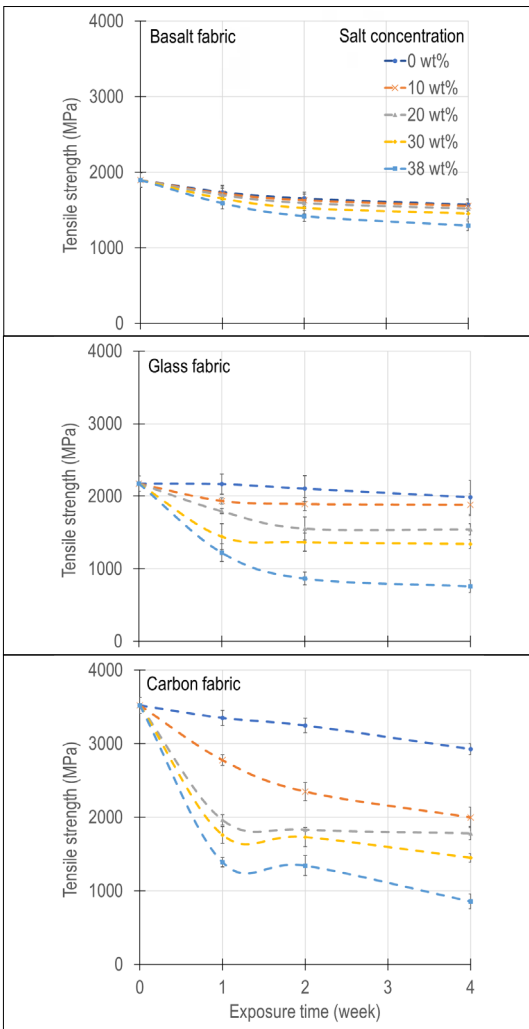


**Figure 1.** The effect of salt-water on the tensile strength of reinforcements.

and the elementary fibres of the basalt fabric, as demonstrated by scanning electron microscopy images shown in **Figure 2**.

The images show that the elementary fibres of the basalt fabric are damaged, cracks and indentations can be observed on their surface.

It is assumed that the treatment has led to the dissolution of a component from the elementary fibres, and to confirm my theory I took samples from the distilled water, and the prepared solution of 38% concentration, which did not contain any reinforcement, and from the solution in which the basalt fibres were left for 4 weeks.

The liquids were analysed by Fourier transform infrared spectroscopy. I performed 3 to 3 measurements for each sample and the spectrograms of the individual spectral curves are displayed (**Figure 3**).

The results show that the difference is only visible between the distilled water used as a reference and the saltwater solution with 38% concentration. The detectable difference is represented merely by a change in transmittance and not by a wavelength difference. The two characteristic peaks are the characteristic signal of aqueous solutions. It is assumed that the wavelength range limits the identification of the leachable elements, so UV spectroscopy was used, which operates in a shorter wavelength range. The average spectra of 3-3 individual spectrum curves were plotted for each sample (**Figure 4**).

The absorbance of the distilled water used as reference is negligible compared to the 38% saltwater solution. The characteristic wavelengths determined for the saltwater solutions are summarised in **Table 3**. Based on the literature [17–19] the values between 190–220 nm (199.76;

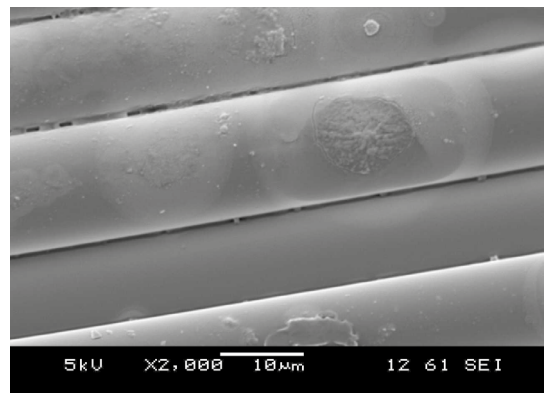
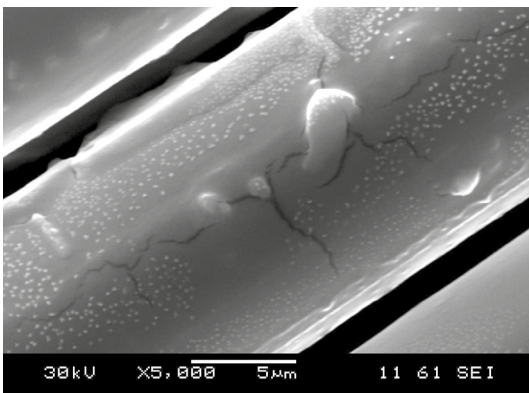


**Figure 2.** Damage of elemental basalt fibres by salt water treatment; 38% concentration 4 weeks (upper), 30% concentration 4 weeks (lower).

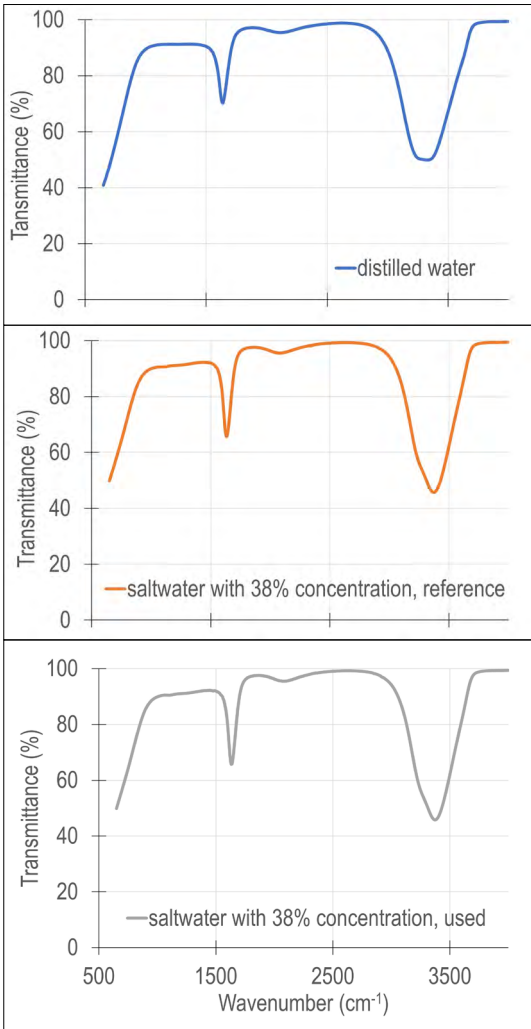


**Figure 3.** Results of Fourier transform infrared spectroscopic measurements

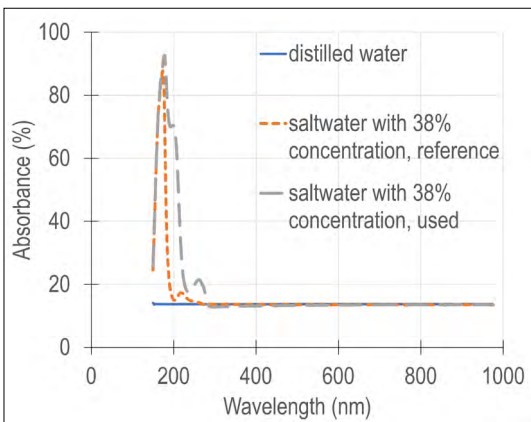


**Figure 4.** Results of ultraviolet spectroscopic studies.

**Table 3.** Characteristic peaks of the recorded UV spectra

Type of saltwater with 38% concentration	Characteristic peaks (nm)		
	1.	2.	3.
reference	173.57	218.1	–
used	178.81	199.76	262.62

218.10) recorded for the used saltwater solution are for sodium and potassium, while the higher peak value (262.62 nm) falls in the range of the characteristic peak for iron and iron oxide.

Spectroscopic studies confirmed that the mechanical properties of the basalt fibre fabric were reduced due to leaching caused by the interaction of the iron or iron oxide that builds up the basalt with salt-water.

**3.2. The effect of salt water on the properties of composites**

After the reinforcement fabrics, I analysed the effect of salt water on the mechanical properties of basalt mono- and hybrid composites by tensile, three-point bending and Charpy tests. Manufactured edges of the specimens were sealed with wax to avoid direct penetration of salt water into the composite material. The results of the tensile tests are shown in Figures 5 and 6.

The results of the tensile tests show that the composite reinforced with basalt fabric was damaged the least by salt water, due to the better resistance of the basalt fibre to saltwater penetrating through the micropores and micro cracks of the matrix material, which is a consequence of the metallic elements that compose the basalt. Compared to glass fibre fabric, basalt fibre is approximately 30% more resistant. The results for the basalt and carbon fibre fabrics show no significant difference compared to the reference. The studies show that replacing glass fibre fabric with basalt fibre fabric in a saltwater environment can lead to a significant increase in lifetime, which also leads to a cost reduction, so the use of basalt fabric in offshore wind turbines can have a positive impact on the lifetime of turbine blades. The flexural strength and flexural modulus values of the composites determined in the flexural testing are summarised in Figures 7 and 8.

The trend determined from the tensile test is consistent with the results of the flexural test, with the basalt fibre reinforced composites proving less sensitive to saltwater treatment than the glass fibre reinforced composites.

The basalt fabric was 36% more resistant in flexural strength and 26% more resistant in flexural modulus of elasticity after 4 weeks of exposure, compared to the glass fibre fabric. The results of the bending tests show that the basalt fibre can be used effectively even when the structural elements are subjected to bending stress.

In conclusion, the use of glass fabric can be substituted by basalt fabric. According to my test results, basalt fibre is more resistant to the saltwater environment. The results of the Charpy impact test are shown in Figure 9. The results of the Charpy test also support the results of the tensile

and bending tests. The saltwater treatment also degraded the matrix material as well as the elementary fibres that compose the reinforcing materials, as evidenced by the 50% impact strength loss of the glass fibre reinforced composite after 4 weeks in 38% solution.

### 4. Conclusions

The results of the tests carried out show that a significant degradation of reinforcement fabrics and composites occurs as the result of saltwater treatment, irrespective of the reinforcing material used to produce them. It can be seen, however,

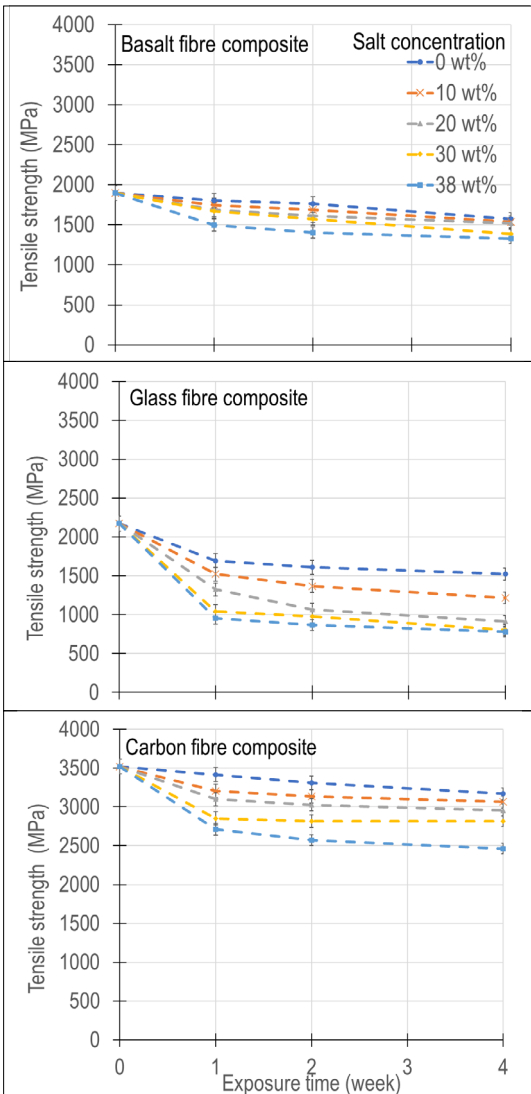


Figure 5. Tensile strength values of composites determined during the tensile test.

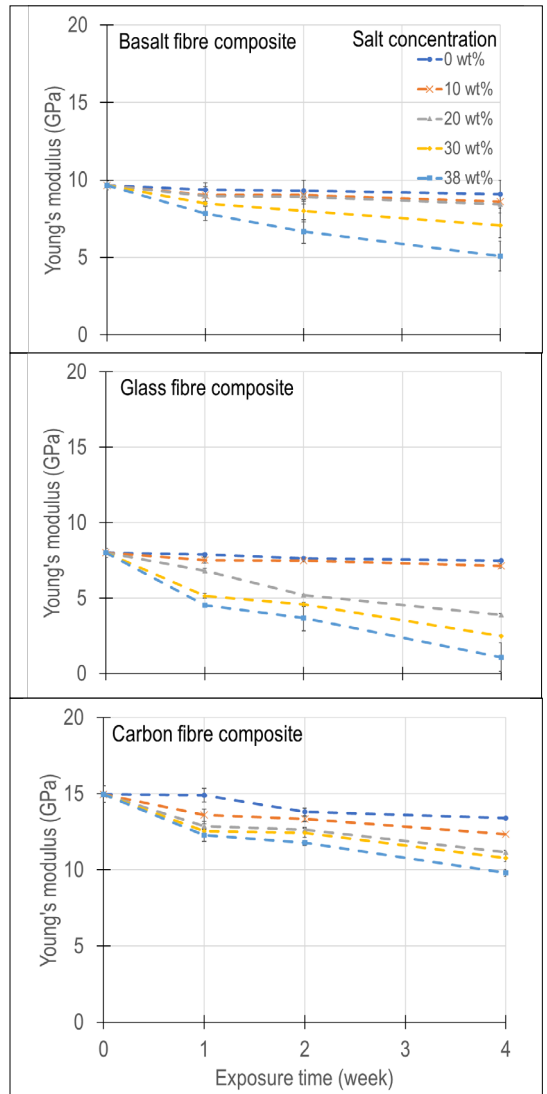


Figure 6. Tensile modulus of elasticity values of composites determined during tensile tests.

that the extent of degradation is already significantly influenced by the constituents that compose the reinforcing material. The results of the tensile, flexural and Charpy tests show that the basalt fibre reinforced specimens are the most resistant of all those tested, due to the metallic elements and their oxides that build up the basalt fibre. Due to this behaviour and resistance, the basalt fibre fabric could become the base material for some components of composite structures operating in different seawater environments, such as offshore wind turbines, and thus its further expansion is predicted.

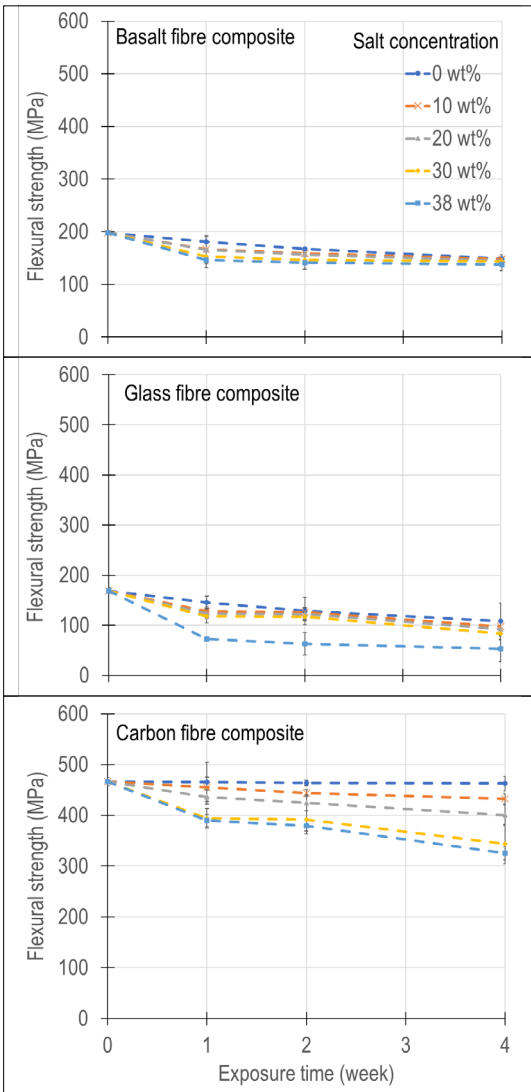


Figure 7. Flexural strength values of composites determined during bending tests.

References

[1] Haldar S. K., Tišljár J.: *Igneous Rocks*. In: *Introduction to Mineralogy and Petrology*. (Szerk.: Haldar S. K., Tišljár J.) Elsevier, Waltham, 2014. 93–120. <https://doi.org/10.1016/B978-0-12-408133-8.00004-3>

[2] Kogan F. M., Nikitina O. V.: *Solubility of chrysotile asbestos and basalt fibers in relation to their fibrogenic and carcinogenic action*. Environmental Health Perspectives, 102. (1994) 205–206. <https://doi.org/10.1289/ehp.94102s5205>

[3] Jamshaid H., Mishra R.: *A green material from rock: basalt fiber – a review*. The Journal of The Textile Institute, 107/7. (2015) 923–937. <https://doi.org/10.1080/00405000.2015.1071940>

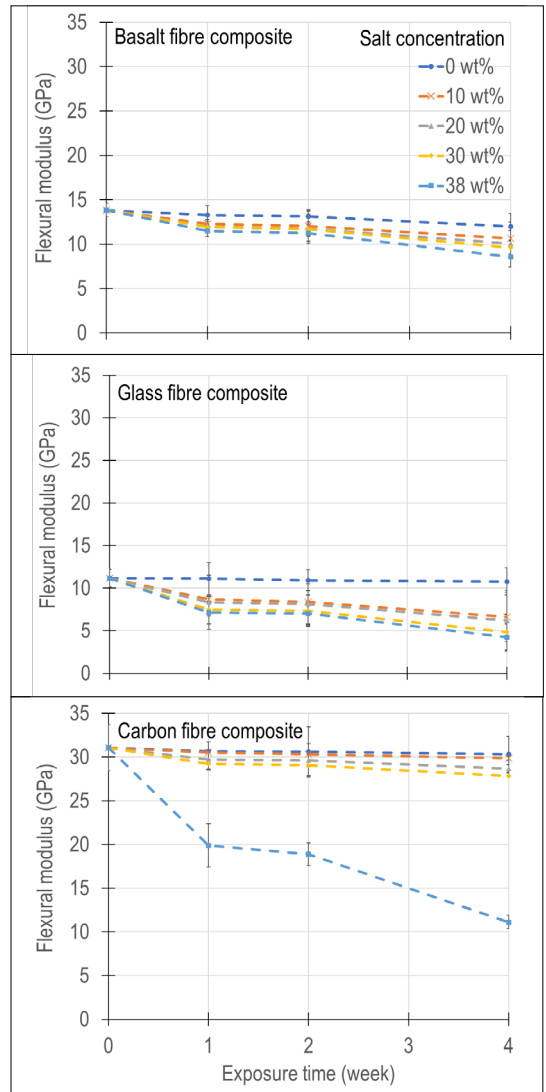
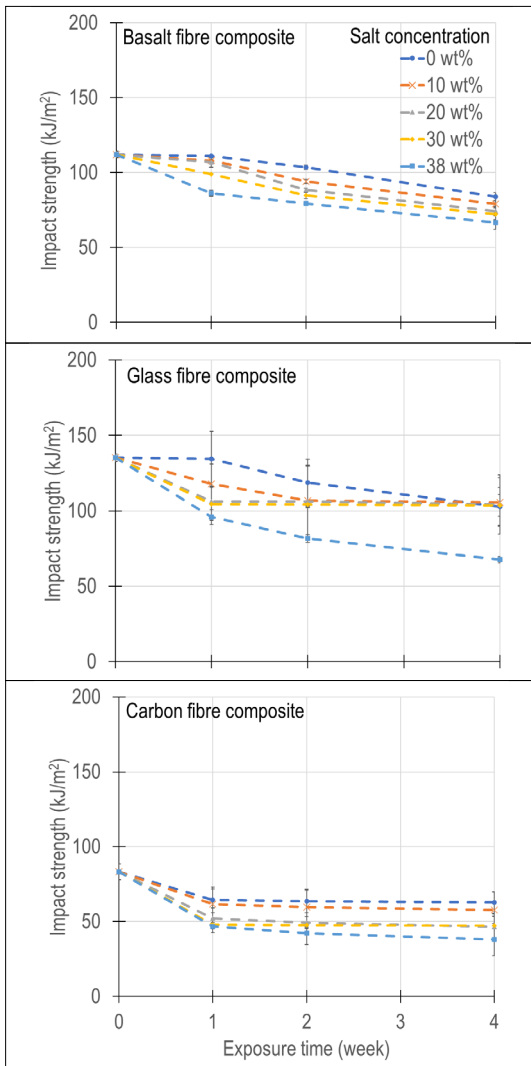


Figure 8. Flexural elastic modulus values of composites determined by bending tests.



**Figure 9.** Impact strength values of composites determined by the Charpy impact test.

- [4] Wei B., Cao H., Song, S.: *Tensile behavior contrast of basalt and glass fibers after chemical treatment*. *Materials & Design*, 31/9. (2010) 4244–4250. <https://doi.org/10.1016/j.matdes.2010.04.009>
- [5] Širok B., Bizjan B., Orbanić A., Bajcar T.: *Mineral wool melt fiberization on a spinner wheel*. *Chemical Engineering Research and Design*, 13. (2013) 1–48. <https://doi.org/10.1016/j.cherd.2013.06.014>
- [6] Wojnárovits I., Rendessy E.: *A szilikátszálak mechanikai tulajdonságait befolyásoló tényezők*. *Építőanyag*, 45. (1993) 50–55.
- [7] Hussnain S. M., Shah S. Z. H., Megat-Yusoff P. S. M., Hussain M. Z.: *Degradation and mechanical performance of fibre-reinforced polymer composites*

*under marine environments: A review of recent advancements*. *Polymer Degradation and Stability*, 215. (2023) 110452.

<https://doi.org/10.1016/j.polymdegradstab.2023.110452>

- [8] Wei B., Cao H., Song, S.: *Degradation of basalt fibre and glass fibre/epoxy resin composites in seawater*. *Corrosion Science*, 53/1. (2011) 426–431. <https://doi.org/10.1016/j.corsci.2010.09.053>
- [9] Bonsu A. O., Liang W., Mensah C., Yang B.: *Assessing the mechanical behavior of glass and basalt reinforced vinyl ester composite under artificial seawater environment*. *Structures*, 38. (2022) 961–978. <https://doi.org/10.1016/j.istruc.2022.02.053>
- [10] Bonsu A. O., Mensah C., Liang W., Yang B., Ma Y.: *Mechanical Degradation and Failure Analysis of Different Glass/Basalt Hybrid Composite Configuration in Simulated Marine Condition*. *Polymers*, 14. (2022) 3480. <https://doi.org/10.3390/polym14173480>
- [11] Davies P., Verbouwe W.: *Evaluation of Basalt Fibre Composites for Marine Applications*. *Applied Composite Materials*, 25/2. (2017) 299–308. <https://doi.org/10.1007/s10443-017-9619-3>
- [12] Kaybal H. B., Ulus H., Avci A.: *Seawater Aged Basalt/Epoxy Composites: Improved Bearing Performance with Halloysite Nanotube Reinforcement*. *Fibers and Polymers*, 22. (2021) 1643–1652. <https://doi.org/10.1007/s12221-021-0671-0>
- [13] Sukur E. F., Onal G.: *Long-term salt-water durability of GNPs reinforced basalt-epoxy multiscale composites for marine applications*. *Tribology International*, 158. (2021) 106910. <https://doi.org/10.1016/j.triboint.2021.106910>
- [14] Shi J., Wang X., Wu Z., Zhu, Z.: *Fatigue behavior of basalt fiber-reinforced polymer tendons under a marine environment*. *Construction and Building Materials*, 137. (2017) 46–54. <https://doi.org/10.1016/j.conbuildmat.2017.01.063>
- [15] Chowdhury I. R., O'Dowd N. P., Comer, A. J.: *Experimental study of hygrothermal ageing effects on failure modes of non-crimp basalt fibre-reinforced epoxy composite*. *Composite Structures*, 275. (2021). 114415. <https://doi.org/10.1016/j.compstruct.2021.114415>
- [16] Fiore V., Scalici T., Di Bella G., Valenza, A.: *A review on basalt fibre and its composites*. *Composites Part B: Engineering*, 74. (2015) 74–94. <https://doi.org/10.1016/j.compositesb.2014.12.034>
- [17] Machado L. C., Marins A. A. L., Muri E. J. B., Biondo A., Matos J. do R., Mazali I. O.: *Complexation of the Fe(III) and Fe(II) sulphates with diphenyl-4-amine barium sulphonate (DAS) Synthesis, thermogravimetric and spectroscopic studies*. *Journal of Thermal Analysis and Calorimetry* 97/289. (2009) 289–296. <https://doi.org/10.1007/s10973-009-0259-1>

[18] Mielczarski J. A., Atenas G. M., Mielczarski E.: *Role of iron surface oxidation layers in decomposition of azo-dye water pollutants in weak acidic solutions*. *Applied Catalysis B: Environmental*, 56/4. (2005) 289–303.  
<https://doi.org/10.1016/j.apcatb.2004.09.017>

[19] Diallo H., Rabiller-Baudry M., Khaless K., Chaufer B.: *On the electrostatic interactions in the transfer mechanisms of iron during nanofiltration in high concentrated phosphoric acid*. *Journal of Membrane Science*, 427. (2013) 37–47.  
<https://doi.org/10.1016/j.memsci.2012.08.047>.



# Effect of Heat Treatment on the Properties of Tool Steel

Tóth László

*Bánki Donát Faculty of Mechanical and Safety Engineering, Óbuda University, Budapest, Hungary,  
toth.laszlo@bgk.uni-obuda.hu*

---

## Abstract

Tool production has deep importance for the industry. The developed tool steels are suitable for the requirements. These tool steels contain large amounts of alloying elements and carbon. The required properties are determined by the chemical composition and microstructure of the tool steel. High hardness, wear resistance, strength, toughness, and corrosion resistance can be achieved by heat treatment which can modify the microstructure. Sub-zero treatment, shallow cryogenic treatment, and deep cryogenic treatment technology, and the resulting microstructure, are given a prominent place in this paper. The review is summarized based on literature research on the experimental results of heat treatment of tool steels..

**Keywords:** *tool steel, heat treatment, retained austenite, high tempering temperature, cryogenic treatments.*

---

## 1. Introduction

Tool steels are unalloyed or alloyed steels, which are primarily used for processing and forming other materials. The applicability of tool steels is determined by their properties. The main properties of tool steels are wear resistance, hardness, toughness, heat resistance, corrosion resistance, polishability, compressive strength, nitriding ability, coating ability [1]. These properties are influenced by the chemical composition and microstructure. Thus, for example, carbon determines the available hardness, strength, hardenability and the start ( $M_s$ ) and finish ( $M_f$ ) temperature of the martensitic transformation [2]. Chromium increases hardenability, wear resistance, edge durability and corrosion resistance [3]. Vanadium refines the primary grains, thereby increasing toughness, wear resistance, edge retention and heat resistance. The tungsten carbides increase the heat resistance and high temperature wear resistance. Cobalt prevents grain growth at high temperatures [4–6].

The structure and grain size of the tool steels also have an effect on the properties [7, 8], which may depend on the manufacturing technology of the raw material, i.e. conventional, remelted or powder metallurgy, hot or cold forming and heat treatment [9–11].

Tool steels are widely used where wear resistance, high strength, toughness and corrosion resistance are required. The microstructure can be modified or adjusted by heat treatment [12, 13]. Heat treatment technologies consist of three cycles : heating, temperature maintaining (ramping or holding time) and cooling [14]. Stress relieving, annealing, normalizing, hardening and tempering are the most important heat treatments that are often used to modify the microstructure of steel and achieve the desired mechanical properties [15]. Heat treatment may be applied before, during or after production. For example, during the production of a tool , the starting raw material is subjected to soft annealing heat treatment in order to make it easily workable, during production a stress relieving heat treatment is performed to reduce the stresses created in the material. The finished tool is hardened and then tempered to the desired hardness and if required surface treated or coated [16–18].

Based on the above, it can be concluded, that heat treatment can be one of the technologies to obtain the desired properties of the tools. In my work I will discuss in more detail the optimal heat treatment procedures required for the appropriate hardness of tools and the importance of the surface treatments and coatings.

## 2. Hardening of tool steels

The hardening consists of heating to the austenitizing temperature, holding to this temperature and quenching faster than the critical cooling rate (Figure 1).

Figure 1 shows the hardening diagram of steel as a function of temperature and time. During heating, thermal stresses arise in the material, which can cause dimensional changes and distortions. To avoid this problem, slow heating is recommended. In the heating process below the transformation temperatures, a ramping step is performed at 650°C and 850°C, to equalize the temperature between the core and the surface of the tool. In Figure 1, the green curve shows the temperature measured on the surface of the material, while the blue curve shows the temperature in the core of the tool. At the austenitization temperature, after the ramping step (when the core of the parts in the furnace reach the chosen temperature) the temperature is maintained constant for a certain amount of time. This is for the formation of homogeneous austenite and it called the holding time [16].

The austenitization temperature of a specific steel grade can also affect the properties. Austenitization can be carried out at lower or higher temperatures within the austenitic area. The hardness of the Sverker 21 cold work tool steel manufactured by Uddeholms AB after quenching and tempering at 1020°C was 62 HRC, and at 1075°C was 61 HRC [17]. The lower hardness value after high-temperature hardening is due to the amount of retained austenite that has not been transformed to martensite due to the increased austenite grains [18, 19].

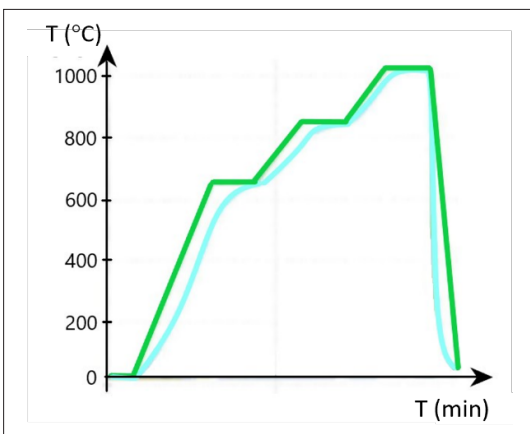


Figure 1. Hardening diagram.

Retained austenite is formed during quenching, when a part of the austenite can not transform into martensite. This transformation is a diffusion-free transformation that begins at  $M_s$ : the martensite starts and ends at  $M_f$ , which is the martensite finish transformation. The  $M_s$  and  $M_f$  temperatures are determined by the carbon content of the steel, which is high in the case of tool steels. In this case  $M_s$  is at low temperatures, and  $M_f$  is in the negative range [45]. This is the reason why cryogenic treatment is necessary. The retained austenite is an undesirable phase in tool steels because it causes stress and dimensional changes. The stress is generated within the material where the untransformed austenite is found, because the volume of the austenite is smaller than that of the martensite, thus drawing-compression stress is generated between the phases. Retained austenite is a soft and unstable phase, which in addition to reducing the hardness during the operation of the tool, transforms into martensite due to stresses and thus can cause cracks in the tool and tool breakage [20–22]. Cryogenic treatment is the most effective method for reducing the amount of retained austenite after quenching [23–25].

### 2.1. Cryogenic treatment and its effect

Cryogenic treatment means that steel is cooled to a negative temperature in order to achieve the specific properties of the material.

Cryogenic treatment can be divided into three different temperature ranges. The first is the range below 0°C called subzero treatment, and ranges down to minus 80°C. In this range, most of the retained austenite transforms into martensite, the fatigue resistance of the steel improves, the dimensional stability and the wear resistance increases [26]. The second domain, called shallow cryogenic treatment, covers the range between minus 80 and minus 160°C. In this range, the amount of retained austenite can be reduced below 1,8%, which ensures dimensional stability, wear resistance and, last but not least an increase in tool life [27, 28]. Table 1 shows the X-ray diffraction test results of a K340 Böhler cold work tool steel produced by electroslag remelting method, one sample heat treated conventionally (CHT), and another heat treated with shallow cryogenic treatment at minus 150°C. The result shows that the retained austenite content of the shallow cryogenic treated specimen is more than three times less than the conventionally heat-treated specimen, and the carbide content is 20% higher,

**Table 1.** Steel K340, XRD analyses results [27]

Phases (mass %)	1- CHT	2- SCT (–150 °C)
Martensite	62.8	55.8
Retained austenite	6.2	1.8
M <sub>2</sub> C (V,Nb)	5.2	4.8
M <sub>7</sub> C <sub>3</sub> (Cr, Fe)	16.7	24.6
M <sub>23</sub> C <sub>6</sub> (Cr, Fe)	9.1	5.3
M <sub>3</sub> C <sub>2</sub> (Cr,Fe)	0	7.7

which is due to secondary carbide precipitation. In addition to an increase in hardness, this also ensures better wear properties for the steel.

The third range (from minus 160 to minus 196 °C) is called deep cryogenic treatment, which not only ensures the dimensional stability of the tool, but also significantly increases its wear resistance, hardness and strength, and, in some cases, even its corrosion resistance [29, 30].

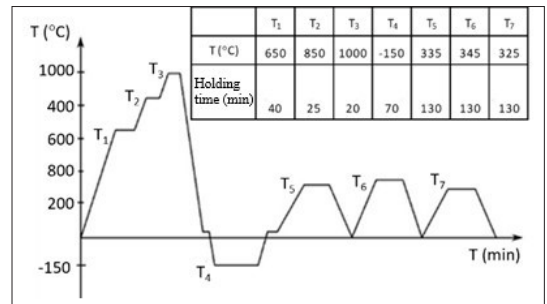
Due to the positive effects of deep cryogenic treatments, they have found application in many areas, such as in the case of additive manufacturing processes[31], electrodes [32], welded joints [33], and during the processing of materials [34–36]. The applications of deep cryogenic treatment are also widespread in nanotechnology [37] and in other industries such as medicine, space research, music, and the automotive industry [38–40]. The tool life is also extremely dependent on the applied heat treatment technologies. Deep cryogenic treatment can greatly improve the mechanical, thermo-chemical and tribological properties of tool steels [41, 42].

Cryogenic treatment has great potential for improving the properties of metallic materials and increasing the lifetime of tools.

We compared the Böhler M340 Isoplast electroslag remelted plastic mould steel cryogenic treated and three times high temperature tempered specimen properties with a conventionally heat-treated sample without cryogenic treatment [43]. Figure 2 show the cryogenic treated specimen diagram.

The hardness of the cryogenic treated specimen was with 1HRC higher than that of the conventionally treated specimen, its wear coefficient was 45% more favourable, while the corrosion mass lost was reduced by 15%.

Cryogenic treatment is usually performed after quenching and before tempering [44].

**Figure 2.** Böhler M340 ISOPLAST steel cryogenic heat treatment

### 3. Tempering and its effect

The martensitic microstructure, after quenching, is brittle and is not recommended for practical use. The material should be tempered immediately after quenching (unless cryogenic treatment is used). When heated to 200-600°C, the stresses are relieved. The microstructure of tool steels after quenching contains martensite, retained austenite and primer carbides, but reheated to a specific temperature below A<sub>c1</sub> (phase transformation temperature), its stresses and the amount of retained austenite are decreased.

During tempering of tool steels, the goal is to achieve a homogeneous spheroidic microstructure.

With low temperature tempering, only the martensite tempering can be achieved, while with high temperature tempering, the amount of retained austenite can also be reduced.

After the first tempering, in the case of a high temperature tempering, the microstructure contains tempered martensite, newly formed martensite from retained austenite, retained austenite and carbides. In this case new carbides are formed (precipitated) called secondary carbides which can increase the hardness with the newly formed martensite. This is called secondary hardening.

Tool steels must be tempered at least twice at high temperatures. After the first tempering, the martensite that has been tempered becomes spheroidite, and the retained austenite transforms into martensite.

A third high temperature tempering is recommended for high-speed steels, hot work tool steels, especially for casting tools, for the heat treatment of larger plastic mould tools, and for highly dimensionally accurate pieces with complex geometry. The essence of the third temper-

ing is the achievement of homogenous spheroidite microstructure and the stress reduction of the material after heat treatment.

Patricia Jovicevic-Klug and her colleagues investigated the changing properties of high-speed steels as a result of deep cryogenic treatment (DCT) [45], and concluded that deep cryogenic treatment increases the compressive strength, and improves fatigue resistance, increases compressive strength, and improves impact performance and thus toughness. However, in addition to deep cryogenic treatment, all these properties are affected by the austenitization temperature and the tempering temperature. Their research also shows that a low austenitization temperature and a high temperature tempering provide more favourable properties for high-speed steels than a high austenitizing temperature and low temperature tempering.

Based in our research, we found that the mechanical properties of the Böhler K110 cold work tool steel are most favourable using high austenitizing temperature, cryogenic treatment, and triple high temperature tempering [46]. After high temperature austenitizing (1070 °C) and low temperature tempering (200 °C), the hardness was 641 HV, while high temperature austenitizing (1070 °C), subzero cooling treatment (-80 °C) and three times high temperature tempering (480 °C), we measured 738 HV hardness, which represented a 14% increase.

Experiments prove that the favourable properties of tool steels can be achieved by forming homogenous spheroidite microstructures with small uniformly distributed secondary carbides. This microstructure can be achieved by using high austenitizing temperature followed by cryogenic treatment and high temperature triple tempering. This microstructure has high hardness, good toughness, high wear resistance, corrosion resistance and last but not least, an increase in service life. Achieving these properties requires a well-developed optimal heat treatment technology. Higher surface hardness and wear resistance can be achieved through surface treatment.

## 4. Surface treatment of tool steels

The purpose of the surface treatment of the tool is to increase wear resistance, reduce adhesion and improve the quality of the finished tool.

During tool production, the most common surface treatments are nitriding and coating technologies.

### 4.1. Nitriding of tool steels

During nitriding, nitrogen atoms are diffused into the surface layer of the tool, which forms a hard wear-resistant compound with the nitride forming elements in the steel. The most suitable steels for nitriding are tool steels with a medium carbon content, which are alloyed with aluminium, chromium, molybdenum or vanadium. It is important that the last tempering temperature is below the nitriding temperature otherwise the hardness in the steel decreases.

The most common nitriding processes are gas nitriding and plasma nitriding.

#### 4.1.1. Gas nitriding

The nitrided crust consists of a compound white layer and a diffusion layer. The compound layer is responsible for resistance to wear, friction and sticking, while the diffusion layer is for resistance to fatigue. The thickness of the compound layer is in the order of microns (around 10 µm), while that of the diffusion layer is around 0,1–1 mm.

Gas nitriding is usually carried out with ammonia in a nitrogen-rich gas. When ammonia comes into contact with the heated workpiece, it breaks into nitrogen and hydrogen, the nitrogen diffuses into the surface of the workpiece. The hardness of the nitrided layer on the surface of tool steel can reach 950–1200 HV. The gas nitriding temperature can vary between 500–570 °C. In the case of nitrided M50NiL steel, Guo-meng Li et al achieved the best wear resistance using a temperature of 500 °C [47].

#### 4.1.2. Plasma nitriding

Plasma nitriding is usually performed at a temperature between 480–520°C. The great advantage of this process is that, compared to other nitriding process, it is well controllable, easily reproducible, takes a short time, and can be performed at a relatively low temperature [48, 49].

Zoltán Kolozsváry investigated the structure and properties of the nitrided layer in his work [50].

During our experiments, we measured a hardness of 1144 HV on the 200µm thick layer after plasma nitriding at a temperature of 520°C on an H13 grade hot work tool steel [51]. Based on the determined wear coefficient, the sample with a plasma nitrided surface has better wear resistance than the hardened and tempered sample.

Dorina Kovács et al investigated the wear behaviour of stainless steel after plasma nitriding [52].

One variant of plasma nitriding is active screen plasma nitriding (ASPEN). In Ilona Szilágyiné Bíró's thesis [53] she studied the edge effect causing discoloration on specimens during active screen plasma nitriding and then compared the nitrified layer after conventional and active screen plasma nitriding.

## 4.2. Surface coating of tool steels

Surface coating of tool steels has become a common practice. The general goal of this process is to create a surface layer with high hardness and low friction, which results in good wear resistance, minimizing the risk of adhesion and sticking.

The coating is typically a thin ceramic layer (below 4µm), characterized by very high hardness and low friction. The most commonly used coating processes are PVD (physical vapour deposition) and CVD (chemical vapour deposition).

During our experiments, we examined the properties of X40CrMoV5-1 quality hot work tool steel under the influence of different coatings [43]. The highest surface hardness of 2938 HV, was achieved with the TiN/AlTiN PVD coating, which also produced the best wear properties.

## 5. Conclusions

The properties of tool steels are determined by the manufacturing technology chemical composition and microstructure. The microstructure can be adjusted by heat treatment, which ensures the appropriate properties during the application of tools.

In my work, I reviewed the heat treatment technologies of tool steels using a number of relevant literatures, during which I compared the properties achieved by heat treatment. The main properties are hardness, wear resistance, strength, absorbency, resistance to cracking, heat resistance, corrosion resistance and dimensional stability. Based on the latest research results, the best properties of the tools and at the same time the longest service tool life can be achieved by using the cryogenic treatment. Wear resistance, surface hardness, and corrosion resistance can be improved even further with surface treatment and coating.

The use of optimal heat treatment technology is the key to achieving the desired properties and service tool life.

## References

- [1] Gaard A., Krakhamler P., Bergström J.: *Wear mechanism in deep drawing of carbon steel-correlation to laboratory testing*. Tribotest, 14. (2008) 1–9. <https://doi.org/10.1002/tt.49>.
- [2] Staia M. H., Pérez-Delgado Y., Sancho C., Castro A., Le Bourhis E., Pucho Cabrera E.: *Hardness properties on high-temperature wear behaviour of nitrified AISI D2 tool steel, prior and after PAPVD coating*. Wear, 267. (2009) 1452–1461. <https://doi.org/10.1016/j.wear.2003.03.045>.
- [3] Brezinová J., Vinos J., Guzanova A., Zivcak J., Brezina J., Sailer A., Voidka M. et al.: *Selected Properties of Hardfacing Layers Created by PTA Technology*. Metals, (2021). <https://doi.org/10.3390/met11010134>.
- [4] Böhler-Uddeholm Hungary Kft.: *Szerszámacélok. Nemesacélok katalógus*. [www.boehler.hu](http://www.boehler.hu) (2014)
- [5] Böhler Uddeholm AG: *Heat Treatment of Tool Steel*. [www.uddeholm.com](http://www.uddeholm.com) (2012) 39.
- [6] Tóth László: *Reduction of Retained Austenite in Tool Steels*. MTK, 16. (2022) 52–57. <https://doi.org/10.33894/mtk-2022.16.10>
- [7] P. Bala: *The Kinetics of Phase Transformations During Tempering of Tool Steels With Different Carbon Content*. Archives of Metallurgy and Materials, 2/54. (2009) 491–498.
- [8] Soares E. Jr., Vatavuk J., Panelli R., Pillis M. F.: *Evaluation of Mechanical Properties and Microstructure of a High Carbon-vanadium Tool Steel Produced by Powder Metallurgy*. Materials Science Forum, 530–531. (2006) 140–144.
- [9] Bostjan Arh, Bojan Podgornik, Jaka Burja: *Electroslag Remelting: A Process Overview*. Materials Technology, 50. (2016) 6, 971–979.
- [10] Schickbichler M., Ramesh Babu S., Hafok M., Turk C., Schneeberger G., Fölzer A. & Michelis S. K.: *Comparison of methods for characterising the steel cleanliness in powder metallurgical high-speed steels*. Powder Metallurgy. <https://doi.org/10.108/00325899.2023.2170848>.
- [11] Korotkov A. N., Korotkova L. P., Laschinina S. V.: *Influence of production technology on the structure and properties of powder high-speed steels*. IOP Conf. Series: Materials Science and Engineering, 971. (2020) 022096. <https://doi.org/10.1088/1757-899x/971/2/022096>.
- [12] Bahrami A., Anijdon S. H. M., Shamanion M., Varahvam N.: *Effects of conventional heat treatment on wear resistance AISI H13 tool steel*. Wear, 258. (2005) 846–851. <https://doi.org/10.1016/j.wear.2004.09.008>
- [13] Réger Mihály, Horváth Richárd, Széll Attila, Réti Tamás, Gonda Viktor, Felde Imre: *The Relationship between Surface and In-Depth Hardness for the Nitrocarburizing Treatment Process*. Metals, 11. (2021) 812. <https://doi.org/10.3390/met11050812>

- [14] Htun Min Shan, Kyaw Si Thu, Lwin Kay Thi: *Effect of Heat Treatment on Microstructure and Mechanical Properties of Spring Steel*. Journal of Metals, Materials and Minerals, 18/2. (2008) 191–197.
- [15] Fadare D. A., Fadara T. G., Akanbi O. Y.: *Effect of Heat Treatment on Mechanical Properties and Microstructure of NST 37-2 Steel*. Journal of Minerals and Materials Characterization and Engineering, 10/3. (2011) <https://doi.org/10.4236/jmmce.2011.103020>
- [16] Bede Martin, Tóth László: *Optimális paraméterek meghatározása dievar melegelakító szerszámacél hőkezelése során*. XXX. Hőkezelő és anyagtudomány a gépgyártásban országos konferencia és szakkiallítás, Hőkezelő proceeding (2022).
- [17] Tóth László: *A maradék ausztenit mennyiségének csökkentése szerszámacélok esetében*. Műszaki Tudományos Közlemények, 16. (2022) 52–57. <https://doi.org/10.33895/mtk-2022.16.10>
- [18] Yiwa Luo, Hanjie Guo, Xiaolin Sun, Mingtao Mao, Jing Guo: *Effect of Austenitizing Conditions on The Microstructure of AISI M42 High-Speed Steel*. Metals, 7. (2017) 27, <https://doi.org/10.3390/met7010027>
- [19] Sola R., Veronesi P., Giovanardi R., Forti A., Parigi G.: *Effect of heat treatment before cryogenic cooling on the properties of AISI M2 steel*. Metall. Ital., 109. (2017) 5–16.
- [20] R. Pierer, R. Schneider, H. Hiebler: *The behavior of two new steels regarding dimensional changes*. 6th International Tooling Conference, 2022, 611–624.
- [21] P. Sekhbar Babui: *Effects of Cryogenic Treatment on H13 Tool steel - An Experimental Investigation*. International Journal of Metallurgical & Materials Science on Engineering, 3/2. (2013) 53–58.
- [22] M. Arbab Rehan, Anna Medvedeva, Lars-Erik Svensson, Leif Karlsson: *Retained Austenite Transformation during Heat Treatment of a 5 Wt Pct Cr Cold work Tool Steel*. Metallurgical and Materials Transaction, 481. (2017). <https://doi.org/10.1007/s11661-017-4232-5>
- [23] Arunram S. P., Nishal M., Thirumugham M., Raghunath A. G.: *Effect of deep and shallow cryogenic treatment on high speed steel grade M2 drilling tool*. Materials Today: Proceedings, 46/19. (2021), 9444–9448.
- [24] Dumasia C. A., Kulkarni V. A., Sonar K. A.: *Review on the effect of cryogenic treatment on metals*. International Research Journal of Engineering and Technology, 4/7. (2017). ISSN: 2395-0072.
- [24] Podgornik B., Paulin I., Zajec B., Jacobson S., Leskovšek V.: *Deep cryogenic treatment of tool steels*. Journal of Materials Processing Technology, 229. (2016) 398–406. <https://doi.org/10.1016/j.jmatprot.2015.09.045>
- [25] Chopra Swamini A., Sargade V. G.: *Metallurgy behind the Cryogenic Treatment of Cutting Tools: An Overview*. 4th International Conference on Materials Processing and Characterization, 2015. <https://doi.org/10.1016/j.matpr.2015.07.119>.
- [26] Yarasu Venu, Jurci Peter, Gogola Peter, Podgornik Bojan, Sedlacek Marko: *Sliding wear behaviour of conventional and cryotreated PM Cr-v (Vanadis 6) ledeburitic tool steel*. Wear, (2023) 532–533. <https://doi.org/10.1016/j.wear.2023.205107>
- [27] Jovicevic-Klug Patricia, Tóth László, Podgornik Bojan: *Comparison of K340 Steel Microstructures and mechanical properties using shallow and Deep Cryogenic Treatment*. Coatings, 12. (2022) 1296. <https://doi.org/10.3390/coatings12091296>
- [28] Tóth László, Fábrián Enikő Réka: *Possibility for Improving the Properties of the Plastic Mold Tool In order to Increase its Service Life*. European Journal of Materials Science and Engineering, 7/4. (2022) 299–305. <https://doi.org/10.36838/ejmse.2022.07.04.299>
- [29] Essam M. A., Shash A. Y. El-Fawakhry M. K., El-Kashif E., Megahed, H.: *Effect of Deep Cryogenic Treatment on Wear Behavior of Cold Work Tool Steel*. Metals, 13. (2023) 382. <https://doi.org/10.3390/met13020382>
- [30] Voglar J., Novak Ž., Jovicevic-Klug P., Podgornik B., Kosec, T.: *Effect of Deep Cryogenic Treatment on Corrosion Properties of Various High-Speed Steels*. Metals, 11. (2021) 14. <https://doi.org/10.3390/met11010014>
- [31] Bartolomé E., Bozzo B., Sevilla P., Martínez-Pasarell O., Puig T., Granados X.: *ABS 3D printed solutions for cryogenic applications*. Cryogenics, 82. (2017) 30–37. <https://doi.org/10.1016/j.cryogenics.2017.01.005>
- [32] Zhisheng W., Ping S., Jinrui L., Shengsun H.: *Effect of deep cryogenic treatment on electrode life and microstructure for spot welding hot dip galvanized steel*. Materials and Design (2003) 24. 687–692.
- [33] Lin Y. T., Wang M. C., Zhang Y., He Y. Z., Wang D. P.: *Investigation of microstructure evolution after postweld Heat Treatment and cryogenic fracture toughness of the weld metal of AA2219 VPTIG joints*. Materials and Design, 113. (2017) 54–59. <https://doi.org/10.1016/j.matdes.2016.10.010>
- [34] Paul S., Chattopadhyay A. B.: *Environmentally conscious machining and grinding with cryogenic cooling*. Machining Science and Technology, 10. (2007) 87–131. <https://doi.org/10.1080/10910340500534316>
- [35] Govindaraju N., Shakeel A. L., Pradeep Kumar M.: *Experimental investigations on cryogenic cooling in the drilling of AISI 1045 Steel*. Materials and Manufacturing Process, 29. (2014) 1417–1421. <https://doi.org/10.1080/10426914.2014.930952>
- [36] Su Y., He N., Li L., Zhao W.: *Effects of cryogenic nitrogen gas jet on machinability of Ti-alloy in high-speed milling*. China Mechanical Engineering, 17. (2006) 1183–1187.

- [37] La Rocca A., Di Liberto G., Shayler P. J., Fay M. W.: *The nanostructure of soot-in-oil particles and agglomerates from an automotive diesel engine*. Tribology International, 61. (2013) 80–87. <https://doi.org/10.1016/j.triboint.2012.12.002>
- [38] Iacopi F., Choi J. H., Terashima K., Rice P. M., Dubois G.: *Cryogenic plasmas for controlled processing of nanoporous materials*. Phys. Chem. Chem. Phys., 13. (2011) 3634–3637. <https://doi.org/10.1039/c0c02660c>
- [39] Thornton R., Slatter T., Jones A. H., Lewis R.: *The effects of cryogenic processing on the wear resistance of grey cast iron brake discs*. Wear, 271. (2011) 2386–2395. <https://doi.org/10.1016/j.wear.2010.12.014>
- [40] Ming C. J. E. R.: *Cryogenic Treatment of Music Wire*. Master's Thesis, Department of Mechanical Engineering, National University of Singapore, Singapore, 2004. <https://scholarbank.nus.edu.sg/haler/10635/14397>
- [41] Mahdi Koneshlon, Kaveh Meshinchi, Farzad Khomamizadeh: *Effect of cryogenic treatment on microstructure, mechanical and wear behaviours of AISI H13 hot work tool steel*. Cryogenics, 51. (2011) 55–61. <https://doi.org/10.1016/j.cryogenics.2010.11.001>
- [42] Debdulal D. Das & Ray K. K.: *On the mechanism of wear resistance enhancement of tool steels by deep cryogenic treatment*. Philosophical Magazine Letters, 92/6. (2012) 295–303. <https://doi.org/10.1080/09500839.2012.669052>
- [43] Körösi Gábor, Dr. Tóth László, Dr. Pinke Péter: *Vizsgálatok a PVC granuláló szerszám élettartamának növelésére*. Mérnöki Szimpózium a Bánkin, ESB, 2022. 194–199. <http://bgk.uni-obuda.hu/esb>, ISBN 978-963-449-306-8
- [44] Jovicevic-Klug Patricia, Podgornik Bojan: *Effect of Deep Cryogenic treatment of Metallic Materials in Automotive Application*. 2020. <https://doi.org/10.3390/met10040434>.
- [45] Jovicevic-Klug Patricia, Pus Gasper, Jovicevic-Klug Matic, Zuzek Borut, Podgornik Bojan: *Influence of heat treatment parameters on effectiveness of deep cryogenic treatment on properties of high-speed steels*. Materials Science & Engineering, A829. (2021) 142157. <https://doi.org/10.1016/j.msea.2021.142157>
- [46] Tóth L., Fábíán E. R.: *The Effects of Quenching and Tempering Treatment on the Hardness and Microstructures of a Cold Work Steel*. International Journal of Engineering and Management Sciences, 4/1. (2019). <https://doi.org/10.21791/IJEMS.2019.1.36>
- [47] Guo-meng Li, Yi-long Liang, Hao Sun, Yun-gang Cao: *Nitriding behaviour and mechanical properties of carburizing and nitriding duplex treated M50NiL steel*. Surface and Coatings Technology, 384. (2019) 125315. <https://doi.org/10.1016/j.surfcoat.2019.125315>.
- [48] Podgornik B., Majdic F., Leslovsek V., Vizintin J.: *Improving tribological properties of tool steels through combination of deep-cryogenic treatment and plasma nitriding*. Wear, 288. (2011) 88–93. <https://doi.org/10.1016/j.wear.2011.04.001>.
- [49] Georges J., Lebrun J.: *Plasma-nitriding and post-oxidizing: An innovative and eco-friendly solution with strong reduced consumption of gas and energy*. Nitriding and Nitrocarburising Conference Proceedings, Aachen, Germany, 2010.
- [50] Kolozsváry Z.: *Nitriding Structure and Properties of Nitriding Layers*. ASM Handbook, Volume 40, Treating of Iron and Steels, 2014. ISBN: 978-1-62708-066-8.
- [51] Tóth László, Kovács Tünde Anna, Nyikes Zoltán, Ghica Valeriu-Gabriel: *Increasing the H13 Tool Steel Wear Resistance by Plasma Nitriding and Multilayer PVD Coating*. U. P. B. Sci. Bull, Series B, 83/2. (2021). ISSN 1454-2331.
- [52] Kovács Dorina, Blücker József, Dobránszky János, Fábíán Réka: *Nemesíthető acélok és rozsdamentes acélok plazmanitridálása*. 2016, XXI. FMTÜ. <https://doi.org/10.33895/mtk2016.05.50>
- [53] Szilágyiné Bíró Andrea: *The Influence of Bios Voltage on The Layer Structure in Active Screen Plasma Nitriding*. Booklet of PHD Theses, University of Miskolc, 2017.
- [54] Bitay Enikő, Tóth László, Kovács Tünde Anna, Nyikes Zoltán, Gergely Attila Levente: *Experimental Study on the Influence of TiN/AlTiN PVD Layer on the Surface Characteristics of Hot Work Tool Steel*. Appl. Sci., 11. (2021) 9309. <https://doi.org/10.3390/app11199309>



# Examination of Damage Processes of Orthopaedic Orthosis

Vincze Kata Dóra

*Budapest University of Technology and Economics, Faculty of Mechanical Engineering, Department of Material Science and Technology, Budapest, Hungary. dori.vincze99@gmail.com*

---

## Abstract

In my work, I examined a palmar forearm splint manufactured by a Hungarian medical device producer. Considering the test results that come from failure analysis, material composition analysis, hardness testing, macroscopic and microscopic examination, scanning electron microscopy and implemented on a product damaged under real conditions, I concluded that the medical device, returned by the customer, had broken prematurely due to improper use. The results of the fatigue test carried out as a physical simulation of the load show that the medical device can withstand more than 850 cycles of micromotion without any problems. Macrofractographic comparisons were performed between the fracture surfaces of the device returned by the users and those of that dismantled under laboratory conditions, thus confirming the validity of my measurement.

**Keywords:** *medical device, orthosis, failure analysis, validation, scanning electron microscopy.*

---

## 1. Introduction

Basically, orthoses (orthosis = A material, device or appliance that protects or fixes damaged parts of the musculoskeletal system, such as casts and splints.) have a long history in the literature.

Haarman describes a device to support hand function that can significantly improve the quality of life of patients with muscle weakness. The authors have developed a novel force transmission mechanism based on tape springs for use in hand orthosis. The actuator force is transmitted to the finger by a system consisting of a tape spring, two sliding blocks and one end-stop per finger. The tape spring allows bending in one direction and resists bending in the other direction. The new mechanism has been prototyped. The small profile (thickening effect) and the ability to transmit high forces make this mechanism suitable for manual orthoses [1].

Hansen points out that strokes often cause flexor hypertonia and weakness of finger extension. In this article, the authors detail the development of DigEx and MIDAS passive arm orthoses. They implemented a quick-change cam system that provides one-handed cam exchange. Belt pulleys and bearings were added to the tool to reduce friction

caused by mechanical contact and material defects. Initial tests of the prototype were promising [2].

Gábor László investigated whether overnight immobilization as a monotherapy significantly improves clinical symptoms, hand functionality and patient quality of life in CMC joint arthrosis. An easy-to-fit wrist and glenohumeral joint orthosis with plaster-like circumferential stability (immobilization) at night was the only allowable therapy. The doctor interviewed the patients by telephone after the end of the study about any night-time complaints. None of the patients complained of night pain [3].

The purpose of the analysis I performed was to compare the fracture surface properties of a fractured orthosis received from the manufacturing company with a complaint and returned to the company with the fracture surface properties of a fractured device subjected to fatigue testing under laboratory conditions. This comparison may shed light on whether the patient wore their orthosis correctly and in accordance with the rules of use. In addition, I will determine whether the device meets the quality and durability expectations of the manufacturer and the current relevant medical technology regulations.

## 2. Examination of suborthoses

### 2.1. An overview of the orthoses studied

Judging by the size of the palmar forearm tendon tested in this article, it is intended for children. The palmar forearm splint is used to immobilise or completely immobilise the wrist, hand and fingers after dislocation, surgery or casting. It may also be used as a substitute for a plaster cast. It is also used for the conservative treatment of tendinitis and degenerative lesions of the wrist, hand and fingers as a resting splint, as a post-operative rehabilitation period and as adjuvant therapy [5].

The device under investigation is composed of the layers illustrated in **Figure 1**. First, the Al sheets of different thicknesses arriving in rolls are corrugated and then stamped to the specified shape. In many cases, several plates have to be riveted or stapled together to produce a suitable aluminium frame. In the assembly process, a layer of polyphom (cross-linked polyethylene foam) is placed on a layer of fabric, followed by the aluminium frame, another layer of polyphom and a final layer of fabric. This layered, flat frame is heat-formed and then cut out of the laminated, hybrid material using a die-cutter. Each flat frame is then individually perforated for better ventilation, sewn around the frame with a sewing machine and then bent to the required shape by hand or with the aid of suitable counter dies (tools). The straps are only put in place after bending and then packaged and shipped with patient information leaflets to orthopaedic shops worldwide.

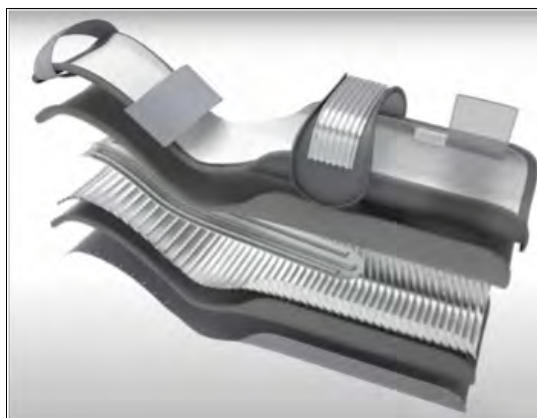


**Figure 1.** Exploded view of the layers of the palmar forearm. [5]

### 2.2. Diagnostics by X-ray microscopy

The medical device was subjected to X-ray microscopy radiography to examine the deterioration of the metal parts of the orthoses used. The type of X-ray microscope used is DAGE XiDAT XD6600.

In all cases, measurements were made at a tube voltage of 140 kV and a power of 11 W.

It can be noted that, in addition to complaints regarding fractures and weakening in the flexio-extension direction at the wrist of the device, several unknown issues were found on the medical device. It can also be concluded that the perforations serve as stress collection points in many places, and the examples suggest that these perforations are the origin of the cracks. The X-ray images have given me an accurate picture of the alignment and number of layers within the orthoses.

The product, illustrated in **Figure 1** was assembled from two types of plate (thickness 0.2 mm and 1.1 mm) with rivet fixation. The thinner plate provides the bending onto the arm and the thicker plate is responsible for the actual fixing. The X-ray microscope image immediately showed that the product was broken at the height of the wrist, across its entire width. On the device investigated, the distinct fracture only affected the thicker reinforcement plate, which was 1.1 mm thick. The thin corrugated aluminium, 0.2 mm thick plate, was only partially broken under load, or in the case of the stressed device, not broken at all (**Figure2**).

From this property, it can be inferred that the thicker the reinforcing plate, the more rigid it behaves and therefore is less resistant to fatigue.

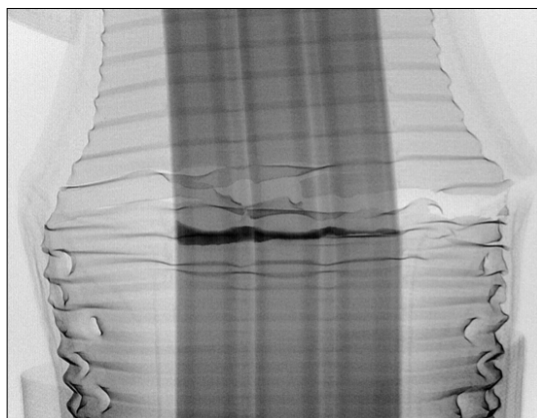


**Figure 2.** X-ray of the fractured part of the wrists of the palmar forearm.

A higher magnification image, examined with a stereomicroscope, shows that this fracture is not a pure fatigue fracture. In the second phase of the fracture, static rupture may have been involved in the fracture process.

### 2.3. Testing of corrugated aluminium reinforcing plate

To test the corrugated aluminium sheet in the orthoses, I made a resin embedded abrasive from a piece of factory corrugated aluminium strip, Lot: 76, 0.4 mm thick. The first striking observation I made was that even at low magnification it was possible to see that the profile of the corrugated aluminium sheet was not symmetrical, i.e. not sinusoidal.

The aluminium profile has unexpected indentations. Since this phenomenon is seen in the same part for all corrugations, I conclude that there is a bulge or a machining defect in the corrugating tool. The aluminium is 7-8  $\mu\text{m}$  thinner in the chipped areas than in other areas (Figure 3). These spalls and thins act as stress accumulation sites. These areas are more likely to develop cracks and subsequent fractures. A small depression runs longitudinally along the bottom of the corrugations. This depression is present on all the corrugations, so I conclude that there is some kind of tooling defect along the entire length of the corrugator.

### 2.4. Description of the fatigue test

The small-cycle fatigue test demonstrates that the material part has undergone ductile deformation in the vicinity of the stress collection sites. At these locations, the stress exceeds the yield stress

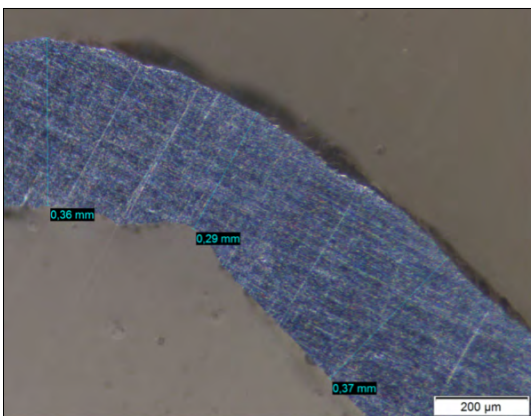


**Figure 3.** Thickness values measured during the plate profile test.

in each cycle. In such cases, typically the number of load cycles to failure is less than 10 000 [6].

The fatigue test was performed using an INSTRON 8872 servo-hydraulic loading machine provided by the BME Biomechanical Research Centre, with the orthosis held in the device as shown in Figure 4. The machine has a maximum load capacity of 20000 N and a crosshead movement speed range of 0.001–1000 mm/min.

The fatigue test was carried out in two parts. Firstly, I loaded the device without quick-clamping, at a test frequency of 1 Hz, with a position control of 10 mm, for a duration of approximately 400 cycles. This method proved not to be suitable. The second method was the quick-clamp clamping method (Figure 4). In this case, I subjected the rail to a real load for about 1500 cycles at a frequency of 2 Hz, also with 10 mm position control. The evaluation was performed only for the test simulating the real load using the second clamping method. MATLAB 2021 (The MathWork, Inc., Massachusetts, USA) software was used to calculate the results and generate the graphs.

In all cases, the position varies by 10-10 mm both downward and upward at an offset of 15 mm. The measurement was performed for less than 800 seconds.

The force varies in a sinusoidal curve over time during fatigue and is repeated many times. In the initial stage, there was a gradual loss of elastic behaviour of the material and the damage to the aluminium stiffener plate - strain hardening, local thinning - which later gave rise to the cracks. Initially, a load of 120 N was required to move the



**Figure 4.** The orthosis in the apparatus designed for fatigue testing.

compression head by 10 mm. This was the resistive force exerted by the orthosis on the machine. After this, a long stretch of maximum resistance value of about 80 N and then the breaking phase begins. Full breakage occurs at the 850th cycle. Here the resistance curve was set to the maximum value of 40 N. This resistance is only due to the tissues in the hybrid structure.

Macrofractographic examination of the fracture surfaces was performed by stereomicroscopy. In the case of the fatigued device, we can say with certainty that the splint has suffered fatigue fracture. The resulting burr surfaces were compared with the surface of the investigated device.

In general, for both devices, the reinforcing aluminium plate is of uneven thickness. On the curved parts it is sometimes up to 0.3 mm thinner than on the straight ones. As I am testing an essentially uneven cross-section, several crack formation sites should be expected. Cracking, the irreversible movement of dislocations caused by cyclic movements, is the result of deformation and microcavitation. In such cases, the load is reduced and deformation may continue at other locations. However, the crack that is created propagates, i.e. the crack tip progresses. Crack initiation points are shown in **Figure 5 a)** for the fatigued and **Figure 5 b)** for the investigated rail. A crack with microscale extent will propagate if the adjacent crystallite is also in the correct position. Once the microcrack reaches a certain size, it becomes macroscale (macroscale is the range of extensions larger than about 1 mm). From then on, tensile stresses will control its propagation rather than shear stresses. The crack will mostly turn and propagate in a plane perpendicular to the maximum tensile stress. As the crack grows under the effect of cyclic loading, cyclicity in the form of regular grooves is also noticeable on the developed strut surface.

Both figures above clearly show semicircular grooves growing away from the crack initiation point. In the case of the fatigued device, the fatigue frequency was probably higher than in the case of the investigated rail, resulting in the formation of several grooves closer together. In the case of the investigated device, the grooves are spaced further apart.

Once the crack reaches a critical size, the propagation becomes unstable and the piece then breaks due to some static fracture. The pointed convexities that are visible in the circled part of **Figure 5 b)** have undergone plastic deformation in the compressive half-cycles, dulling down

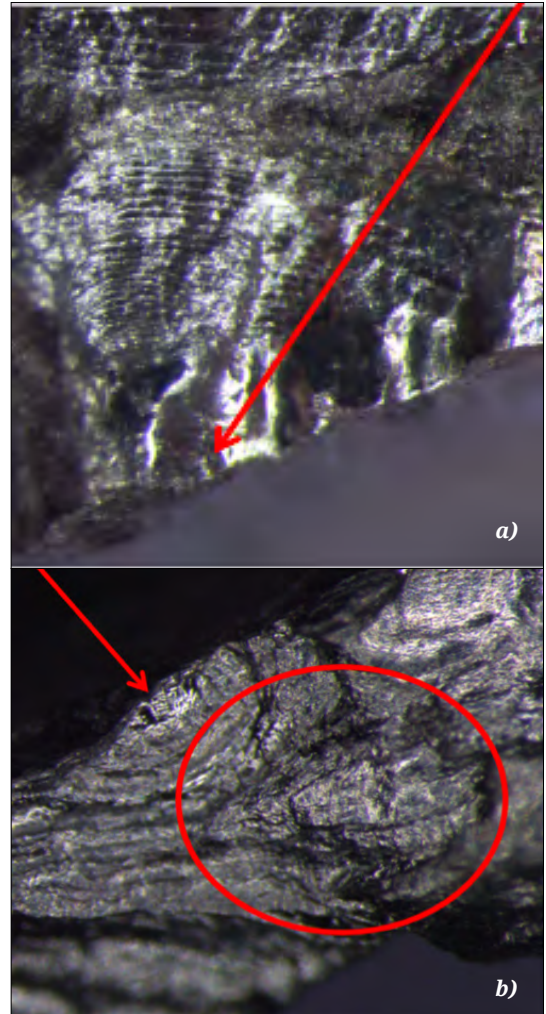


**Figure 5.** (a) Crack initiation site on the proximal burst surface of the fatigued and the investigated (b) orthosis, marked with an arrow.

and losing their original fractographic features. It is interesting to note that in the case of the fatigued tool, cracks were so densely formed as a result of the regular cyclicity that sometimes the semicircular grooves, starting from several directions, overlap. The resistance to fatigue can be improved by mechanical (rolling, spraying) or thermochemical hardening (nitriding) of the surface layer, or by surface coating (e.g. PVD). In the factory, the application of a polychromic coating to aluminium sheet is not considered as heat treatment.

## 2.5. Hardness testing of aluminium reinforcing plate

Hardness measurements can be used to determine the mechanical properties of the material as a good approximation and provide comparative data to tensile test data [4]. The measured data are approximate values of 40 HV. Proportionally deduced from the table in DIN EN ISO 18265:2004, a value of 40 HV corresponds to a tensile strength of approximately 125 MPa. This value is within the range of 105-145 MPa required in the technical certificate of the plate and the material is therefore suitable.

## 2.6. Scanning electron microscopy of aluminium stiffener plate

A scanning electron microscope is a device that scans the surface of a sample in a vacuum with a well-focused electron beam. Using secondary or back-scattered electrons from the sample or X-rays, the equipment can image the surface of the sample as set by modulating the signal from the sample with the light intensity of a cathode ray tube operating synchronously with the electron beam of the microscope. Using this technique, we can image the sample at a magnification of more than 16 000 times [7].

For my studies I used a ZEISS EVO MA10 scanning electron microscope. The machine was used in secondary electron detector mode, at a standard accelerating voltage of 20 kV, an anode current of 200 pA and a working distance of about

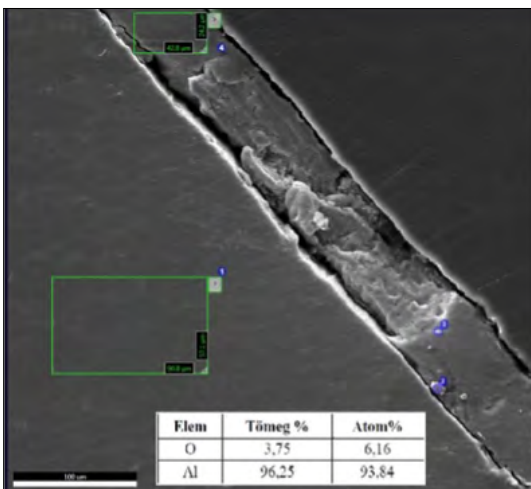


**Figure 6.** Scanning electron microscope image of a part of the sample and the composition of the material measured by EDS in tabular form.

10 mm. From the images taken, it was found that there were no inclusions, foreign material, cracks or breaks in the plate. That is, the material of the plate can be considered homogeneous. The material of the stiffener plate was also examined by energy dispersive X-ray spectrometry (EDS).

The measurement proved that the plate contains only aluminium, since the oxygen peak can be considered as an artificial product caused by molecules adhering to the surface: in this case, too, it is found in the sample due to contact with air.

## 3. Conclusion

Examination of the stiffening plate of the hand orthoses tested on the basis of user complaints has also revealed characteristics that could be considered as manufacturing defects and certainly impair the resistance of the stiffening plate to fatigue. This discovery can be considered in the manufacturing development process.

Based on the hardness test, it can be stated that the tensile strength of the device meets the required specifications. Compliance with the requirements is also confirmed by the material composition measured by EDS. The damage to the tool subjected to the fatigue test proves that the faulty tool has suffered fatigue fracture due to micromovements. Based on the measured data, the device should not break after approximately two weeks of normal use. It can therefore be clearly established that the user did not comply with the conditions of use established to avoid overloading.

## Acknowledgements

My supervisor, János Dobránszky, the Department of Polymer Engineering, the Biomechanics Cooperative Research Centre and the Department of Materials Science and Technology contributed to the research. I am also grateful to the staff of the Laboratory of Failure Analysis of the Department of Electronic Technology (ETT) of the BME for the use of the X-ray microscope. I would also like to thank Peter Mersitz, chief engineer of Chrisofix Ltd. for his support and for the equipment provided.

## References

- [1] Haarman Claudia J. W., Hekman Edsko E. G., Rietman Hans S., Kooij Herman van der: *Pushing the limits: A novel tape spring pushing mechanism to be used in a hand orthosis*. In: Carrozza M. C. et al. (eds.): WeRob 2018, BIOSYSROB 22, Springer Nature Switzerland AG, 2019. 475–479. [https://doi.org/10.1007/978-3-030-01887-0\\_92](https://doi.org/10.1007/978-3-030-01887-0_92)

- [2] Titus S. Hansen, Bitikofer Chris K., Sobbi Bahram E., Perry Joel C.: *Design of mobile digit assistive system (MIDAS): A passive hand extension exoskeleton for post stroke rehabilitation*. In: Haarmann Claudia J. W., Hekman Edsko E. G., Rietman Hans S., Kooij Herman van der: Pushing the limits: A novel tape spring pushing mechanism to be used in a hand orthosis. In: M. C. Carrozza et al. (eds.): WeRob 2018, BIOSYSROB 22, 2019. 535–539.  
[https://doi.org/10.1007/978-3-030-01887-0\\_104](https://doi.org/10.1007/978-3-030-01887-0_104)
- [3] László Gábor, Fűrész József, Sandra Sándor, Bolla Kálmán: *A mozgást a gipszhez hasonló mértékben gátló ortézis terápiás hatásosságának vizsgálata CMC I ízület arthrózisa esetén*. A Magyar Reumatológusok Egyesületének éves vándorgyűlése, 2017. szeptember, Siófok.
- [4] BME ATT: Keménységmérés laboratórium sillaszusz
- [5] Chrisofix. (accessed on: 2022. 07. 26.)  
<https://chrisofix.com/hu/project/universal-resting-shell-orthosis-for-hand-wrist-tenosynovitis-night-use/>
- [6] Anyagvizsgálat (accessed on: 2022. 07. 28.)  
[http://www.sze.hu/~hargitai/Anyagvizsga%E1lat/5\\_kifaradas.pdf](http://www.sze.hu/~hargitai/Anyagvizsga%E1lat/5_kifaradas.pdf)
- [7] Pozsgai Imre: *A pásztázó elektronmikroszkópia és az elektronsugaras mikroanalízis alapjai*. ELTE Eötvös Kiadó, Budapest, 1995.